MIKES Metrology

Espoo 2010

ADVANCED APPLICATIONS OF WAVELENGTH TUNABLE LASERS IN METROLOGY AND FUNDAMENTAL PHYSICS

Doctoral Dissertation

Ville Ahtee

Dissertation for the degree of Doctor of Science in Technology to be presented with due permission of the Faculty of Electronics, Communications, and Automation for public examination and debate in Auditorium S1 at the Aalto University School of Science and Technology (Espoo, Finland) on the 19th of November 2010 at 12 noon.

Aalto-yliopisto

ABSTRACT OF DOCTORAL DISSERTATION	
Author Ville Ahtee	
Name of the dissertation Advanced Applications of Wavelength Tunable Lasers in Metrology and Fundamental Physics	
Manuscript submitted 14.6.2010	Manuscript revised 22.10.2010
Date of the defence 19.11.2010	
☐ Monograph	☒ Article dissertation (summary + original articles)

Faculty	Faculty of Electronics, Communications, and Automation
Department	Department of Signal Processing and Acoustics
Field of research	Measurement Science and Technology
Opponent(s)	Dr. Alan Madej, National Research Council of Canada
Supervisor	Prof. Erkki Ikonen
Instructor	Dr. Mikko Merimaa

Abstract

In this thesis, measurement systems based on wavelength tunable lasers have been developed and studied to improve measurement capabilities in the fields of optical metrology and quantum optics.

In the first work presented in this thesis, techniques for precision measurements of absolute spectral irradiance responsivity of detectors were investigated. Two laser-based methods and a traditional monochromator based method were compared in the near infrared wavelength region. The results between absolute responsivity measurements using the three different measurement systems demonstrated agreement at the uncertainty level of less than 0.1 % ($k = 1$).

The second work consists of an acetylene-stabilized laser and an optical single-frequency synthesizer that were constructed and characterized for precision optical frequency measurements at telecommunication wavelengths. The acetylene-stabilized laser was designed by taking a fiber-based approach, which enabled a relatively straightforward implementation of the optical set-up. The frequency of the stabilized-laser was measured absolutely using an optical frequency comb generator. The results agree well with the recommendation by the International Committee for Weights and Measures (CIPM).

The single-frequency synthesizer was designed for generating a single user-specified frequency from an atomic time base within the 192–196 THz gain bandwidth of an erbium-doped fiber amplifier (EDFA). The synthesizer was utilized for studying spectral lineshapes of acetylene transitions near 1540 nm. The recorded spectra were investigated by theoretical fits and the obtained line-center frequencies were compared to line-center frequencies measured with the acetylene-stabilized laser using the third harmonic technique. The results agreed well with each other.

Final part of the thesis describes a set-up that is capable of emitting indistinguishable single photons using single molecules as photon sources. This was achieved by combining high resolution laser spectroscopy and optical microscopy at cryogenic conditions. Two single molecules in separate microscopes were identified and DC-Stark effect was exploited to shift the resonance frequencies of given molecules for perfect spectral overlap. Excitation by pulsed laser enabled triggered generation of identical single photons from two independent single molecules. The results can be utilized in the development of a number of different quantum information processing schemes.

Keywords	wavelength tunable laser, spectral irradiance, optical frequency measurement, single-photon source		
ISBN (printed)	978-952-5610-63-5	ISSN (printed)	1235-2704
ISBN (pdf)	978-952-5610-64-2	ISSN (pdf)	1797-9730
Language	English	Number of pages	71 p. + appendix 55 p.
Publisher	Centre for Metrology and Accreditation		
Print distribution	Centre for Metrology and Accreditation		
☒ The dissertation can be read at http://lib.tkk.fi/Diss/2010/isbn9789525610642/			

Aalto-yliopisto

VÄITÖSKIRJAN TIIVISTELMÄ	
Tekijä Ville Ahtee	
Väitöskirjan nimi Aallonpituussäädettävien lasereiden pitkälle kehittyneet sovellukset metrologiassa ja perusfysiikan tutkimuksessa	
Käsikirjoituksen päivämäärä 14.6.2010	Korjatun käsikirjoituksen päivämäärä 22.10.2010
Väitöstilaisuuden ajankohta 19.11.2010	
☐ Monografia	☒ Yhdistelmäväitöskirja (yhteenveto + erillisartikkelit)
Tiedekunta Elektroniikan, tietoliikenteen ja automaation tiedekunta Laitos Signaalinkäsittelyn ja akustiikan laitos Tutkimusala Mittaustekniikka Vastaväittäjä(t) Dr. Alan Madej, National Research Council of Canada Työn valvoja Prof. Erkki Ikonen Työn ohjaaja TkT Mikko Merimaa	

Tiivistelmä

Tässä väitöskirjassa on tutkittu sekä kehitetty aallonpituussäädettäviin lasereihin perustuvia mittausjärjestelmiä ja täten parannettu mittauskyvykkyyttä optisen metrologian ja kvanttioptiikan tieteenaloilla.

Väitöskirjan ensimmäisessä työssä on tutkittu menetelmiä, joita sovelletaan spektrisen irradianssin mittaamiseen käytettävien ilmaisimien herkkyyksien absoluuttiseen määrittämiseen. Tutkittavana oli kaksi laseriin perustuvaa ja yksi perinteinen monokromaattoriin perustuva menetelmä, joita verrattiin toisiinsa lähi-infrapuna-alueen mittauksin. Eri menetelmillä saavutetut mittaustulokset olivat keskenään yhtäpitäviä alle 0,1 %:n epävarmuustasolla (k =1).

Toinen väitöskirjassa esitettävä työ koostuu asetyleenistabiloidun laserin ja optisen yksitaajuussyntetisaattorin kehittämisestä ja karakterisoinnista. Kehitetyt laserjärjestelmät toimivat optisen tietoliikenteen aallonpituusalueella. Asetyleenistabiloitu laser suunniteltiin hyödyntäen optisia kuituja, mikä mahdollisti järjestelmän verrattain suoraviivaisen toteuttamisen. Stabiloidun laserin taajuus mitattiin absoluuttisesti optisen taajuuskamman avulla. Tulokset olivat yhteneviä kansainvälisen mitta- ja painokomitean (CIPM) suositusten kanssa.

Optinen yksitaajuussyntetisaattori suunniteltiin tuottamaan käyttäjän valitsema yksittäinen optinen taajuus atomikellon taajuudesta erbium-seostetun kuituvahvistimen (EDFA) 192–194 THz:n vahvistuskaistalla. Tässä työssä syntetisaattoria käytettiin asetyleenin 1540 nm:n ympäristössä olevien spektriviivojen tutkimiseen. Mitattuihin viivanmuotoihin tehtyjen sovitusten perusteella määritettiin spektriviivojen keskitaajuudet ja näitä verrattiin vastaaviin asetyleenistabiloidulla laserilla kolmannen harmonisen menetelmällä mitattuihin arvoihin. Tulokset olivat keskenään yhtäpitäviä.

Väitöskirjan kolmannessa työssä toteutettiin järjestelmä, jolla voidaan tuottaa yksittäisistä molekyyleistä yksittäisiä, keskenään täysin identtisiä, fotoneja. Järjestelmä toteutettiin yhdistämällä korkearesoluutioinen laserspektroskopia ja mikroskopia kryogeenisissä olosuhteissa. Kahden erillisissä mikroskoopeissa olevan yksittäisen molekyylin resonanssitaajuudet siirrettiin vastaamaan toisiaan DC-Stark-efektiä hyödyntäen. Molekyylien virittäminen pulssitetulla laserilla mahdollisti yksittäisten fotonien samanhetkisen tuottamisen erillisistä molekyyleistä. Työn tuloksia voidaan hyödyntää useissa kvanttilaskentaan ja kvanttitiedonkäsittelyyn tähtäävien järjestelmien kehittämisessä.

Asiasanat aallonpituussäädettävä laser, spektrinen irradianssi, optisen taajuuden mittaaminen, yksifotonilähde	
ISBN (painettu) 978-952-5610-63-5	ISSN (painettu) 1235-2704
ISBN (pdf) 978-952-5610-64-2	ISSN (pdf) 1797-9730
Kieli englanti	Sivumäärä 71 s. + liitteet 55 s.
Julkaisija Mittatekniikan keskus	
Painetun väitöskirjan jakelu Mittatekniikan keskus	
☒ Luettavissa verkossa osoitteessa http://lib.tkk.fi/Diss/2010/isbn9789525610642/	

Preface

The research work presented in this thesis has been carried out at the Centre for Metrology and Accreditation (MIKES), at the Metrology Research Institute of Helsinki University of Technology (TKK), and at the Laboratory of Physical Chemistry of Swiss Federal Institute of Technology Zurich (ETH) over the years 2005-2008.

I am thankful to my supervisor Professor Erkki Ikonen for the opportunity to work with the research in the interesting field of optical metrology and laser physics, and for giving me the chance to work with so many great people in various institutes during the years spent with this thesis.

I am grateful to my instructor Dr. Mikko Merimaa and Docent Kaj Nyholm for excellent guidance in research at MIKES and during writing process of this thesis. I want to thank Tuomas Hieta for giving me a hand with building up the set-ups and for the refreshing discussions we had while sharing an office. Dr. Heikki Isotalo and Dr. Antti Lassila are thanked for offering the possibility to carry out research at MIKES Metrology.

Dr. Mart Noorma is very much thanked for sharing his knowledge on optical radiometry and guiding me with research in radiation thermometry at TKK and MIKES.

From ETH I would like to thank Professor Vahid Sandoghdar and his group for introducing me to the field of single-molecule spectroscopy and for very nice companionship during my stay at Zurich. Especially, I want to mention Dr. Andreas Walser, Dr. Robert Pfab, Dr. Robert Lettow, Dr. Alois Renn, and Dr. Stephan Götzinger. Thanks for great support and for many moments to remember.

I want to thank Dr. Steven Brown and Dr. Keith Lykke from the National Institute of Standards and Technology (NIST) for collaboration in research with optical radiometry. Steven Brown and his family are especially thanked for great hospitality during my visit at NIST.

The preliminary examiners of the thesis, Dr. Petr Balling and Professor Tapio Niemi, are thanked for their efforts.

The financial support by the Finnish Foundation for Technology Promotion, Magnus Ehrnrooth Foundation, and the Academy of Finland is acknowledged.

Special acknowledgement for their support goes to my wife Anna and to our lovely little daughter, “Peippo”!

Espoo, October 2010

Ville Ahtee

Contents

List of Publications

This thesis consists of an overview and the following publications.

[I] V. Ahtee, S. W. Brown, T. C. Larason, K. R. Lykke, E. Ikonen, and M. Noorma, "Comparison of absolute spectral irradiance responsivity measurement techniques using wavelength-tunable lasers," Appl. Opt. **46**, 4228–4236 (2007).

[II] V. Ahtee, M. Merimaa, and K. Nyholm, "Fiber-based acetylene-stabilized laser," IEEE Trans. Instrum. Meas. **58**, 1211–1217 (2009).

[III] V. Ahtee, M. Merimaa, and K. Nyholm, "Single-frequency synthesis at telecommunication wavelengths," Opt. Express **17**, 4890–4896 (2009).

[IV] V. Ahtee, M. Merimaa, and K. Nyholm, "Precision spectroscopy of acetylene transitions using an optical frequency synthesizer," Opt. Lett. **34**, 2619–2621 (2009).

[V] R. Lettow, V. Ahtee, R. Pfab, A. Renn, E. Ikonen, S. Götzinger, and V. Sandoghdar, "Realization of two Fourier-limited solid-state single-photon sources," Opt. Express **15**, 15842–15847 (2007).

[VI] V. Ahtee, R. Lettow, R. Pfab, A. Renn, E. Ikonen, S. Götzinger, and V. Sandoghdar, "Molecules as sources for indistinguishable single photons," J. Mod. Opt. **56**, 161–166 (2009).

Author's contribution

All publications included in the thesis are results of team work. The author has prepared the manuscripts for Publications I, II, III, and VI.

In the work reported in Publication I the author has been responsible for the measurements done for the comparison at TKK. He has also analyzed all the measurements presented in this publication.

The author has contributed to the design of the measurement set-ups presented in Publication II and III and he has constructed and characterized the set-ups. He has carried out and analyzed all the measurements presented in these publications. In Publication IV the author has carried out all the measurements and made the numerical simulations.

In the work presented in Publications V and VI the author was involved in the planning of the project, constructed the initial measurement set-up and made the first proof-of-the-principle measurements that demonstrated spectrally overlapping two natural lifetime limited single-molecule resonances. He also analyzed the measurements presented in Publication VI.

1 Introduction

1.1 Background

The proposal for the realization of Light Amplification by Stimulated Emission of Radiation (LASER) in 1958 [1] followed by the demonstration of the first lasing device, a ruby laser in 1960 [2], have been one of the most remarkable landmarks in the history of modern science. Not only that the demonstration of the laser action is a great manifestation of the physical phenomena by itself but, above all, it has opened a door for experiments and technological innovations that would have been impossible to carry out using traditional light sources.

Today, lasers have become an everyday tool in research laboratories where fundamental physical phenomena are investigated. They are used, for example, in spectroscopy to probe atomic and molecular structures and hence to obtain information from the interaction between light and matter [3] or to test the theories of modern physics [4]. Also in other fields of science lasers are extensively used. In metrology, lasers are used for the realization of SI units [5]. The meter, for instance, can be realized by the radiation of a frequency-stabilized laser system [6], and the most stable clocks are based on optical transitions in single ions [7,8,9] or neutral atoms in an optical lattice [10] probed by lasers. Another example from the field of metrology is the realization of the unit for luminous intensity, the candela [11], for which detector responsivity calibrations are made using optical power from a laser source at specific wavelengths.

In telecommunication, lasers have enabled long haul optical data transmission [12], which today forms the backbone of the physical layer of the Internet. Other examples of applications based on laser sources range from consumer products to industrial processing tools and state-of-the art medical instruments. In 2008 the estimated total value of global laser market was $7.40 billion [13].

What then makes the laser so special? The answer lies in the mechanism of the photon generation. In classical light sources, the photons are generated by a spontaneous emission process, which produces photons with random phase and direction over a

broad spectral range. The laser operation, in contrary, is based on stimulated emission where the photons generated are exact copies of one another. As the light emitted form a laser is highly coherent, phase is well defined over long distance and coherent phenomena can be used in measurements.

The first operational laser, a ruby laser, was a solid-state laser acting in pulsed mode at 694 nm [2]. Soon after the pulsed ruby laser was introduced, continuous wave (cw) lasing was demonstrated in a gaseous helium neon mixture pumped by electrical discharge [14] providing the first truly coherent light source at 633 nm. Since then, in addition to various solid-state and gas lasers, several other types of laser have been developed, for example, semiconductor lasers [15] and dye lasers [16]. Laser operation on numerous wavelengths over a spectral range from a few nanometers to hundreds of micrometers has been reported [17].

In most cases, the gain of the lasing medium is restricted to a narrow spectral range, which results into a very limited wavelength tuning range. However, some laser types have a broad gain bandwidth and are operable over fairly large wavelength ranges. These include liquid dye lasers [18], solid-state Ti:Sapphire lasers [19], and external-cavity diode lasers (ECDL) [20]. Using frequency mixing processes provided by non-linear optics, e.g., second harmonic generation (SHG) and optical parametric oscillation (OPO), the wavelength range can be further extended. A number of applications benefit from the broad gain bandwidth. For example, in spectroscopy, wide atomic or molecular absorption bands can be recorded by continuous frequency sweeps. Broad gain bandwidth also enables mode-locked operation and generation of wide continuums.

In this work, several measurement systems based on broad wavelength range lasers have been developed and studied to improve measurement capabilities in the field of optical metrology and in quantum optics. The following chapter summarizes the progress of this work.

1.2 Aim and scope of this thesis

In Chapter 2, techniques for precision measurements of spectral irradiance and radiance responsivity of detectors are discussed. Publication I reports results of a work where three different methods for the measurement of the absolute spectral irradiance responsivity were compared and studied. In the study, two laser-based methods and a traditional monochromator based method were compared in the near infrared wavelength region. The aim of the work was to validate the uncertainty level of the laser-based measurement systems developed at the Metrology Research Institute (MRI) of the Helsinki University of Technology (TKK) [21] and at the National Institute of Standards and Technology (NIST) [22]. The work was the first detailed study of different spectral irradiance responsivity measurement methods reported in the near infrared. The results between the different measurement systems demonstrated agreement at the uncertainty level of less than 0.1 % ($k = 1$).

In Chapter 3 a research work carried out at the MIKES is presented. The work aimed for developing an optical single-frequency synthesizer for precision optical frequency measurements at telecommunication wavelengths near 1.5 μm. To study the feasibility of the scheme based on fiber optics, a fiber-based acetylene-stabilized laser, described in Publication II, was first constructed and characterized. For the first time, standard fiber optic components were utilized almost exclusively in a construction of a frequency-stabilized laser. In the set-up, the light is coupled to free space only to pass through a gas cell, where the Doppler-free spectrum of acetylene is detected. The length of the optical path in the spectroscopy arrangement was dithered with a piezoelectric transducer to average out interference effects. This enabled performing high precision spectroscopy with a fiber-based set-up. The absolute frequency of the laser stabilized to five different transitions of $^{13}C_2H_2$ at ($\nu_1 + \nu_3$) band was measured using an optical frequency comb generator. The results agree well with the recommendation by the International Committee for Weights and Measures (CIPM).

The developed optical single-frequency synthesizer is presented in Publication III. The synthesizer was designed for generating a single user-specified frequency from an

atomic time base within the 192–196 THz gain bandwidth of an erbium-doped fiber amplifier (EDFA). A phase-coherent link between an atomic time base and optical frequencies is established using an optical frequency comb generator. Continuous frequency scanning of the synthesized optical frequency is possible in sub-kilohertz resolution, in principle, over the entire gain bandwidth of the EDFA. The capability of repeating the measurements on the absolute frequency scale and the extremely high intensity stability of the synthesizer allows performing optical frequency measurements at telecommunication wavelengths in unprecedented accuracy. The synthesizer is directly applicable for characterization of optical components used in telecommunication networks or as a frequency reference when calibrating acetylene-stabilized lasers as well as for performing high precision spectroscopy without modulation techniques.

In Publication IV, we reported of a work where the synthesizer was utilized for studying spectral lineshapes of acetylene transitions near 1540 nm. The high signal-to-noise ratio (SNR) of the recorded spectra allowed investigating the lineshapes by theoretical fits and comparing the line-center frequencies to line-center frequencies obtained with a frequency-stabilized laser using the third harmonic technique. Thus, using the synthesizer the effect of line-shape asymmetries and modulation techniques to the lock-point of a frequency-stabilized laser could be studied.

Chapter 4 describes a work done at ETH in the field of quantum optics. The objective of the research was to develop a set-up for demonstrating quantum mechanical two-photon interference using independent single molecules as single-photon sources.

A first step towards the goal is presented in Publication V, where emission of indistinguishable single photons, required for the two-photon interference experiment, was reported. For the first time, two independent solid-state sources were used for producing indistinguishable single photons. In the set-up organic single-molecules in crystalline host matrix were used as sources. The emission of indistinguishable single-photons was achieved by combining high resolution laser spectroscopy and optical microscopy at cryogenic conditions. Wavelength tunable liquid dye lasers were used to excite two individual molecules under two independent microscopes. DC-Stark effect

was exploited to shift the resonance frequencies of given molecules for perfect spectral overlap.

In the further step of the project, reported in Publication VI, a pulsed laser was introduced to the set-up for triggered generation of single photons. For the first time, pulsed excitation was combined with high spectral and spatial resolution in single-molecule spectroscopy. The experimental arrangement set the ground for the realization of a two-photon interference experiment reported recently [23]. The results of this work are important for the development of various quantum information processing schemes utilizing quantum interference.

2 Characterization of absolute spectral irradiance responsivity of detectors using wavelength-tunable lasers

Optical radiometry is a field of science that studies the measurement of energy of the electromagnetic radiation and its propagation in a wavelength range between 5 nm and 100 μm [24]. The quantities of interest are often related to the spectral power distribution of the studied electromagnetic radiation field. Such quantities are, e.g., spectral radiance and irradiance. Radiance is a measure of radiant power through a surface to a specified direction within a given solid angle and has a unit of [$W \cdot m^{-2} \cdot sr^{-1}$]. Irradiance is a measure of radiant power falling on a certain area of a surface and has a unit of [$W \cdot m^{-2}$]. In this thesis, characterization methods of spectral irradiance responsivity of detectors using laser sources have been studied. The motivation for the work was to develop the accuracy of absolute radiation thermometry [25,26,27,28]. In metrology, applications of radiometric temperature measurements include realization of the spectral irradiance scale [29]. In industry, these measurements are needed for monitoring high temperature materials processes. Examples of other applications that benefit from high precision measurements of spectral irradiance include thermal imaging, night vision and solar irradiance measurements.

2.1 Radiometric temperature measurements

Radiometric methods are needed for measurement of high temperatures, for which methods utilizing contact sensors cannot be applied. Traditionally, high temperature measurements have been based on the ratio pyrometry using the Planck radiance law [24]. For an ideal blackbody, the spectral radiance $L(\lambda,T)$ is given by:

$$L(\lambda,T) = \frac{c_1}{\lambda^5\left[\exp(c_2/\lambda T)-1\right]}, \qquad (1)$$

where λ is the wavelength, and T is the temperature, $c_1 = 1.9104282\times10^{-16}$ Wm^2/sr is the first radiation constant, and $c_2 = 1.4387752\times10^{-2}$ mK is the second radiation constant.

Figure 1 shows the spectral radiance of an ideal blackbody, calculated using equation (1), at three different temperatures. The spectral power density at all wavelengths is a monotonic function of temperature, which enables determining the temperature by measuring the radiance on a known wavelength band anywhere on the curve.

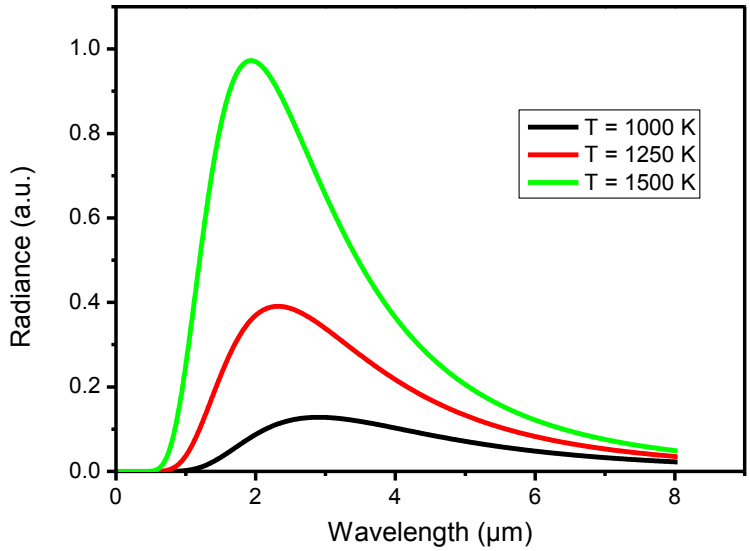

Figure 1. Spectral radiance emitted by an ideal blackbody at three different temperatures.

In the International Temperature Scale of 1990 (ITS-90) [30] the temperatures above the freezing temperature of silver (961.78 °C) are defined in terms of spectral radiance ratios to the silver-, gold- or copper-freezing temperature fixed point blackbody sources. The realization is obtained by relative measurements against one of the fixed points as

$$\frac{L_\lambda(T_{90})}{L_\lambda[T_{90}(X)]} = \frac{\exp\left\{c_2\left[\lambda T_{90}(X)\right]^{-1}\right\}-1}{\exp\left\{c_2\left[\lambda T_{90}\right]^{-1}\right\}-1}, \qquad (2)$$

where $T_{90}(X)$ is the temperature of any one of the silver-, gold-, or copper-freezing points, $L_\lambda(T_{90})$ and $L_\lambda[T_{90}(X)]$ are the spectral radiances emitted by a blackbody at the wavelength λ at T_{90} and at $T_{90}(X)$, respectively.

In the ITS-90, the assigned temperatures for the Ag, Au, and Cu freezing points, result from thermometry using ratio pyrometry referenced to constant-volume gas thermometry (CVGT) measurements at lower temperatures [31]. The thermodynamic

temperature uncertainties of these fixed points arise primarily from the uncertainties in the lower temperature gas thermometry.

The uncertainty of a temperature measurement of higher temperature blackbodies referenced to the fixed points can be estimated by applying Wien's approximation [24]

$$L(\lambda,T) = \frac{c_1}{\lambda^5\left[\exp(c_2/\lambda T)\right]}. \tag{3}$$

From the derivative of $L(\lambda,T)$ with respect to temperature

$$\frac{dL(\lambda,T)}{dT} = \frac{c_1 c_2}{\lambda^6 T^2\left[\exp(c_2/\lambda T)\right]}, \tag{4}$$

it follows that

$$\frac{\Delta L}{L} = \frac{c_2}{\lambda}\frac{\Delta T}{T^2}, \tag{5}$$

which relates the changes in L with the changes in T. When combined with equation (2) this shows that the temperature uncertainty of an ITS-90 assigned blackbody, $u(T_{BB})$, increases as the square of the temperature ratio:

$$u\left(T_{BB}\right) = u\left(T_{FP}\right)\left(\frac{T_{BB}}{T_{FP}}\right)^2, \tag{6}$$

where T_{FP} and $u(T_{FP})$ are the temperature and the uncertainty of the fixed point blackbody and T_{BB} is the temperature of the higher temperature blackbody.

Using absolutely characterized filter radiometers or pyrometers to measure the spectral radiance or irradiance, the thermodynamic temperature of a blackbody can be determined directly and the uncertainty at high temperatures can be reduced [32]. Such detector based methods were long limited by capability of measuring absolute radiation power. The introduction and further development of cryogenic radiometers [33,34] has offered a direct link between optical power and electrical units. This has significantly decreased uncertainties associated to optical power measurements and has made the detector-based absolute radiometric temperature measurements feasible.

2.1.1 Sources of uncertainty

The major sources of uncertainty in the detector-based radiation temperature measurement arise from the spectral responsivity characterization of the detector. In addition to uncertainty in optical power, the wavelength uncertainty is often also a major component in the uncertainty budget. Figure 2 shows radiance of a gold point blackbody source together with responsivity curve of a near infrared filter radiometer that is typically used for radiometric temperature measurements at TKK. Figure 2 shows that as the radiance of the source is highly wavelength dependent on the measurement band, accurate wavelength determination of the detector's responsivity is essential. Also, the out-of-band attenuation of a narrow-band detector has to be well known as the total amount of optical power at the long-wavelength end is significant and the power coupled to the detector cannot be neglected.

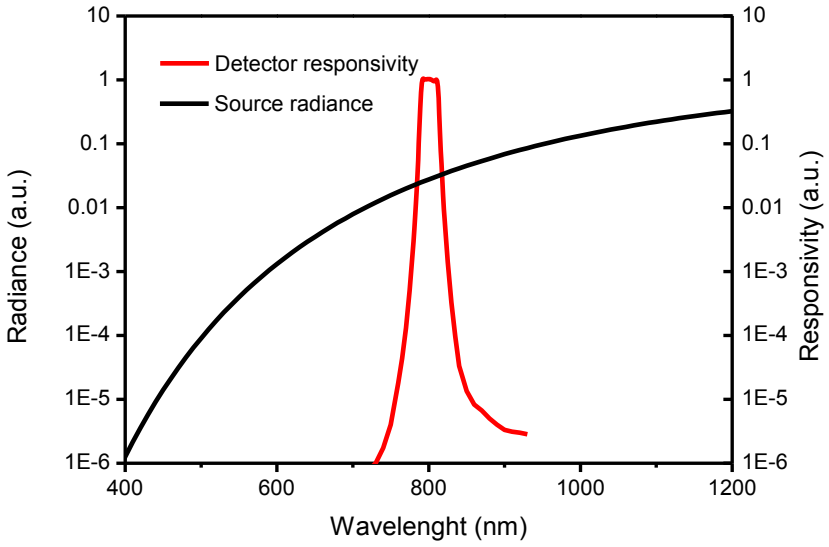

Figure 2. Spectral radiance of a gold point blackbody (T = 1064.18 °C) shown together with the responsivity of a narrow-band near infrared filter radiometer.

2.2 Spectral irradiance responsivity measurement techniques

Traditionally the spectral irradiance responsivity of a detector has been calibrated using a lamp and a monochromator as a radiation source [35,36]. This approach is convenient as broad spectral range can be covered using one source and calibration can be

performed rapidly. However, the achievable uncertainty is often limited by the low radiant flux and the relatively broad spectrum of the source. The low radiant flux limits measurements especially at the out-of-band regions. Broad spectral width, on the other hand, limits the accuracy of determining the responsivity as a function of the wavelength due to convolution effects, especially, at steep transition bands of the device under study.

Using single-mode wavelength tunable dye and Ti:Sapphire lasers, whose output powers range from a few hundred milliwatts up to several watts, the wavelength range from 450 nm to 1100 nm can be continuously covered. Using nonlinear optics this wavelength range can be readily extended, albeit at lower optical power. By stabilizing the laser intensity, relative intensity variations can be reduced below 0.01 %. An active control of the laser cavity and the use of wavelength selective elements provide stable operation in a single longitudinal mode with less than 1-MHz linewidth. These properties make laser sources an attractive alternative for calibrations of detectors [21,22,37]. Indeed, when using wavelength tunable lasers instead of a lamp and a monochromator, the limitations of the traditional calibration methods can be overcome. However, because of the high spatial and temporal coherence of the laser sources, care has to be taken to avoid errors due to interference effects inside the device under test [21, Publication I].

One way to circumvent the interference effect could be to use a pulsed laser instead of a cw source [38]. A Gaussian pulse with duration of a few tens of picoseconds would lead to a linewidth of approximately 100 GHz, which could be utilized in fringe reduction through averaging. However, the center wavelength of spectrally wide pulsed radiation cannot be controlled or measured as accurately as the center wavelength of a narrow cw source. Also, care has to be taken not to saturate a detector under study with high peak power pulses.

Another recently studied approach is provided by supercontinuum laser sources [39], where spectrally broad radiation is generated using a pulsed laser and a photonic crystal fiber (PCF). A supercontinuum source could replace a lamp as a monochromator's light source providing orders of magnitude increased spectral power densities. As the

radiation from a fiber source can easily be focused into small spot size, the radiation can be coupled into a monochromator using a small entrance slit. This would enable both high spectral resolution and high spectral power density at the monochromator's output.

2.2.1 Comparison of laser-based calibration methods at TKK and NIST

In this work, two laser-based spectral irradiance responsivity characterization methods were comparatively studied in the near infrared range. The studied measurement systems were the laser scanning facility (LSF) [21] at TKK and the facility for Spectral Irradiance and Radiance responsivity Calibrations using Uniform Sources (SIRCUS) [22] at NIST. The laser-based methods were compared also to a conventional lamp and a monochromator based method. Earlier comparisons of different calibration methods of spectral irradiance responsivity have revealed deviations which have exceeded the stated uncertainties [40,41]. One reason for these discrepancies has been reported to be due higher than expected uncertainties in the wavelength scales at the comparison laboratories [41]. From this point of view, the laser-based calibration methods are likely to be more exact because of the narrow linewidth of the laser radiation and the ability for accurate real-time wavelength monitoring.

The construction of the filter radiometer used in this work as a measurement artifact is shown in Figure 3. It consists of a precision aperture with a nominal diameter of 3 mm, a band-pass interference filter with a bandwidth of 24 nm (full width at half maximum, FWHM), and a three-element silicon trap detector [42]. The temperature of the aperture and the filter are stabilized during measurements to (25 ± 0.5) ºC.

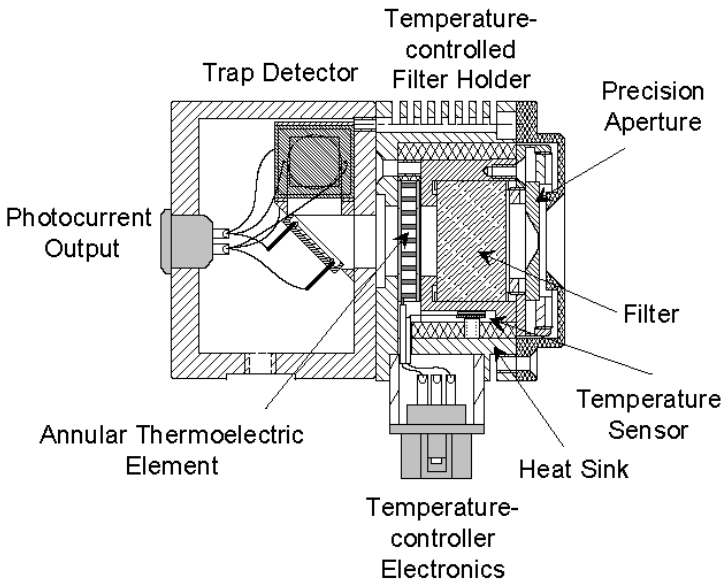

Figure 3. The construction of a typical filter radiometer used in TKK. Figure reproduced from Ref. [41].

Description of the laser-based measurement systems

The studied measurement set-ups have completely independent traceability chains from two independent primary standard cryogenic radiometers. Wavelength-tunable Ti:Sapphire lasers are used at both laser-based set-ups as the light sources and calibrated silicon trap detectors as the reference standards for spectral power responsivity. At TKK the trap detector calibration is based on optical power responsivity measurements at three visible laser wavelengths with a cryogenic radiometer. The responsivity is modeled up 1150 nm. At NIST the reference detector is calibrated directly against national primary standards for spectral power responsivity [34].

The method to generate a uniform monochromatic irradiance is completely different between the two set-ups. SIRCUS at NIST uses an integrating sphere to generate a uniform irradiance field, while LSF at TKK is based on the raster scanning a single collimated laser beam relative to a device under test [43]. The irradiance responsivity on LSF measurement is calculated by summing the resulting photocurrent I at each point, multiplying by the step sizes, and dividing by the incident power P_L as

$$S(\lambda) = \frac{\sum_{j=1}^{n_x} \sum_{k=1}^{n_y} I_{j,k} \Delta x \Delta y}{P_L}. \qquad (7)$$

In equation (7), n_x and n_y are the numbers of measurement points in horizontal and vertical directions, Δx and Δy are the horizontal and vertical distances between the measurement points.

The measurements made with the two laser based set-ups were compared to a measurement made on the monochromator based Visible to Near-Infrared Spectral Comparator Facility (SCF) [35] at NIST, which utilizes a 100 W quartz halogen lamp as a light source. The measurements were done using 4-nm bandwidth. In the SCF the measurement principle is also based on raster scanning the monochromator's output beam.

Interference effects

As explained above, interference effects have to be taken into account when lasers are used in spectral responsivity calibrations. The interference can be minimized by proper coatings on optical surfaces and by using a suitable geometry. In this measurement, for example, the filter of the detector was antireflection coated and the filter surfaces were slightly wedged. However, an interference pattern with 0.2 nm period and 0.5 % peak-to-peak amplitude is still present.

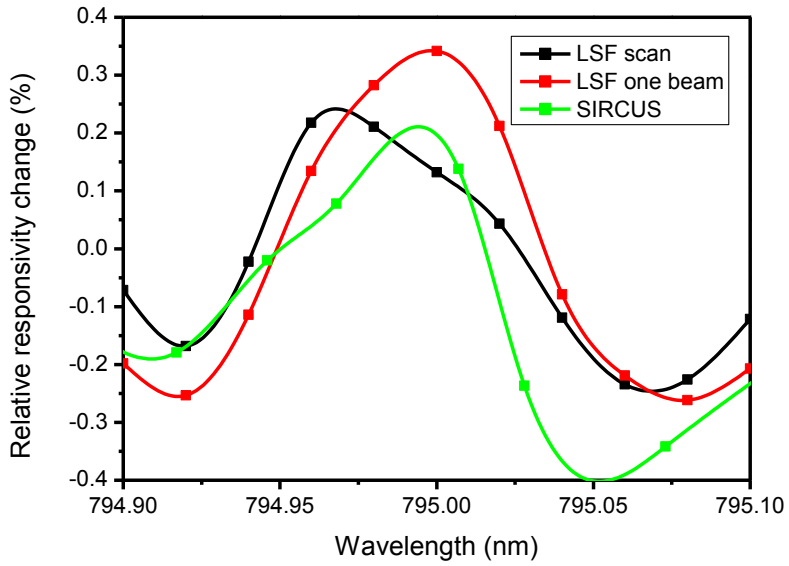

Figure 4. Interference pattern on the filter radiometer's responsivity measured close to 795 nm on SIRCUS, LSF, and with single beam technique on LSF [Publication I].

On SIRCUS calibration the effect of interference was taken into account by taking measurements with 0.02 nm intervals on average, which enabled determination of the true responsivity curve. On LSF, where the scanning method limits the practical number of measurement points, a correction was made to every measurement point. This was done by measuring a relative responsivity of the detector over an oscillation cycle around an absolute raster scanned measurement point using a single beam at the center of the aperture. Based on the single beam measurements, the absolute responsivity was corrected to correspond to the average of the interference pattern. The applicability of the single beam method was confirmed by measuring a period of an oscillation pattern with single beam and raster scanning techniques. The result of this measurement is shown in Figure 4 together with a SIRCUS measurement.

Results of the comparison

Figure 5 shows the results of the measurements performed with the three set-ups. The irradiance responsivity measurements obtained with the two laser-based methods have an excellent agreement. The shape of the responsivity curve obtained from the

measurements on SCF is highly affected by the large bandwidth of the source, which makes the individual measurement points to represent values that are spectrally averaged over several nanometers.

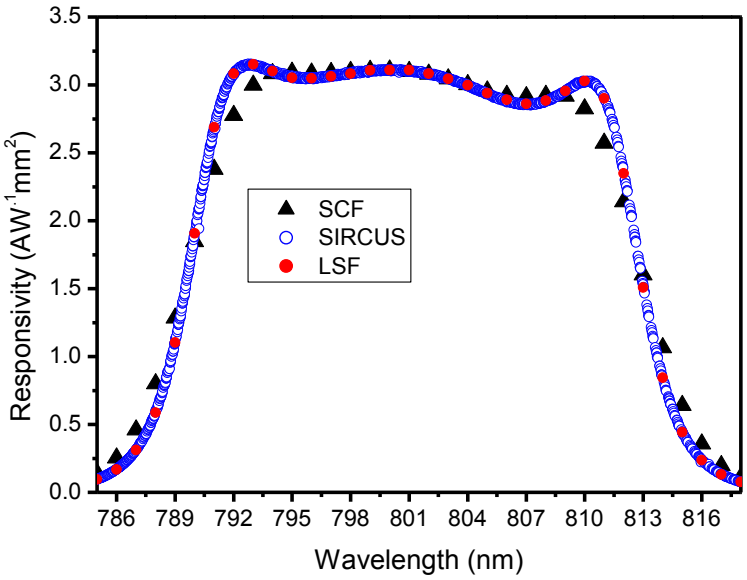

Figure 5. Spectral irradiance responsivity of the near infrared filter radiometer measured on SIRCUS, LSF, and SCF [Publication I].

To quantitatively compare the measured data, the integrated irradiance responsivity and the effective wavelength were calculated. The results are shown in the Table I as relative differences to the weighted average of all three methods together with the stated standard uncertainties for each set-up. The weighted averages were calculated as

$$\bar{x} = \frac{\sum_{i=1}^{3} x_i u_i^{-2}}{\sum_{i=1}^{3} u_i^{-2}}, \tag{8}$$

where x_i are the calculated integrated responses/effective wavelengths obtained with each method and u_i are the corresponding standard uncertainties.

It should be noted that the effective wavelength in SCF measurements is affected by the convolution effect due 4-nm source linewidth. The effect was estimated to be approximately 0.01 nm.

Table I. Integrated responses and effective wavelengths obtained on each set-up as compared to weighted average of the three measurements. Results are calculated from the measurement data over 785 - 818 nm range. The corresponding standard uncertainties are shown.

	Integrated irradiance responsivity		Effective wavelength	
	Relative difference to weighted average × 10^{-4}	Relative standard uncertainty × 10^{-4}	Difference to weighted average [nm]	Standard uncertainty [nm]
SIRCUS	-1.0	5.2	0.001	0.001
LSF	3.0	8.9	-0.006	0.003
SCF	-0.6	59	0.016	0.1

All three methods agree well with each other in terms of the integrated responsivities; the laser-based methods offering significantly lower uncertainties than the monochromator-based method. The calculated effective wavelength values on SIRCUS and LSF measurements match well with each other, within expanded (k = 2) uncertainties. Also, the effective wavelength extracted from the SCF agrees well with the average of all three methods, although the uncertainty is much higher.

The results of this comparison have implications for a number of radiometric applications where high-accuracy spectral radiance and irradiance measurements are crucial. For instance, the uncertainty in an absolute detector-based radiometric temperature scale depends mostly on the accuracy of the spectral radiance and irradiance responsivity scales. Freezing temperatures of gold, silver, and aluminum fixed points, defined by ITS-90, have been measured using radiometric detectors traceable to absolute cryogenic radiometers, with uncertainties similar to the thermodynamic measurements of temperature reported in the ITS-90. For example, such a measurement was conducted using the filter radiometer characterized in this work in a study where thermodynamic temperatures of blackbody radiators were measured at MIKES [28]. The thermodynamic temperature measurement of a silver fixed-point cell using the filter radiometer gave excellent agreement with the ITS-90 determined temperature (961.78 °C), the deviation being only 0.05 K with standard uncertainty of 0.109 K.

The results of this comparison may also have implications in photometry where tunable lasers can be utilized to measure the spectral responsivity of photometers with low uncertainty. In such measurements the advantage of using lasers arises primarily because of the improved accuracy of the wavelength scale.

3 Precision optical frequency measurements at telecommunication wavelengths

Frequency can be measured at the lowest uncertainty of all physical quantities. This applies also at the optical domain where the most accurate atomic clocks operate today [7,8,9,10], although the definition of the second is still tied to the ground state hyperfine splitting of Cesium at microwave region. Past measurements of optical frequencies have led to a number of technological breakthroughs, one of the most significant being the current definition of the meter adopted by General Conference on Weights and Measures (CGPM) in 1983 [44]: "The Meter is the length of the path traveled by light in vacuum in 1/299792458 of a second." This definition fixes the speed of light and relates the SI-base unit of length, the meter, with that of the time, the second.

3.1 Absolute measurement of optical frequency

A measurement is absolute when it is referenced to the definition of the appropriate SI unit(s). An absolute frequency measurement must be based on the time unit second and thus referenced to a Cs-clock. The measurement of optical frequency at hundreds of terahertz is anything but trivial. Direct frequency counting using electronic circuits is limited to frequencies up to a few tens of gigahertz. Thus, to measure visible optical frequencies a method to cover orders of magnitude wide frequency gap between an atomic time base and optical frequencies is needed. Until last decade, this was one of the trickiest challenges in metrology and diverse techniques to do this were investigated.

3.1.1 Traditional approach

Optical frequencies were first absolutely measured in the beginning of 1970's using synthesis by harmonics approach to construct a frequency chain [45,46,47,48,49,50]. Although the frequency chains were the only viable option at that time, the limitations of such systems were obvious. The complexity of the approach required resources that were available only at a few major metrology institutes and the chain had to be designed

to measure a particular frequency. Also, the multiplication of phase noise with harmonic synthesis limited the performance of frequency chains. Nevertheless, successful measurement of an iodine-stabilized He-Ne laser at 633 nm in 1982 led to re-definition of the meter.

In 1990's optical frequency measurement methods based on difference-frequency syntheses were developed. Probably the most notable of these techniques was frequency interval bisection [51], which relied on subdividing a frequency gap between two optical frequencies (f_1 and f_2) by phase locking a third frequency f_3 to the exact average of the frequencies f_1 and f_2. In principle, concatenation of approximately 12 bisection stages links visible optical frequencies to microwave region.

3.1.2 Full octave optical frequency comb technique

Advances in mode-locked laser technology in the end of 1990's provided ever wider measurement ranges [52] and paved a way for a quantum leap in the measurement of optical frequencies. At the turn of millennium the introduction of a full-octave optical frequency comb generator revolutionized the field of optical frequency metrology by providing direct phase coherent link between optical and microwave frequencies [53,54,55]. Using a Ti:Sapphire femtosecond mode-locked laser and a photonic crystal fiber (PCF) [56], a dense comb of equally spaced frequencies spanning over an optical octave was produced. The comb could be directly stabilized to a microwave standard giving each frequency component an absolutely known value. This enabled practical absolute measurements of any optical frequency over the entire visible spectrum extending to near infrared. Soon after, an octave spanning comb spectrum at near infrared was demonstrated using an erbium-doped fiber laser [57,58].

In this work, a Ti:Sapphire frequency comb generator has been utilized to measure the absolute frequency of the constructed acetylene-stabilized laser and for optical single-frequency synthesis at near infrared. In the next section, the operating principle of a full octave optical frequency comb generator is briefly reviewed.

3.1.3 Ti:Sapphire femtosecond laser comb

Operation of a conventional full octave spanning optical frequency comb generator is typically based on a mode-locked laser, which produce pulses whose duration is in the femtosecond scale with a repetition rate in between 100 MHz and 1 GHz. By Fourier transforming such a pulse train from time domain to frequency domain, it is seen that the result is a comb like structure of evenly spaced frequency components [59].

The spacing between the frequency components is directly given by the repetition rate (f_{rep}) of the pulsed laser. The location of each frequency component is, however, not an integer number times the repetition rate. This is due to the fact that the group and phase velocities differ inside the laser cavity and the center of envelope with respect to carrier changes from pulse to pulse. In frequency domain, this phenomenon causes an offset frequency for the frequency comb structure, commonly referred as the carrier-envelope-offset (CEO).

The spectral width of the output of a femtosecond laser is determined by the duration of the emitted pulses. The width of the spectrum resulting from Gaussian shaped pulses with duration of 30 fs is approximately 15 THz (FWHM). To broaden the spectrum, the pulse train from the laser is taken through a PCF. The size of the core and the dispersion properties of a PCF can be tailored for efficient pulse compression in the fiber. The resulting self-phase modulation (SPM) and other non-linear effects broaden the spectrum [60] and at the fiber output a spectrum spanning over an octave in frequency can be obtained. It has also been demonstrated that octave-spanning spectra can be achieved directly from a Ti:Sapphire laser using double-chirped mirrors and a second intracavity focus in a glass plate for additional SPM effects [61].

In order to generate a comb of absolutely known optical frequencies, the repetition rate and the CEO frequency have to be phase-locked to an atomic time base. A hydrogen maser [62] is very desirable reference clock as it has excellent short- and long-term stability and it can be tuned with high precision to match the frequency distributed by the Cs-clock. When the repetition rate and the CEO frequency are stabilized, the frequency of every comb component can directly be calculated as

$$f_n = nf_{rep} \pm f_{CEO}, \quad (9)$$

where n is the number of the comb component and f_{CEO} is the carrier-envelope-offset frequency.

Stabilization of the repetition rate is relatively straightforward as it can be directly measured at the output of the femtosecond laser using a high speed photodetector and synchronized to a microwave source using an analog mixer, loop-filter, and a piezoelectric transducer (PZT) to control the cavity length.

In contrast to the repetition rate stabilization, the stabilization of the CEO frequency is not trivial because the offset cannot be accessed directly. The possibility to broaden the spectrum over an optical octave allows an elegant method, self-referencing, to be used to solve this problem. In self-referencing, shown schematically in Figure 6, the red end of the comb spectrum is frequency doubled, thus frequency doubling also the CEO frequency. When the frequency-doubled part of the comb spectrum is overlapped with the blue end of the original comb spectrum, having original offset, the resulting beat-note is exactly equal to the CEO frequency, which can then be stabilized using a PLL controlling the cavity dispersion. This can locally be done by adjusting the power of the pump laser. The complication of this method is that obtaining a proper beat signal requires that the frequencies contributing to the signal in corresponding pulses must overlap both spectrally and temporally at high precision. As the signal path contains a number of non-linear and dispersive components, slight deviations in laser parameters and in coupling to the PCF may have dramatic effect to SNR of the measured offset frequency. However, careful control of vibrations and temperature stabilization in addition to active control of the PCF in the coupling provides continuous operation exceeding hours.

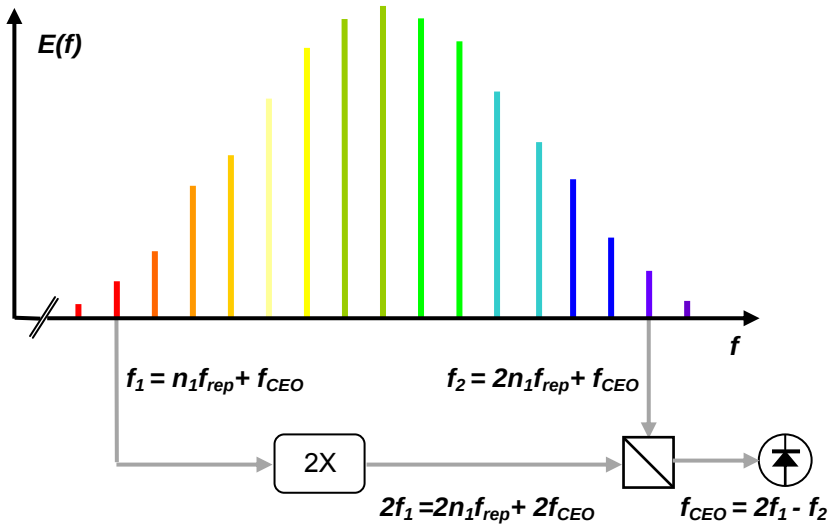

Figure 6. Schematical illustration of self-referencing technique used for measuring the CEO frequency.

3.2 Optical frequency standards

Schemes of using the laser frequency stabilized on an atomic or molecular transition as a wavelength standard have been explored since late 1960's [63] and in 1983 stabilized lasers superseded ^{86}Kr discharge lamps as working wavelength standards. The International Bureau of Weights and Measures (BIPM) maintains a list of radiations recommended by the CIPM for the realization of the definition of the meter as well as for other optical frequency standards covering the wavelength range from 200 nm to 10 μm [6]. A conventional and highly successful method for laser stabilization utilizes saturation absorption spectroscopy [64] and the third harmonic-locking method [65,66] with gas cells. Relative stabilities below 1×10^{-13} at 1 s averaging time can readily be achieved with these systems [67].

An ultimate frequency-stabilized laser is an optical atomic clock. The most stable clocks are based on nearly forbidden transitions in single ions [7,8,9] or in neutral atoms trapped to an optical lattice [10]. The instability of an atomic clock arising from quantum projection noise as a function of the averaging time τ is [68]

$$\sigma(\tau) = \frac{\Delta\nu}{\nu_0}\sqrt{\frac{T}{N\tau}}, \qquad (10)$$

where ν_0 is the transition frequency, $\Delta\nu$ the linewidth, T the cycle time, and N the number of atoms. As the electronic transitions of atoms or ions at visible or near infrared have approximately five orders of magnitude higher frequency compared to a ground state hyperfine structure transition, the fractional uncertainty and instability of an optical clock are potentially extremely small. The utilization of an optical frequency comb generator in reverse direction has enabled transferring the stability of optical frequency references to the microwave region and comparison of different optical clocks. The best optical clocks demonstrate fractional uncertainties less than 10^{-17} [9], which is more than an order of magnitude better than obtained with the best Cs-clocks.

3.2.1 Laser stabilization using gas-cell absorbers

Lasers frequency-stabilized on an atomic or a molecular transition using a gas-cell absorber are widely used, for example, in calibration of lasers used in interferometric length measurements [67,69,70] and in calibration of measurement instruments used in development and maintenance of optical telecommunication networks [Publication II, 71,72,73].

Although absolute optical frequency measurements using frequency combs are now used everyday in today's optical frequency metrology laboratories and ultra precise optical clocks are emerging, the set-ups are still far from simple and are not practical enough to be used as routine working standard calibrations. Thus, development of compact and practical frequency-stabilized lasers is still useful.

As shown by equation (10) the obtainable stability of a stabilized-laser depends inherently on the frequency resolution of such a system, i.e., on the relation of the observed linewidth to the center frequency of the line. A direct measurement of the width of a molecular line in gaseous phase is limited by Doppler-broadening [3]. This inhomogeneous broadening arises from the Doppler-effect and thermal velocity distribution of the molecules leading to a linewidth in the gigahertz range, which is several orders of magnitude higher compared to the natural linewidth of the molecular lines.

A common method to observe Doppler-free spectra is to use saturation spectroscopy, in which counter-propagating pump and probe beam are used for velocity group selection. Pump beam saturates the molecules while the probe beam is used to measure the absorption. When the laser frequency is swept over a molecular line, the spectrally narrow pump and probe beams generally interact with molecules belonging to different velocity groups. However, when the frequency is tuned close to the centre of the line both beams interact with molecules whose velocity components are essentially zero in the direction of the beams. In such conditions the absorption measured by the probe is reduced due to the saturation of the molecules by the pump. This so called Lamb dip [74] ideally shows the natural Lorentzian line shape of the molecule. The excited-state lifetimes of ro-vibrational transitions in molecules can have long lifetimes leading to natural linewidths below the technical broadening mechanism of the spectroscopic system. In such a case, effects like laser linewidth, pressure broadening, or transit time broadening [3] determine the observable linewidth. Nevertheless, it is usually possible to achieve linewidth in the order of one megahertz or below.

A powerful and well known method for stabilizing a laser to an atomic or a molecular line uses frequency modulated measurement and phase sensitive detection (PSD). When the third harmonic of the modulation frequency is detected, the Doppler broadened background is effectively cancelled and the laser can be locked to the steep zero crossing indicating the line center frequency. In addition, the modulation transfers the measurement away from DC-region where 1/*f*-noise dominates and the noise bandwidth can be optimized at detection. This is useful as the detected signals can be small and almost covered by noise. Figure 7 shows typical third-harmonic signal when a modulated laser frequency is tuned over a Doppler-free molecular line.

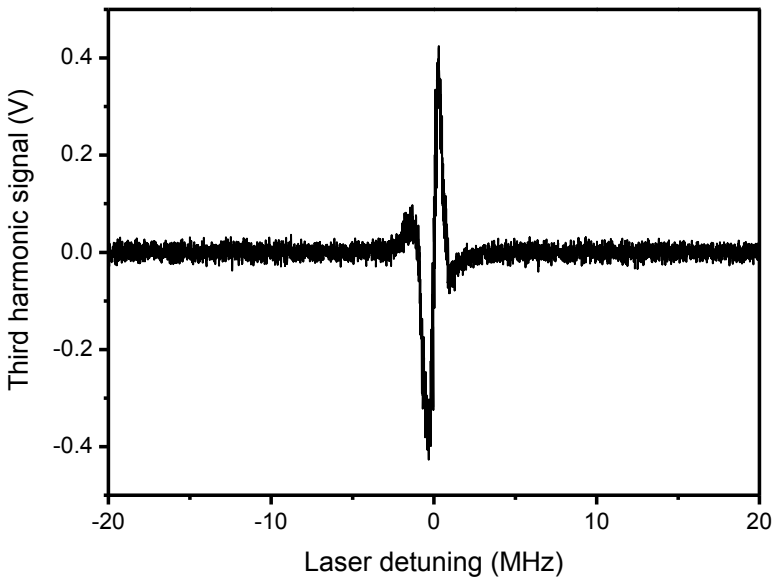

Figure 7. Third-harmonic signal recorded in a measurement where the laser frequency was tuned over a Doppler-free acetylene line. The laser was modulated at 2.94 kHz with a modulation amplitude of (1.0 ± 0.2) MHz peak-to-peak. Sample time was 3 ms [Publication II].

3.2.2 Optical single-frequency synthesizers

An absolute optical frequency reference with a user-specified frequency can be realized with an optical single-frequency synthesizer. In such a device, a single optical frequency is generated with a cw laser, whose frequency is phase-locked to an optical frequency comb referenced to an atomic time base. By proper design of the servo loops, the frequency stability of the synthesizer follows that of the microwave frequency reference.

In addition to frequency metrology, applications in spectroscopy benefit from an absolutely known monochromatic light source. While frequency combs can be used directly for spectroscopy [75,76], the low optical power in each comb component limits the signal-to-noise ratio of the measurements and the techniques needed to extract individual frequency components from the dense comb structure complicate the measurement set-ups. Recently, the development of optical single-frequency

synthesizers have gained much interest in metrology institutes [Publication III,77,78,79,80].

Generally, the structure of an optical single-frequency synthesizer resembles that of some microwave synthesizers. The frequency of a reference oscillator is transferred to a higher frequency using a frequency comb generator and a voltage controlled oscillator is phase-locked to a predetermined comb component. In an optical single-frequency synthesizer, a self-referenced optical frequency comb generator is used and the voltage controlled oscillator is replaced by a tunable cw laser. The phase lock between the cw laser and the optical frequency comb can be established either by optical injection [79,81] or by using an electronic phase-locked loop [Publication III,77,80]. Frequency tuning of the synthesized frequency has been demonstrated by several different methods. One method is to use a fixed frequency comb and by external locking circuits control the beat note between the cw laser and the frequency comb [77] or the output of the cw laser can be shifted by an electro-optical modulator (EOM) [82]. Another approach for sweeping the synthesized frequency is to adjust the frequency comb. This can be accomplished by tuning the repetition rate of the frequency comb [Publication III,80,83]. If the repetition rate is tuned by df then the n^{th} comb tooth and the frequency of the cw laser locked to this component is tuned by $n \cdot df$.

The optical single-frequency synthesizer offers an interesting tool to explore the line shapes of atomic and molecular transitions at high precision. The main advantage of a single-frequency synthesizer is the accuracy and the repeatability of the synthesized frequency. The synthesized frequency is produced at the fractional uncertainty of the microwave reference, which enables long measurement times and averaging over large number of similar measurements. Thus, it is possible to measure a line shape profile with superior signal-to-noise ratio. When a theoretical line profile is fitted to the results, the absolute line center frequency can be determined with low uncertainty. Such measurements are useful in investigations of frequency shifts in lasers stabilized on atomic or molecular transitions. In particular, one of the major sources of uncertainty in frequency stabilized lasers utilizing the third-harmonic technique is the frequency shift

due to modulation, which arises from asymmetry of the observed line. Using a single-frequency synthesizer, insight to the origin of the asymmetry can be obtained.

3.3 Experimental set-ups

In this thesis, two experimental set-ups for precision optical frequency measurements at near infrared telecommunication wavelengths are described. The goal of the work was to construct and characterize a tunable optical single-frequency synthesizer suitable for precision characterization of optical components used in telecommunication networks. To study the feasibility of a fiber-based approach to be utilized on the construction of the single-frequency synthesizer, we first constructed and characterized a fiber-based acetylene-stabilized laser [Publication II]. The absolute frequency of the acetylene-stabilized laser was measured using an optical frequency comb generator. Next, exploiting the results obtained with the acetylene-stabilized laser we re-configured the set-up and constructed the optical single-frequency synthesizer [Publication III]. The optical part of the set-up was essentially the same between the two set-ups. However, instead of locking the frequency of the laser to acetylene lines, we utilized a phase-locked loop to synchronize the laser to an atomic time base via the optical frequency comb generator. We measured spectral lineshapes of acetylene transitions with the synthesizer using unmodulated optical frequency [Publication IV]. In the next chapter the experimental work is described.

3.3.1 Acetylene-stabilized laser

The realization of the acetylene-stabilized laser is based on a commercial fiber coupled external cavity diode laser (ECDL, Photonetics Tunics-PRI) and standard fiber optic components commonly available for the telecommunication wavelengths. In the set-up, the light is coupled to free space only to pass through a 50 cm long acetylene cell at 2.8 Pa pressure. Spectroscopy is performed utilizing saturated absorption in a counter-propagating pump-probe beam configuration. To cancel frequency shifts related to

interference arising from reflections at fiber ends, the length of the optical path in the spectroscopy arrangement was dithered using a piezoelectric transducer (PZT) attached to the end mirror behind the gas cell. This technique has previously been demonstrated in spectroscopy with multi-pass absorption cells [84]. Here the technique was utilized with frequency-stabilized lasers for the first time. To effectively average the interference signal the dithering frequency (125.1 Hz) and amplitude of the mirror (3.1 μm), the modulation frequency of the laser (2.94 KHz), and the time constant of the lock-in amplifier (3 ms) were selected in such a way that the signal arising from dithered interference was sufficiently averaged, while the time constant was still short enough for frequency stabilization. The dithering frequency was synchronized to the modulation frequency and their ratio was chosen to be exactly a half-integer to avoid shifting the harmonics of the dither-frequency to the detection band of the lock-in amplifier. The amplitude of the mirror dither was chosen to be an integer number of half wavelengths of the laser radiation, thus diminishing the residual interference, which scales as inverse to the number of interference cycles averaged. Figure 8 demonstrates the effect of the mirror-dither technique on a laser frequency sweep over P(16) line of $(\nu_1 + \nu_3)$ band of $^{13}C_2H_2$ recorded from the low-pass filtered output of the photodiode amplifier used for detection. The optical power used in the experiment was 100 mW.

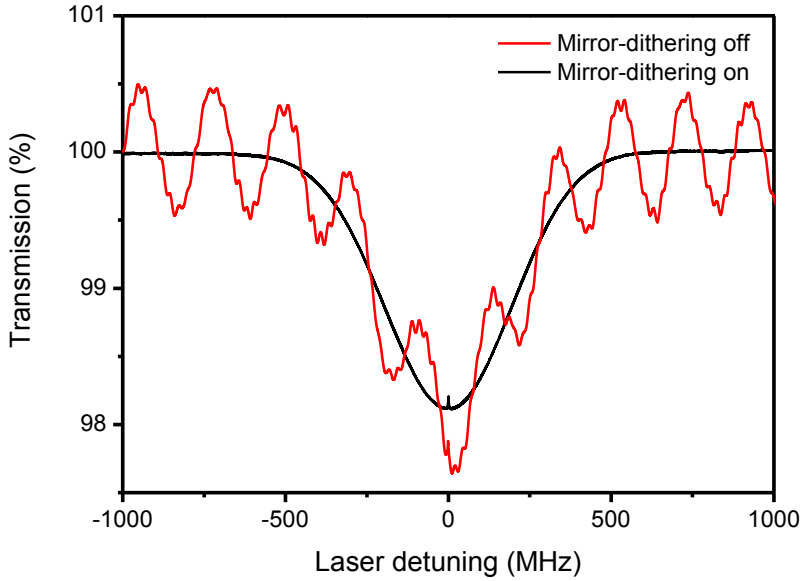

Figure 8. Unmodulated laser swept over a Doppler-broadened P(16) transition of $^{13}C_2H_2$ in a 2.8 Pa gas cell without and with the mirror dithering applied [Publication II].

Another factor strongly affecting the frequency of the laser's lock-point is the geometric arrangement of the pump and probe beams inside the gas-cell absorber. An angular mismatch between the wave fronts traveling to opposite directions inside the gas cell causes a frequency shift to the saturated absorption signal as the wave fronts interact with molecules belonging to a group that has a non-zero velocity component in the direction of the beams [Publication IV,85]. Unlike in our set-up, in the arrangements where resonators are employed to enhance the signal from the gas-cell absorber, the resonator fields inherently overlap. In our set-up, the collimation of the beams was ensured by carefully adjusting the position of the beam waist to the end mirror right behind the acetylene cell by maximizing the amount of light coupled back to the fiber. An aspheric lens with a relatively long focal length was employed to maximize the Rayleigh-range (,i.e., the distance from the waist of a Gaussian beam to the point where the beam cross-section area is doubled), and thus to minimize the wavefront curvature along the free-space beam traveling inside the acetylene cell.

Related to our fiber-based scheme an interesting approach to acetylene spectroscopy presented by Henningsen et al. in [86] is worth mentioning here. They have measured

saturated absorption of C_2H_2 molecules confined in the hollow core of a photonic bandgap fiber. However, SNR of the measurement needs to be improved to fully exploit this technique in realization of accurate wavelength standards.

Absolute frequency measurement results

It is possible to lock the acetylene-stabilized laser to over 25 lines in the ($\nu_1+\nu_3$) overtone band of $^{13}C_2H_2$ on covering a frequency band of wider than 2 THz. We measured the absolute frequency of the stabilized-laser locked to five different transitions of acetylene with a Ti:Sapphire optical frequency comb generator. For the measurements, the output of the acetylene-stabilized laser at 1.5 μm was frequency doubled using a periodically poled lithium niobate (PPLN) waveguide device to reach the wavelength range of the comb. The periodicity of the structure in the custom made PPLN waveguide device was chirped along the length of the crystal to enable frequency conversion over extended frequency band. The device provides about 1 mW of power at second harmonic when 250 mW of power within the wavelength range of 1530–1570 nm is taken to its input. Table II shows the results of the absolute frequency measurements compared to the values recommended by CIPM [6]. The values were consistent with CIPM values within the uncertainties of 3.6 kHz ($k = 2$).

Table II. Measured frequencies of the laser locked to five transitions of $^{13}C_2H_2$.

$^{13}C_2H_2$ transition	Frequency (kHz)	u_c (kHz)	Difference to the CIPM [6] value (kHz)
P(16)	194369569384.3	1.8	0.3
P(15)	194446632391.8	1.8	0.8
P(14)	194523020608.7	1.8	-1.3
P(11)	194748141655.4	1.8	-0.6
P(10)	194821826415.7	1.8	-0.3

The main uncertainty components arise from the repeatability of the measurements, the uncertainty of the modulation amplitude, and the uncertainty of the cell pressure. The

frequency shifts due possible changes in alignment have also been taken into account in the uncertainty estimate. The relative long-term stability (t = 1000 s) of the acetylene-stabilized laser is better than 10^{-12} and limited by white frequency noise. The measured Allan standard deviation [87] of the laser frequency is shown in Figure 9.

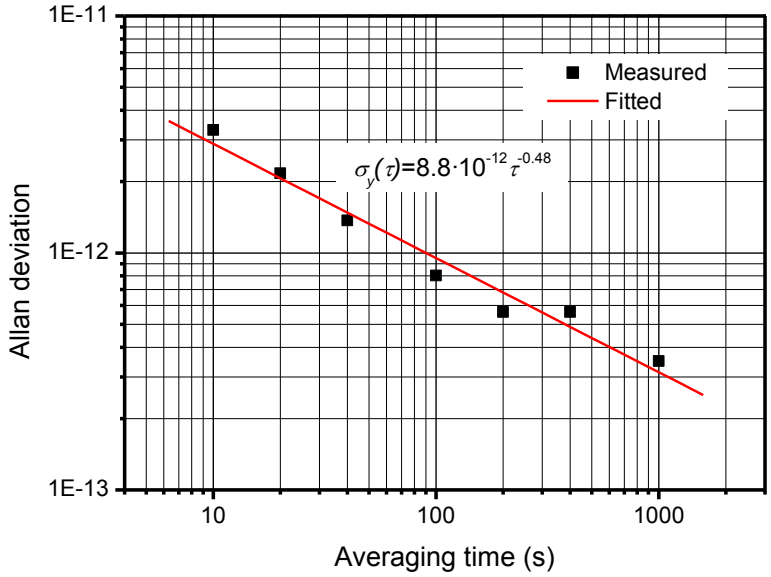

Figure 9. Typical Allan standard deviation of an acetylene P(16) line frequency measurement. [Publication II].

3.3.2 Optical single-frequency synthesizer

The single frequency synthesizer constructed in this work was designed for generating a single user-specified frequency from an atomic time base within the 192–196 THz gain bandwidth of an erbium-doped fiber amplifier (EDFA). The synthesizer is based on the ECDL, whose output is frequency doubled using a PPLN waveguide device and phase locked to a predetermined frequency component of a Ti:Sapphire optical frequency comb generator using an electrical PLL. By tuning the repetition rate of the Ti:Sapphire laser, the synthesized optical frequency can be swept with sub-kilohertz resolution. Frequency sweeps of several gigahertz are realized by automatically re-locking the ECDL to adjacent comb components during a frequency sweep. Figure 10 shows the principle of the frequency tuning. The re-locking method, demonstrated in this work,

allows sweeping the optical frequency, in principle, over the whole gain bandwidth of the EDFA.

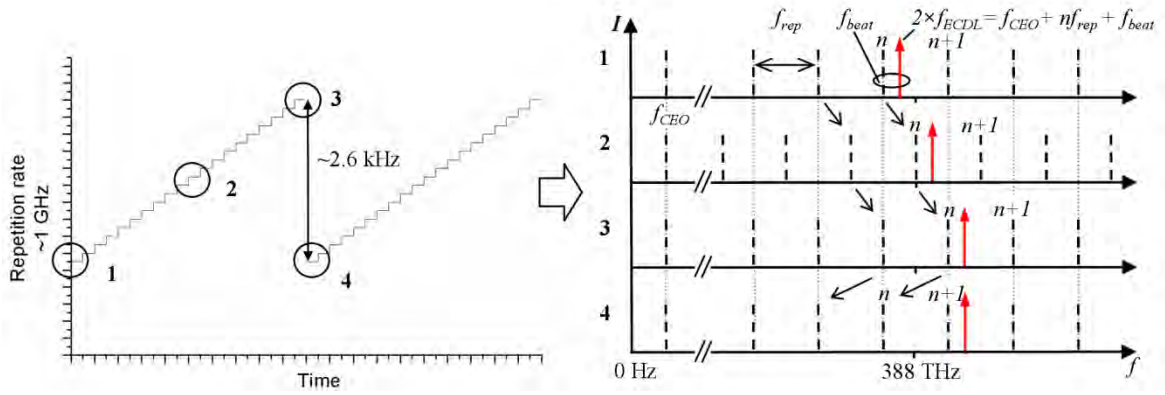

Figure 10. Tuning of the synthesized frequency. The left part of the figure illustrates the stepping of the repetition rate and the right part that of the optical frequencies. 1) The second harmonic of the synthesized frequency is locked to the n^{th} frequency component of the comb. 2-3) By stepping the repetition rate, the n^{th} component is shifted to the initial position of the $(n+1)^{th}$ component. 4) The repetition rate is set back to the start value and the synthesizer locks to the $(n+1)^{th}$ component [Publication III].

Line profile measurements of $^{13}C_2H_2$

We have utilized the synthesizer for direct Doppler-free spectroscopy on acetylene without modulation techniques [Publication III,IV]. High intensity stability of the synthesized signal and the capability of repeating the measurements on absolute frequency scale allowed performing line profile measurements at near infrared in unprecedented accuracy. The optical part of the set-up was essentially the same as that used in the acetylene-stabilized laser measurements. Indeed, we could alternate between these two configurations within minutes, just by rearranging electrical connections of the set-up. This offered an interesting possibility of investigating the effect of the different techniques of measurements of spectral lines.

Figure 11 shows a measurement over Doppler-broadened P(16) line on (ν_1+ ν_3) overtone band of acetylene. The measurement was done using 1-MHz step size. Due to frequency resolution the Lamb dip in the middle of the absorption curve is not shown properly. The inset in Figure 11 shows a measurement over the Lamb dip of the same transition in 79-kHz resolution. The intensity of the Lamb dip is less than 0.1 % of the

total detected power. The graph shown is an average of 31 similar measurements. The amplitude noise of the measurement is suppressed to practically negligible level by averaging.

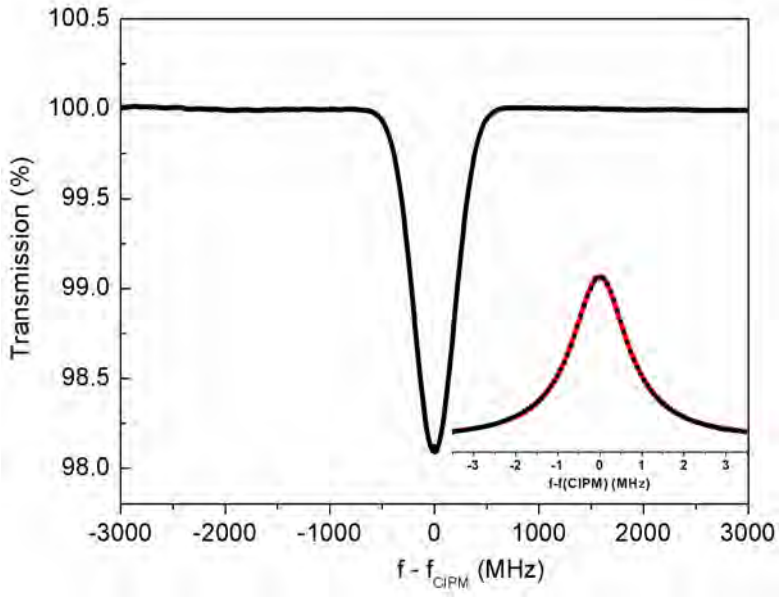

Figure 11. Doppler-broadened P(16) transition of acetylene at (v_1+v_3) overtone band recorded with the synthesizer. Inset: Doppler-free line shape of the same transition. The saturation dip spans a change of 0.08 % in transmission.

When the Gaussian profile of the Doppler-broadened line is subtracted, the true natural line shape of the transition can be investigated. By fitting a Lorentzian profile

$$I(f-f_0) = I_0 + \frac{2A}{\pi}\frac{w}{4(f-f_0)^2 + w^2} \qquad (11)$$

to the measurements, line shape asymmetry and the line center frequency could be determined. In equation (11) I_0 is the detected power offset, f_0 is the central frequency, w is full width at half-maximum, and A is the integrated area under Lorentzian profile. Figure 12 shows a Lorentzian and a Lorentzian with a dispersive term

$$I(f-f_0) = I_0 + [1 + B(f-f_0)]\frac{2A}{\pi}\frac{w}{4(f-f_0)^2 + w^2}, \qquad (12)$$

fitted to the measured line shape. In equation (12) B is a fit coefficient that sets the dispersive term strength. The residuals of the fits are shown in the lower part of Figure 12. The dispersive shape is addressed mainly due to a slight angular mismatch of the pump and probe beam, which might have remained despite of careful alignment.

Further, the residuals in Figure 12 indicate that in addition to dispersive shape, the signal is slightly too peaked. This might be a result of the increased relative contribution of slow molecules to the signal. When the linewidth is transit-time limited as in this measurement, the saturation becomes inhomogeneous for low pump laser powers and low gas pressures, and the line shape tends towards sharper peaking [88].

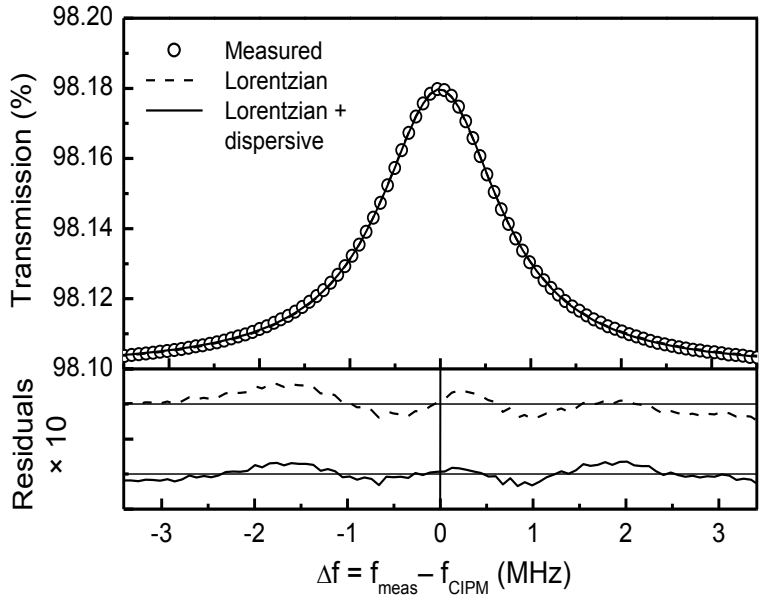

Figure 12. Measured P(16) line, a Lorentzian fit, Lorentzian + dispersive fit. Lower part shows residuals of the fits respectively [Publication IV].

We compared the line center values returned by the fits to the line center frequencies obtained using the acetylene-stabilized laser. To verify that the alignment had not changed between the two sets of measurement, we re-measured the absolute frequency of the P(16) line with the acetylene-stabilized laser right after the line shapes were measured with the synthesizer. The ability of rearranging the set-up between these two measurement modes enabled us to keep all the parameters related to optical set-up

constant. The re-measured absolute frequency of P(16) matched well with the value measured earlier with the stabilized-laser.

When the modulation shift in the acetylene-stabilized laser measurements is taken into account, the line center values obtained with the two methods agree within a few kilohertz, which is well within the combined uncertainty of 4.6 kHz (k = 2) of the measurements. The results gave also a very good match to the CIPM values. Table III sums the result. Regarding the acetylene-stabilized laser measurements the result of the P(16) line represents the re-measured value. The results shown for the lines P(10)–P(15) are taken from the earlier measurements with the stabilized-laser shown in Table II.

Table III. Measured frequencies of five $^{13}C_2H_2$ lines. Calculated modulation shifts are added to synthesizer frequencies.

line	synthesizer f_{synth} (kHz)	$^{13}C_2H_2$-stab.laser f_{stab} (kHz)	CIPM value (kHz)	$f_{synth} - f_{stab}$ (kHz)
P(10)	194821826415.9	194821826415.7	194821826416	0.2
P(11)	194748141655.5	194748141655.4	194748141656	0.1
P(14)	194523020606.4	194523020608.7	194523020610	–2.3
P(15)	194446632391.4	194446632391.8	194446632391	–0.4
P(16)	194369569382.1	194369569384.2	194369569384	–2.1

The effect of the modulation shift was studied also by numerical simulations using MATLAB/SimuLink software. We simulated the third-harmonic locking with lock-in amplifier servo loop and using the Lorentzian with a dispersive line shape component. The average modulation shift (-3.7±0.7) kHz/MHz returned by the simulations on four fitted P(16) line shapes was in good agreement with the experimentally measured modulation shift (-3.1±0.1) kHz/MHz of P(16) line [Publication II].

4 Indistinguishable single photons

A thorough understanding of the physical world requires that natural phenomena are examined not only on macroscopic level, where ensemble averages of particles and events are observed. When the examination is taken to individual particle level, the true quantum mechanical behavior of the events can be investigated.

Photons are often used in quantum mechanical experiments, as photon states are relatively easy to prepare and measure. One of the most fundamental group of experiments is the one where interference effects of single photons are investigated [89,90]. Interestingly, the results on a single-photon level differ drastically from that of the ensemble average. Although the motivation for the early experiments on the field was testing the theories of quantum mechanics [91,92], the recent progress has lead to potential applications in the field of optical quantum information processing. Such applications include optical quantum computing [93], communication, and cryptography [94]. Commercial applications in quantum cryptography already exist [95]. Communication with single photons by quantum teleportation has been demonstrated over long distances [96], and chip scale all-optical quantum computation has been demonstrated in laboratory conditions [97].

4.1 Single-photon sources

The key component for the applications mentioned above is a reliable single-photon source, which emits one and only one photon per defined time interval with high probability. The most straightforward solution would be to utilize a laser producing faint pulsed radiation. Laser output can be attenuated until the probability of finding more than one photon per pulse in a mode gets small. However, this method has a rather severe drawback. As the number of photons in coherent laser output is governed by Poisson statistics, most of the time the number of the photons in the mode would be zero. This limits the applicability of the laser source, as typically when a measurement should be made no photon would exist. Another approach using lasers utilizes a

spontaneous parametric down-conversion (SPDC) process, where correlated photon pairs are generated from higher frequency pump photons in a nonlinear crystal. Although the number of photons is statistically Poisson distributed also in this approach, the measurement of other photon (idler) can be used to inform that the other photon (signal) exists, thus reducing the number of measurements where no photons exist.

A two-level system can be operated as a natural single-photon source, as it inherently emits only one photon per one excitation-relaxation cycle. Single-photon action has been successfully demonstrated with molecules [98], atoms [99], ions [100], quantum dots [101], and diamond nitrogen-vacancy centers [102].

In recent years, active research has been undertaken to develop single-photon sources that are capable of emitting single-photons that are indistinguishable from each other. Motivation for this has been the requirement that quantum computation sets for a single-photon source: As quantum computation with linear optics relies on manipulation of entangled photon states [103], the emitted photons have to be indistinguishable. That is to say, they should be in the same optical mode, hence would share the same spectral and spatial features, and have the same optical polarization. Additionally, the emission process should be natural lifetime limited, i.e., no external influence on emission process should appear. Moreover, for practical applications, the sources should be scalable to multiple similar sources that exhibit mutual indistinguishability.

In the first experiments, trains of indistinguishable single photons were generated using single two-level emitters [104,105,106] as sources. Recently, indistinguishability of photons emitted from independent two-level emitters has been demonstrated in several experiments by quantum interference. This has been shown using independently trapped atomic emitters [107,108], quantum well nano-structures [109], and single molecules [23] as sources.

4.1.1 Characterization of single-photon sources

To validate the single-photon nature of a light source, one has to measure the second order intensity correlation [110]

$$g^{(2)}(\tau) = \frac{\langle I(t+\tau)I(t)\rangle}{\langle I(t)\rangle^2}, \tag{13}$$

where *I(t)* is the average intensity with fixed time delay of τ for the consequently emitted photons, using a Hanbury Brown and Twiss (HBT) type of a set-up [111] shown in Figure 13.

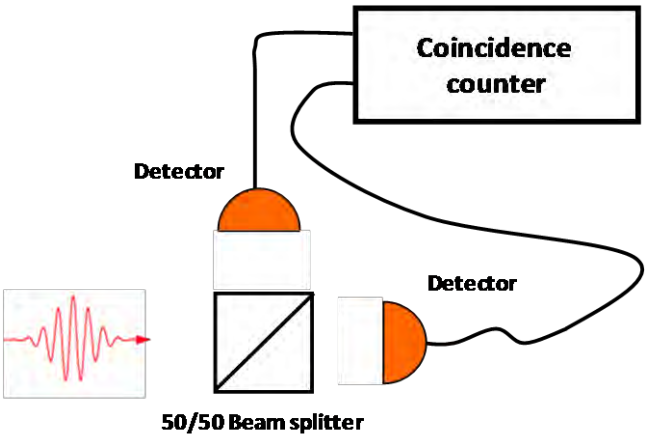

Figure 13. Hanbury Brown and Twiss type of photon correlation set-up.

The photons emitted by a source are sent to a 50/50 beam splitter. Single-photon detectors are placed at both outputs of the beam splitter. Time delays between clicks, i.e. photon arrivals, on the two detectors are recorded. Ideally, in the case of a true single-photon source, both detectors can not click simultaneously. Thus, the $g^{(2)}$-function is suppressed at $\tau = 0$. Figure 14 shows a result of such a measurement recorded from a single-molecule light source using avalanche photon detectors (APD). The fact that the function in Figure 14 does not reach zero at $\tau = 0$ implies that in addition to the signal from the single-molecule, some background signal is also present.

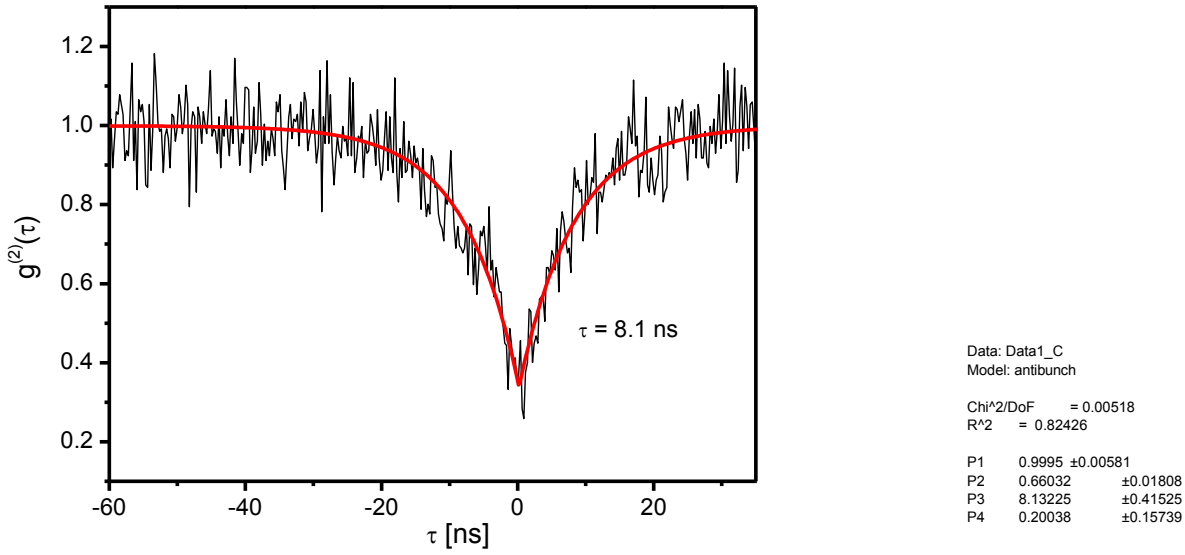

Figure 14. Second order photon correlation measurement of a single-photon source [Publication VI].

Photon indistinguishability is determined by a quantum interference measurement. Two photons are taken to a beam splitter from neighboring input ports. If the photons are in the same polarization state and their spectral and spatial modes perfectly overlap, the photons will coalesce and always leave the beam splitter together to the same direction (see Figure 15).

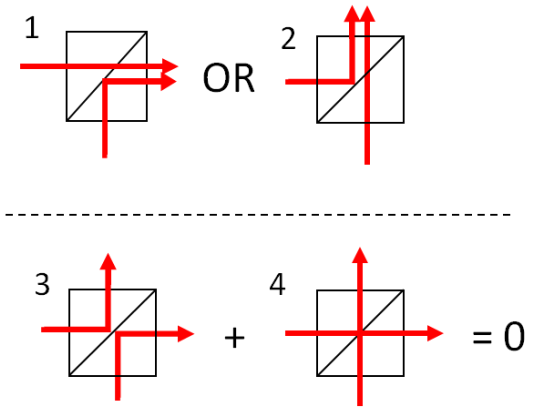

Figure 15. When identical single photons enter a 50/50 beam splitter from neighboring input ports they coalesce and leave the beam splitter always together (1 & 2). The probability amplitudes for the photon states where both photons are reflected or transmitted cancel each other (3 & 4) [92].

Essentially a similar HBT set-up, which was described above, can also be used for a quantum interference measurement. A correlation function is measured as a function of a delay between photon arrivals at a beam splitter. The experimental arrangement is illustrated in Figure 16. In case of an ideal spontaneous-emission single-photon source, a zero reaching dip in the function is observed when the delay between the two photons is tuned to zero as shown in Figure 17 by a theoretical correlation function [104]

$$g^{(2)}(\delta\tau) = 1 - \exp(-|\delta\tau| / \tau_s), \tag{14}$$

where $\delta\tau$ is the delay and τ_s corresponds to the spontaneous emission lifetime. The two-photon interference was experimentally first shown by Hong, Ou, and Mandel in 1987 [92] in an experiment where they used single photons from a SPDC source.

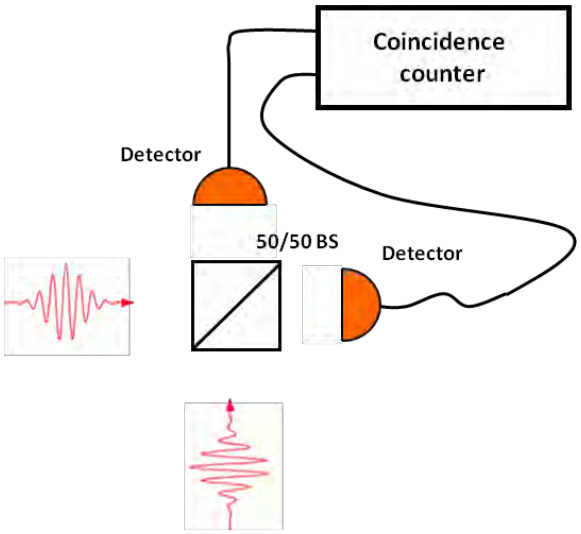

Figure 16. Hanbury Brown and Twiss type of set-up is used for measuring quantum interference between two indistinguishable photons.

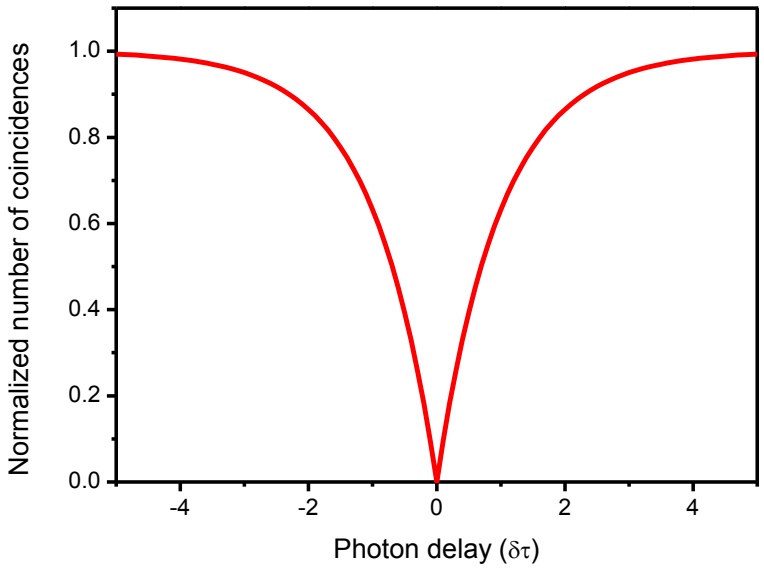

Figure 17. When the delay between indistinguishable single photons at a beam splitter is tuned to zero a deep dip in the measured correlation function occurs.

4.2 Low-temperature single molecules as single-photon sources

Single-molecule spectroscopy originates from 1989 when single molecules were detected for the first time by recording an absorption signal of an organic dye molecule embedded in a solid crystalline host at low temperature [112]. Soon after that, single-molecule detection based on fluorescence excitation spectroscopy was demonstrated [113]. Low temperature, single-molecule spectroscopy takes advantage on the effect of inhomogeneous broadening of molecular lines. A dilute solution of dye molecules in a crystalline host matrix is cooled to liquid helium temperatures ($T < 4$ K). At cryogenic temperatures the lines of the molecules get narrower as thermal effects are dramatically suppressed. Additionally, as the dye molecules are embedded in non-ideal crystalline host matrix, every molecule sees its environment a little differently, which leads to non-uniform shifting of the resonance frequencies of the molecules. Using a frequency tunable single-mode laser, one can individually select molecules by scanning the laser frequency over the inhomogeneously broadened absorption band of the molecules. In

detection, the excitation wavelength is filtered and fluorescence at longer wavelength is measured.

Organic molecules embedded in a crystalline host matrix offer an attractive system for studying quantum interference. At low temperatures, some electronic transitions become natural lifetime limited and offer quantum yield approaching unity. Further, the solid-state approach enables long observation times using the same emitters. In this work, the use of single molecules as sources of indistinguishable single photons was experimentally studied.

4.3 Experimental arrangement

The experimental work presented here has been carried out at the Laboratory of Physical Chemistry of Swiss Federal Institute of Technology Zurich (ETH). The objective of the research was to construct and characterize a set-up for demonstrating quantum interference using independent single molecules as single-photon sources. In Publication V we reported, for the first time, generation of indistinguishable single photons using two distinct single molecules. Organic fluorescent dibenzanthanthrene (DBATT) molecules in n-tetradecane were used as emitters and investigated by means of high resolution laser spectroscopy. DBATT molecules were chosen as candidate as previous studies have shown that DBATT embedded in crystalline host matrix at low temperatures has many properties that are desirable for a indistinguishable single-photon source, including near lifetime-limited linewidth, very weak triplet yield [114], and well defined orientation of the dipole moment [115].

High spatial resolution was obtained by preparing a molecule sample on a solid-immersion lens (SIL) through which the excitation laser radiation was focused using an aspheric lens. Photon correlation measurements on individual molecules under cw laser excitation proved the isolation of single quantum systems. Local electric fields were applied to match the emission wavelengths of the two molecules via DC-Stark effect.

In later state of the project, reported in Publication VI, a pulsed laser was included in the set-up and triggered generation of indistinguishable single photons was demonstrated.

To our knowledge, this was the first demonstration of single-molecule spectroscopy using pulsed excitation combined with high spectral and spatial resolution.

After the work described in this thesis, the set-up has been further developed and at the time of writing a quantum interference experiment using the set-up was reported [23]. The next sections sum up the experimental aspects essential for this work.

4.3.1 Excitation schemes

A dye molecule embedded in solid host matrix can be approximated as a two-level emitter. The energy levels of a dye molecule can be modeled with a simplified level scheme (Jablonsky diagram [116]) shown in Figure 18.

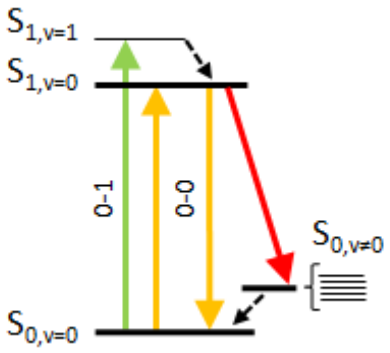

Figure 18. A simplified level scheme of a single dye molecule embedded in solid host matrix [Publication VI].

The relevant energy levels consist of the ground level and the first excited electronic level, denoted by $S_{0,v}$ and $S_{1,v}$ respectively. Both levels further contain a number of vibrational energy levels ($v \neq 0$). In this simplified level scheme, the probability for the molecule to enter to a metastable triplet state is considered negligible and has been ignored. It is possible that the molecule is excited also to a higher electronic state by multiple photon excitation. However, the lifetime of these states is very short (ps) and they decay non-radiatively to the first electronic level thus eliminating a possibility for two or more photon emission. In temperatures below 2 K, the purely electronic zero-phonon-line (ZPL) transition, i.e., the transition between the lowest levels of the ground

($S_{0,v=0}$) and the first excited electronic state ($S_{1,v=0}$) (denoted here as 0-0 ZPL), becomes natural lifetime limited. A DBATT molecule has a natural linewidth of about 17 MHz (FWHM) for a transition at a wavelength of λ = 590 nm.

There are two principal ways to excite the narrow linewidth molecules at cryogenic temperatures. The first method excites the molecule from the ground state $S_{0,v=0}$ into the $S_{1,v=0}$ state. From there the molecule decays back into the ground state and into a manifold of states with $v \neq 0$. The red shifted photons are detected, but the photons from the narrow 0-0 ZPL cannot be separated from the excitation laser light. This technique of photoluminescence excitation spectroscopy can directly measure the linewidth of the 0-0 ZPL by scanning a narrow band laser across the resonance.

In a second method, one excites the molecule into a higher vibrational level of the electronically excited state $S_{1,v=1}$. This state decays non-radiatively within a few ps into the state $S_{1,v=0}$, from which the molecule decays, giving access to photons emitted by the natural lifetime limited 0-0 ZPL. Transition from the ground state to $S_{1,v=1}$ is relatively broadband (about 30 GHz) due to short lifetime of $S_{1,v=1}$.

To identify lifetime limited single photons we spectrally scanned across the sample with a wavelength tunable cw dye laser and measured the 0-0 ZPL linewidths of potential molecules. After finding an isolated single molecule with a narrow 0-0 ZPL a second laser source was switched for pulsed 0-1 excitation. Thus, triggered 0-0 ZPL emission could be collected.

4.3.2 Spatial resolution

In addition to spectral resolution, high spatial resolution is needed. Spatial resolution is needed first of all to be able to locate an individual molecule and to reduce the background signal caused by weak excitation of nearby molecules. Thus, the spatial resolution should be sufficiently high so that no more than one molecule is resonant with the excitation laser in the focal volume at a time. High spatial resolution is especially important when higher vibrational states are excited with a pulsed laser. This

is due to the broad linewidth of the vibronically excited states. This together with the broad linewidth of the laser severely limits the possibility to spectrally select the molecules and hence puts greater emphasis on spatial resolution.

The spatial resolution is fundamentally limited by diffraction. The minimum obtainable FWHM spot size for a plane wave focused with a lens can be approximated as [117]

$$FWHM = \frac{\lambda}{2NA}, \tag{15}$$

where λ is the wavelength of the incident radiation and NA is the numerical aperture of the lens defined as

$$NA = n \cdot \sin(\theta_{½}), \tag{16}$$

where n is the refractive index of the medium where the lens operates and $\theta_{½}$ is the half angle subtended by the lens. We achieved a tight focus by employing an aspheric lens with a NA of 0.55 (in air) together with a solid immersion lens (SIL) made from cubic zirconia (ZrO_2), whose refractive index is 2.2. The sample is prepared in between the flat side of the SIL and a glass substrate. The incident light is focused into the sample through the SIL. Because the light is focused to the center of the hemispherical lens no refraction at the outer edge of the lens occurs. Hence SIL gives direct improvement of the focused spot size by factor of n. It should be noted that in a case where the laser beam is focused through the lens the dimension limiting the spot size is usually the beam diameter. However, equation (15) gives the theoretical upper limit for the resolution of the lens system.

The emitted photons are collected using the same lens system. The high refractive index of the SIL also improves the light collection efficiency, which is crucial in the single-photon applications. Figure 19 shows a schematic view of the arrangement.

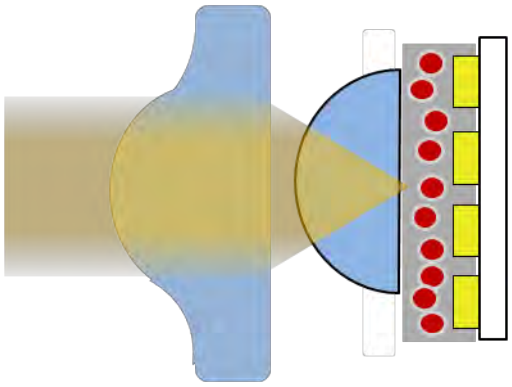

Figure 19. Laser light is focused into the molecule sample using aspheric and solid immersion lenses. The sample has been prepared on gold electrodes to enable Stark shifting the lines.

4.3.3 Stark shifting the lines of the molecules

We exploited the DC-Stark effect to shift the transition frequencies of two molecules in distinct samples to match each other. This was done by applying a static electric field over the molecules on one of the samples. The electric field was applied using gold electrodes under the samples (see Figure 19). The narrow spacing of interdigitated electrodes, 18 μm, makes it possible to reach high electric fields on the order of 10^6 V/m with voltages below 100V. With this configuration we typically found shifts in the zero-phonon-lines of the molecules in the order of ~100 Hz/(V/m). Figure 20 shows an example where nearly natural lifetime limited zero-phonon-lines of two independent DBATT molecules in distinct samples are detected simultaneously. The molecule whose line is initially at higher frequency is frequency shifted across the line of the other molecule, thus making the 0-0 zero-phonon-lines of the molecules spectrally indistinguishable at the point where the lines cross.

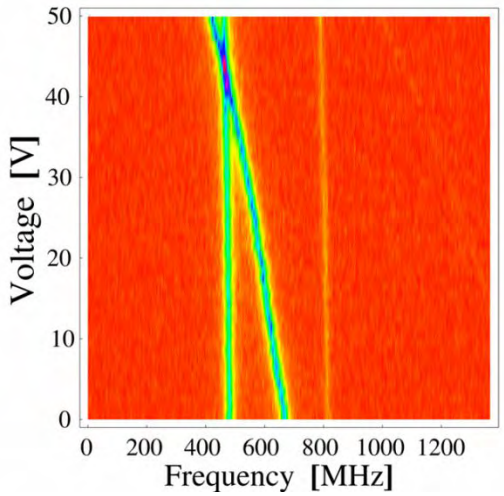

Figure 20. Fluorescence excitation spectra of two molecules in distinct samples. The vertical axis shows the voltage applied on electrodes and horizontal axis the frequency sweep of the laser. An electric field applied to one of the molecules shifts its line to lower frequencies with increasing voltage. [Publication VI].

4.3.4 Continuation of the project

Experimental aspects presented above demonstrated the capability of using independent single molecules to generate indistinguishable single photons. As explained before, true quantum indistinguishability requires identical photons with respect to wavelength, polarization state, and spatial mode. DBATT molecules embedded in a crystalline host matrix have well-oriented transition dipole moments whose emission can be linearly polarized. Thus, the polarization of the emitted photons can readily be matched. Furthermore, the emission from single molecules can be coupled into to a single-mode fiber with an efficiency of 30 % or more, which conveniently ensure spatial mode matching. Indeed, after the work done for this thesis, two-photon interference was demonstrated using the set-up [23]. Single-photon beams from two molecules were coupled into the two arms of a single-mode polarization maintaining fiber beam splitter. Half-wave plates were used to align the input polarizations. A photon correlation measurement at the output arms of the fiber-optic beam splitter showed a clear sign of quantum interference.

The high photostability and the compact solid-state arrangement of the sources allow nearly indefinite measurement times on the same emitter and a straightforward up-

scaling to a larger number of identical single-photon sources. These results are promising for miniaturization and integration of several single-photon sources to ever smaller volumes, even on a single chip.

5 Conclusions

In this work, advanced applications based on the utilization of wavelength tunable lasers in optical radiometry, optical frequency metrology, and quantum optics were studied and developed.

In the field of optical radiometry, a study of different techniques for measuring absolute spectral irradiance responsivity was carried out. A comparative study of spectral irradiance responsivity measurement techniques was performed between measurement systems used for detector calibrations at TKK and NIST. Two laser-based and a monochromator based measurement systems were compared by measuring the absolute spectral irradiance responsivity of a near infrared filter radiometer with each system. The work provided the first reported results of a detailed comparison of different calibration techniques for spectral irradiance responsivity at near infrared wavelength region. The study showed excellent agreement between the three calibration systems and gave validation for the low uncertainty, below the level of 0.1 %, stated for both laser-based calibration systems. The results have significant implications for radiation thermometry and a number of other radiometric applications where high accuracy spectral radiance and irradiance measurements are crucial.

In a work done at MIKES, an acetylene-stabilized laser and an optical single-frequency synthesizer were constructed and characterized. The acetylene-stabilized laser was realized, for the first time, by taking a fiber-based approach. By dithering the length of the optical path in the spectroscopy arrangement, interference inherently present in a fiber-based scheme was effectively suppressed by averaging. Conceivably, the mirror dithering technique could be generally applied to frequency-stabilized lasers based on external gas cells to improve long term stability through the reduction of slowly varying frequency-dependent intensity changes caused by interference. Absolute frequency measurements of the laser stabilized to five different lines of acetylene were in good agreement with the values recommended by CIPM with a standard uncertainty of 1.8 kHz. The relatively straightforward construction of the acetylene-stabilized laser

provides a potential for developing compact and portable wavelength standards in telecommunication wavelengths.

The optical single-frequency synthesizer was designed for generating a user-specified frequency from an atomic time base within the 192–196 THz gain bandwidth of an EDFA. A phase-coherent link between microwave and optical frequencies was established using an optical frequency comb generator. Scanning the optical frequency was realized by stepping the repetition rate of the optical frequency comb generator. Combined with a comb component handover process, this method allows, in principle, scanning the optical frequency over the entire gain bandwidth of the EDFA with sub-kilohertz resolution. The capability of repeating the measurements on absolute frequency scale and the high intensity stability of the synthesizer enabled performing spectroscopy without modulation techniques in unprecedented accuracy at telecommunication wavelengths. In addition to spectroscopy, the developed synthesizer is directly suitable for characterization of optical components used in telecommunication networks.

The synthesizer was utilized for recording the shapes of acetylene transitions and studying their lineshape asymmetries by theoretical fits. The high signal-to-noise ratio of the measurement enabled determination of absolute line-center frequencies with 1.4 kHz uncertainty. The line-center frequencies were in excellent agreement with the frequencies obtained with the acetylene-stabilized laser and with the CIPM values. The calculated modulation shift based on the fitted asymmetrical line shape agreed with the shift determined from acetylene-stabilized laser measurements. Thus, origin of the modulation shift in the third-harmonic measurement could be determined.

The final part of the work presented in this thesis was carried out at ETH in Zurich. A light source emitting indistinguishable single photons from independent single molecules was developed. For the first time, a solid-state source consisting of multiple independent emitters was used to emit indistinguishable single photons.

By means of high resolution laser spectroscopy and optical microscopy in cryogenic conditions, two fluorescent molecules under distinct microscopes were detected. Fluorescence excitation spectroscopy with a wavelength tunable cw dye laser was

utilized to detect and measure natural lifetime limited zero-phonon-lines of the molecules in two distinct samples. Vibronic excitation with a pulsed laser allowed collecting triggered zero-phonon-line emission. The utilization of solid immersion lenses together with aspheric lenses enabled high spatial resolution. By exploiting DC-Stark shifts, the resonances of the detected molecules were shifted to match each other. Later measurements verified the indistinguishability of the photons by quantum interference measurements. The work has implications on the development of various quantum information processing schemes.

The techniques explored in the thesis show the extraordinary power and application that wavelength tunable lasers can provide in exploring limits of measurement science and fundamental studies in physics.

References

[1] A. L. Schawlow and C. H. Townes, "Infrared and optical masers," Phys. Rev. **112**, 1940–1949 (1958).

[2] T. H. Maiman, "Stimulated optical radiation in ruby," Nature **187**, 493–494 (1960).

[3] W. Demtröder, "Laser Spectroscopy," Vol. 1, 4th ed., Springer 2008, 457 p., ISBN 978-3-540-73415-4.

[4] A. Zeilinger, G. Weihs, T. Jennewein, and M. Aspelmeyer, "Happy centenary, photon," Nature **433**, 230–238 (2005).

[5] The International System of Units (SI), 8th Edition Bureau International des Poids et Mesures, Sèvres, France, 88 p. (2006).

[6] R. Felder, "Practical realization of the definition of the metre, including recommended radiations of other optical frequency standards," Metrologia **42**, 323–325 (2005).

[7] H. S. Margolis, G. P. Barwood, G. Huang, H. A. Klein, S. N. Lea, K. Szymaniec, and P. Gill, "Hertz-Level Measurement of the Optical Clock Frequency in a Single $^{88}Sr^{+}$ Ion," Science **306**, 1355–1358 (2004).

[8] P. Dubé, A. A. Madej, J. E. Bernard, and L. Marmet, "A narrow linewidth and frequency-stable probe laser source for the $^{88}Sr^{+}$ single ion optical frequency standard," Appl. Phys. B **95**, 43–54 (2009).

[9] C. W. Chou, D. B. Hume, J. C. J. Koelemeij, D. J. Wineland, and T. Rosenband, "Frequency Comparison of Two High-Accuracy Al^{+} Optical Clocks," Phys. Rev. Lett. **104**, 070802 (2010).

[10] A. D. Ludlow, T. Zelevinsky, G. K. Campbell, S. Blatt, M. M. Boyd, M. H. G. de Miranda, M. J. Martin, J. W. Thomsen, S. M. Foreman, Jun Ye, T. M. Fortier, J. E. Stalnaker, S. A. Diddams, Y. Le Coq, Z. W. Barber, N. Poli, N. D. Lemke, K. M. Beck, and C. W. Oates, "Sr lattice clock at 1×10^{-16} fractional uncertainty by remote optical evaluation with a Ca clock," Science **319**, 1805–1808 (2008).

[11] "Principles governing photometry," Metrologia **19**, 97–101 (1983).

[12] ITU-T standard G.671, Transmission characteristics of optical components and subsystems.

[13] "Laser Marketplace 2009," Laser Focus World, January 2009.

[14] A. Javan, W. R. Bennet Jr., and D. R. Herriot, "Population inversion and continuous optical maser oscillation in a gas discharge containing a He-Ne mixture," Phys. Rev. Lett. **3**, 106–110 (1961).

[15] R. N. Hall, G. E. Fenner, J. D. Kingsley, T. J. Soltys, and R. O. Carlson, "Coherent light emission from GaAs junctions," Phys. Rev. Lett. **9**, 366–368 (1962).

[16] O. G. Peterson, S. A. Tuccio, and B. B. Snavely, "cw operation of an organic dye solution laser," Appl. Phys. Lett. **6**, 245–247 (1970).

[17] M. J. Weber, "Handbook of laser wavelengths," CRC Press LLC 1999, 767 p., ISBN 0-8493-3508-6.

[18] J. M. Yarborough, "cw dye laser emission spanning the visible spectrum," Appl. Phys. Lett. **24**, 629–630 (1974).

[19] P. F. Moulton, "Spectroscopic and laser characterization of Ti:Al_2O_3," J. Opt. Soc. Am. B **3**, 125–132 (1986).

[20] M. Fleming and A. Mooradian, "Spectral characteristics of external-cavity controlled semiconductor lasers", IEEE J. Quantum Electron **17**, 44–59 (1981).

[21] M. Noorma, P. Toivanen, F. Manoocheri, and E. Ikonen, "Characterization of filter radiometers with a wavelength-tunable laser source," Metrologia **40,** S220–S223 (2003).

[22] S. W. Brown, G. P. Eppeldauer, and K. R. Lykke, "Facility for spectral irradiance and radiance responsivity calibrations using uniform sources," Appl. Opt. **45,** 8218–8237 (2006).

[23] R. Lettow, Y. L. A. Rezus, A. Renn, G. Zumhofen, E. Ikonen, S. Götzinger, V. Sandoghdar, "Quantum interference of tunably indistinguishable photons from remote organic molecules," Phys. Rev. Lett. **104**, 123605 (2010).

[24] A. C. Parr, R. U. Datla, and J. L. Gardner, "Optical radiometry," Elsevier Inc. 2005, ISBN 0-12-475988-2.

[25] N. P. Fox, J. E. Martin, and D. H. Nettleton, "Absolute spectral radiometric determination of the thermodynamic temperatures of the melting/freezing points of Gold, Silver and Aluminium," Metrologia **28**, 357–374 (1991).

[26] P. Sperfeld, K.-H. Raatz, B. Nawo, W. Möller, and J. Metzdorf, "Spectral-irradiance scale based on radiometric black-body temperature measurements," Metrologia **32**, 43–439 (1996).

[27] H. W. Yoon, P. Sperfeld, S. Galal Yousef, and J. Metzdorf, " NIST-PTB measurements of the radiometric temperatures of a high-temperature black body using filter radiometers," Metrologia **37**, 377–380 (2000).

[28] M. Ojanen, V. Ahtee, M. Noorma, T. Weckström, P. Kärhä, and E. Ikonen, "Filter radiometers as a tool for quality assurance of temperature measurements with linear pyrometers," Int. J. Thermophysics **29**, 1084–1093 (2008).

[29] H. W. Yoon, C. E. Gibson, and P. Y. Barnes, "Realization of National Institute of Standards and Technology detector-based spectral irradiance scale," Appl. Opt. **41**, 5879–5890 (2002).

[30] H. Preston-Thomas, "The International Temperature Scale of 1990 (ITS-90)," Metrologia **27**, 3–10 (1990).

[31] R. E. Edsinger and J. F. Schooley, "Differences between Thermodynamic Temperature in the Range 230°C to 660°C and t (IPTS-68)," Metrologia **26**, 95–106 (1989).

[32] H. W. Yoon, D. W. Allen, C. E. Gibson, M. Litorja, R. D. Saunders, S. W. Brown, G. P. Eppeldauer, and K. R. Lykke, "Thermodynamic-temperature determinations of the Ag and Au freezing temperatures using a detector-based radiation thermometer," Appl. Opt. **46**, 2870–2880 (2007).

[33] J. E. Martin, N. P. Fox, and P. J. Key, "A Cryogenic Radiometer for Absolute Radiometric Measurements," Metrologia **21**, 147–155 (1985).

[34] J. M. Houston, and J. P. Rice, "NIST reference cryogenic radiometer designed for versatile performance," Metrologia **43**, S31–S35 (2006).

[35] T. C. Larason, S. S. Bruce, and A. C. Parr, "Spectroradiometric Detector Measurements: Part I–Ultraviolet Detectors and Part II–Visible to Near-Infrared Detectors, Natl. Inst. Stand. Technol. Spec. Publ. 250–41, U.S. Govt. Printing Office (1998).

[36] P. Kärhä, A. Haapalinna, P. Toivanen, F. Manoocheri, and E. Ikonen, "Filter radiometry based on direct utilization of trap detectors," Metrologia **35**, 255–259 (1998).

[37] V. E. Anderson, N. P. Fox, and D. H. Nettleton, "Highly stable, monochromatic and tunable optical radiation source and its application to high accuracy spectrophotometry," Appl. Opt. **31,** 536–545 (1992).

[38] S. W. Brown and K. R. Lykke, NIST, Gaithersburg, Md., personal communication, 2007.

[39] J. T. Woodwar, A. W. Smith, C. A. Jenkins, C. Lin, S. W. Browm, and K. R. Lykke, "Supercontinuum sources for metrology," Metrologia **46**, S277–S282 (2009).

[40] H. W. Yoon, P. Sperfeld, S. Galal Yousef, and J. Metzdorf, "NIST-PTB measurements of the radiometric temperatures of a high-temperature black body using filter radiometers," Metrologia **37**, 377–380 (2000).

[41] P. Kärhä, N. J. Harrison, S. Nevas, W. S. Hartree, and I. Abu-Kassem, "Intercomparison of characterization techniques of filter radiometers in the ultraviolet region," Metrologia **40**, S50–S54 (2003).

[42] N. P. Fox, “Trap detectors and their properties,” Metrologia **28,** 197–202 (1991).

[43] P. Toivanen, F. Manoocheri, P. Kärhä, E. Ikonen, and A. Lassila, “Method for characterization of filter radiometers,” Appl. Opt. **38**, 1709–1713 (1999).

[44] Documents Concerning the New Definition of the Metre, Metrologia **19**, 163–177 (1984).

[45] K. M. Evenson, J. S. Wells, F. R. Petersen, B. L. Danielson, and G. W. Day, “Accurate frequencies of molecular transitions used in laser stabilization: the 3.39-μm transitions in CH_4 and 9.33- and 10.18-μm transitions in CO_2,” Appl. Phys. Lett. **22**, 192–195 (1973).

[46] D. A. Jennings, C. R. Pollock, F. R. Peterson, R. E. Drullinger, K. M. Evenson, J. S. Wells, J. L. Hall, and H. P. Layer, “Direct frequency measurement of the I_2-stabilized He-Ne 473-THz (633 nm) laser,” Opt. Lett. **8**, 136–138 (1983).

[47] O. Acef, J. J. Zondy, M. Abed, D. G. Rovera, A. H. Gérard, A. Clairon, Ph. Laurent, Y. Millerioux, and P. Juncar, “A CO_2 to visible optical frequency synthesis chain: accurate measurement of the 473 THz HeNe/I_2 laser ,” Opt. Commun. **97**, 29–34 (1993).

[48] J. E. Bernard, A. A. Madej, L. Marmet, B. G. Whitford, K. J. Siemsen, and S. Cundy, “Cs-Based Frequency Measurement of a Single, Trapped Ion Transition in the Visible Region of the Spectrum,” Phys. Rev. Lett. **82**, 3228–3231 (1999).

[49] H. Schnatz, B. Lipphardt, J. Helmcke, F. Riehle, and G. Zinner, “First Phase-Coherent Frequency Measurement of Visible Radiation,” Phys. Rev. Lett. **76**, 18–21 (1996).

[50] T. G. Blaney, C. C. Bradley, G. J. Edwards, B. W. Jolliffe, D. J. E. Knight, and P. T. Woods, “Measurement of the frequency of the methane-stabilised laser at 3.39 μm and of the R(32) transition of CO_2 at 10.17 μm,” Nature **254**, 584–585 (1975).

[51] H. R. Telle, D. Meschede, and T. W. Hänsch, “Realization of a new concept for visible frequency division: phase locking of harmonic and sum frequencies,” Opt. Lett. **15**, 532–534 (1990).

[52] J. Reichert, R. Holzwarth, Th. Udem, T. W. Hänsch, “Measuring the frequency of light with mode-locked lasers,” Opt. Commun. **172**, 59–68 (1999).

[53] D. J. Jones, S. A. Diddams, J. K. Ranka, A. Stentz, R. S. Windeler, J. L. Hall, and S. T. Cundiff, “Carrier-envelope phase control of femtosecond mode-locked lasers and direct optical frequency synthesis,” Science **288**, 635–639 (2000).

[54] S. A. Diddams, D. J. Jones, J. Ye, S. T. Cundiff, J. L. Hall , J. K. Ranka, R. S. Windeler, R. Holzwarth, Th. Udem, and T. W. Hänsch, “Direct link between microwave and optical frequencies with a 300 THz femtosecond laser comb,” Phys. Rev. Lett. **29**, 5102–5105 (2000).

[55] R. Holzwarth, Th. Udem, T. W. Hänsch, J. C. Knight, W. J. Wadsworth, and P. St. J. Russell, "Optical Frequency Synthesizer for Precision Spectroscopy," Phys. Rev. Lett. **85**, 2264–2267 (2000).

[56] J. K. Ranka, R. S. Windeler, and A. J. Stentz, "Visible continuum generation in air-silica microstructure optical fibers with anomalous dispersion at 800 nm," Opt. Lett. **25**, 25–27 (2000).

[57] B. R. Washburn, S. A. Diddams, N. R. Newbury, J. W. Nicholson, M. F. Yan, and C. G. Jørgensen, "Phase-locked, erbium-fiber-laser-based frequency comb in the near infrared," Opt. Lett. **29**, 250–252 (2004).

[58] T. R. Schibli, K. Minoshima, F.-L. Hong, H. Inaba, A. Onae, H. Matsumoto, I. Hartl, and M. E. Fermann, "Frequency metrology with a turnkey all-fiber system," Opt. Lett. **29**, 2467–2469 (2004).

[59] Th. Udem, R. Holzwarth, and T. W. Hänsch, "Optical frequency metrology," Nature **416**, 233–237 (2002).

[60] G. Genty, M. Lehtonen, H. Ludvigsen, J. Broeng ,and M. Kaivola, "Spectral broadening of femtosecond pulses into continuum radiation in microstructured fibers," Opt. Express **10**, 1083–1098 (2002).

[61] R. Ell, U. Morgner, F. X. Kärtner, J. G. Fujimoto, E. P. Ippen, V. Scheuer, G. Angelow, T. Tschudi, M. J. Lederer, A. Boiko, and B. Luther-Davies, "Generation of 5-fs pulses and octave-spanning spectra directly from a Ti:sapphire laser," Opt. Lett. **15**, 373–375 (2001).

[62] H. M. Goldenberg, D. Kleppner, and N. F. Ramsay, "Atomic Hydrogen maser," Phys. Rev. Lett. **5**, 361–362 (1960).

[63] J. L. Hall, "Stabilized lasers and precision measurements," Science **202**, 147–156 (1978).

[64] T. W. Hänsch, I. S. Shanin, and A. L. Schawlow, "High-resolution saturation spectroscopy of the sodium D lines with a pulsed tunable dye laser," Phys. Rev. Lett. **27**, 707–710 (1971).

[65] A. J. Wallard, "Frequency stabilization of the helium-neon laser by saturated absorption in iodine vapour," J. Phys. E: Sci. Instrum. **5**, 926–930 (1972).

[66] G. R. Hanes, K. M. Baird, and J. DeRemigis, "Stability, reproducibility, and absolute wavelength of a 633 nm He-Ne laser stabilized to an iodine hyperfine component," Appl. Opt. **12**, 1600–1605 (1973).

[67] S. Picard, L. Robertsson, L-S Ma, K. Nyholm, M. Merimaa, T. Ahola, P. Balling, P. Kren, and J.-P. Wallerand, "Comparison of $^{127}I_2$-stabilized frequency-doubled Nd:YAG lasers at Bureau International des Poids et Mesures," Appl. Opt. **42**, 1019–1028 (2003).

[68] H.S. Margolis, "Frequency metrology and clocks," J. Phys. B: At. Mol. Opt. Phys. **42**, 154017 (2009).

[69] M. Merimaa, K. Nyholm, M. Vainio, and A. Lassila, "Traceability of laser frequency calibration at MIKES," IEEE Trans. Instrum. Meas. **56**, 500–504 (2007).

[70] J. Lazar, J. Hrabina, P. Jedlicka, and O. Cíp, "Absolute frequency shifts of iodine cells for laser stabilization," Metrologia **46**, 450–456 (2009).

[71] A. Czajkowski, A.A. Madej, and P. Dubé, "Development and study of a 1.5 μm optical frequency standard referenced to the P(16) saturated absorption line in the ($\nu_1+\nu_3$) overtone band of $^{13}C_2H_2$," Opt. Commun. **234**, 259–268 (2004).

[72] C. S. Edwards, H. S. Margolis, G. P. Barwood, S. N. Lea, P. Gill, G. Huang, W. R. C. Rowley, "Absolute frequency measurement of a 1.5-μm acetylene standard by use of a combined frequency chain and femtosecond comb," Opt. Lett. **6**, 566–568 (2004).

[73] P. Balling, M. Fischer, P. Kubina, and R. Holzwarth, "Absolute frequency measurement of wavelength standard at 1542 nm: acetylene stabilized DFB laser," Opt. Express **13**, 9196–2001 (2005).

[74] W. E. Lamb, "Theory of an optical maser," Phys. Rev. **134**, A1429–A1450 (1964).

[75] V. Gerginov, C. E. Tanner, S. A. Diddams, A. Bartels, and L. Hollberg, " High-resolution spectroscopy with a femtosecond laser frequency comb," Opt. Lett. **30**, 1734–1739 (2005).

[76] M. J. Thorpe and J. Ye, "Cavity-enhanced direct frequency comb spectroscopy," Appl. Phys. B **91**, 397–414 (2008).

[77] J. D. Jost, J. L. Hall, and J. Ye, "Continuously tunable, precise, single frequency optical signal generator," Opt. Express **10**, 515–520 (2002).

[78] H. Inaba, T. Ikegami, F.-L. Hong, Y. Bitou, A. Onae, T. R. Schibli, K. Minoshima, and H. Matsumoto, "Doppler-free spectroscopy using a continuous-wave optical frequency synthesizer," Appl. Opt. **45**, 4910–4915 (2006).

[79] S. E. Park, E. B. Kim, Y.-H. Park, D. S. Yee, T. Y. Kwon, C. Y. Park, H. S. Moon, and T. H. Yoon, "Sweep optical frequency synthesizer with a distributed-Bragg-reflector laser injection locked by a single component of an optical frequency comb," Opt. Lett. **31**, 3594–3596 (2006).

[80] A. K. Mills, Y.-F. Chen, K. W. Madison, and D. J. Jones, "Widely tunable, single-mode optical frequency synthesizer with a 100 kHz uncertainty," J. Opt. Soc. Am. B. **26**, 1276–1280 (2009).

[81] T. M. Fortier, Y. Le Coq, J. E. Stalnaker, D. Ortega, S. A. Diddams, C. W. Oates, and L. Hollberg, "Kilohertz-resolution spectroscopy of cold atoms with an optical frequency comb," Phys. Rev. Lett. **97**, 163905 (2006).

[82] H. Inaba, T. Ikegami, F.-L. Hong, Y. Bitou, A. Onae, T. R. Schibli, K. Minoshima, and H. Matsumoto, "Doppler-free spectroscopy using a continuous-wave optical frequency synthesizer," Appl. Opt. **45**, 4910–4915 (2006).

[83] B. R. Washburn, R. W. Fox, N. R. Newbury, J. W. Nicholson, K. Feder, P. S. Westbrook, and C. G. Jørgensen, "Fiber-laser-based frequency comb with a tunable repetition rate," Opt. Express **12**, 4999–5004 (2004).

[84] J. A. Silver and A. C. Stanton, "Optical interference fringe reduction in laser absorption experiments," Appl. Opt. **27**, 1914–1916 (1988).

[85] S. E. Park, H. S. Lee, T. Y. Kwon, and H. Cho, "Dispersion-like signals in velocity-selective saturated-absorption spectroscopy," Opt. Commun. **192**, 49–55 (2001).

[86] J. Henningsen, J. Hald, and J. C. Peterson, "Saturated absorption in acetylene and hydrogen cyanide in hollow-core photonic bandgap fibers," Opt. Express **13**, 10475-10482 (2005).

[87] D. W. Allan, "Statistics of Atomic Frequency Standards," P. IEEE **54**, 221–230 (1966).

[88] C. J. Bordé, J. L. Hall, C. V. Kunasz, and D. G. Hummer, "Saturated absorption line shape: Calculation of the transit-time broadening by a perturbation approach," Phys. Rev. A **14**, 236–263 (1976).

[89] L. Mandel, "Photon interference and correlation effects produced by independent quantum sources," Phys. Rev. A **28**, 929–943 (1983).

[90] H. Paul, "Interference between independent photons," Rev. Mod. Phys. **58**, 209–231 (1986).

[91] R. Ghosh and L. Mandel, "Observation of nonclassical effects in the interference of two photons," Phys. Rev. Lett. **59**, 1903–1905 (1987).

[92] C. K. Hong, Z. Y. Ou, and L. Mandel, "Measurement of subpicosecond time intervals between two photons by interference," Phys. Rev. Lett. **59**, 2044–2046 (1987).

[93] P. Kok, W. J. Munro, K. Nemoto, T. C. Ralph, J. P. Dowling, and G. J. Milburn, "Linear optical quantum computing with photonic qubits," Rev. Mod. Phys. **79**, 135–174 (2007).

[94] N Gisin, G. Ribordy, W. Tittel, and H. Zbinden, "Quantum cryptography," Rev. Mod. Phys. **74**, 145–195 (2002).

[95] Id Quantique SA, http://www.idquantique.com/, 10.5.2010.

[96] R. Ursin, T. Jennewein, M. Aspelmeyer, R. Kaltenbaek, M. Lindenthal, P. Walther, and A. Zeilinger, "Quantum teleportation across the Danube," Nature **430**, 849 (2004).

[97] A. Politi, J. C. F. Matthews, and J. L. O'Brien, "Shor's quantum factoring algorithm on a photonic chip," Science **325**, 1221 (2009).

[98] Ch. Brunel, B. Lounis, Ph. Tamarat, and M. Orrit, "Triggered Source of Single Photons based on Controlled Single Molecule Fluorescence," Phys. Rev. Lett. **83**, 2722–2726 (1999).

[99] A. Kuhn, M. Hennrich, and G. Rempe, "Deterministic Single-Photon Source for Distributed Quantum Networking," Phys. Rev. Lett. **89**, 067901 (2002).

[100] M. Keller, B. Lange, K. Hayasaka, W. Lange, and H. Walther, "Continuous generation of single photons with controlled waveform in an ion-trap cavity system," Nature **431**, 1075–1078 (2004).

[101] P. Michler, A. Kiraz, C. Becher, W. V. Schoenfeld, P. M. Petroff, L. Zhang, E. Hu, and A. Imamoglu, "A Quantum Dot Single-Photon Turnstile Device," Science **290**, 2282–2285 (2000).

[102] C. Kurtsiefer, S. Mayer, P. Zarda, and H. Weinfurter, "Stable Solid-State Source of Single Photons," Phys. Rev. Lett. **85**, 290–293 (2000).

[103] E. Knill, R. Laflamme1, and G. J. Milburn, "A scheme for efficient quantum computation with linear optics," Nature **409**, 46–52 (2001).

[104] C. Santori, D. Fattal, J. Vučković, G. S. Solomon, Y. Yamamoto,"Indistinguishable Photons from a Single-Photon Device," Nature **419**, 594–597 (2002).

[105] T. Legero, T. Wilk, M. Hennrich, G. Rempe, A. Kuhn, "Quantum Beat of Two Single Photons," Phys Rev. Lett. **93**, 070503 (2004).

[106] A. Kiraz, M. Ehrl, Th. Hellerer, O. E. Müstecaplıoğlu, C. Bräuchle, and A. Zumbusch, "Indistinguishable Photons from a Single Molecule," Phys. Rev. Lett. **94**, 223602 (2005).

[107] J. Beugnon, M. P. A. Jones, J. Dingjan, B. Darquié, G. Messin, A. Browaeys, and P. Grangier, "Quantum Interference between Two Single Photons Emitted by Independently Trapped Atoms," Nature **440**, 779–782 (2006).

[108] P. Maunz, D. L. Moehring, S. Olmschenk, K. C. Younge, D. N. Matsukevich, and C. Monroe, "Quantum Interference of Photon Pairs from Two Remote Trapped Atomic Ions," Nature Phys **3**, 538–541 (2007).

[109] K. Sanaka, A. Pawlis, T. D. Ladd, K. Lischka, and Y. Yamamoto, "Indistinguishable Photons from Independent Semiconductor Nanostructures," Phys. Rev. Lett. **103**, 053601 (2009).

[110] B. Lounis, and M Orrit, "Single-photon sources," Reg. Prog. Phys. **68**, 1129–1179 (2005).

[111] R. Hanbury Brown and R. Q. Twiss, "Correlation between photons in two coherent beams of light," Nature **177**, 27–29 (1957).

[112] W. E. Moerner and L. Kado, "Optical detection and spectroscopy of single-molecules in solids," Phys. Rev. Lett. **62**, 2535–2538 (1989).

[113] M. Orrit and J. Bernard, "Single pentacene molecules detected by fluorescence excitation in a *p*-terphenyl crystal," Phys. Rev. Lett. **65**, 2716–2719 (1990).

[114] A.-M. Boiron, B. Lounis, and M. Orrit, "Single molecules of dibenzanthanthrene in n-hexadecane," J. Chem. Phys. **105**, 3969-3974 (1996).

[115] G. Wrigge, I. Gerhardt, J. Hwang, G. Zumhofen, and V. Sandoghdar, "Efficient coupling of photons to a single molecule and the observation of its resonance fluorescence," Nature Phys. **4**, 60-66 (2008).

[116] J. R. Lakowicz , "Principles of Fluorescence spectroscopy," 3rd ed., Springer 2006, 954 p., ISBN 0-387-31278-1.

[117] F. Träger, "Handbook of Lasers and Optics," 7th ed. Springer 2007, 1332 p., ISBN 0-387-95579-8.

I

Publication I

V. Ahtee, S. W. Brown, T. C. Larason, K. R. Lykke, E. Ikonen, and M. Noorma, "Comparison of absolute spectral irradiance responsivity measurement techniques using wavelength-tunable lasers," Appl. Opt. **46**, 4228–4236 (2007).

Comparison of absolute spectral irradiance responsivity measurement techniques using wavelength-tunable lasers

Ville Ahtee,[1,2,*] Steven W. Brown,[3] Thomas C. Larason,[3] Keith R. Lykke,[3] Erkki Ikonen,[1,2] and Mart Noorma[1,3]

[1]Metrology Research Institute, Helsinki University of Technology (TKK), P.O. Box 3000, FI-02015 TKK, Finland
[2]Centre for Metrology and Accreditation (MIKES), P.O. Box 9, FI-02151 Espoo, Finland
[3]National Institute of Standards and Technology (NIST), Gaithersburg, Maryland 20899, USA

*Corresponding author: ville.ahtee@tkk.fi

Received 19 December 2006; revised 23 February 2007; accepted 26 February 2007; posted 2 March 2007 (Doc. ID 78288); published 20 June 2007

Independent methods for measuring the absolute spectral irradiance responsivity of detectors have been compared between the calibration facilities at two national metrology institutes, the Helsinki University of Technology (TKK), Finland, and the National Institute of Standards and Technology (NIST). The emphasis is on the comparison of two different techniques for generating a uniform irradiance at a reference plane using wavelength-tunable lasers. At TKK's Laser Scanning Facility (LSF) the irradiance is generated by raster scanning a single collimated laser beam, while at the NIST facility for Spectral Irradiance and Radiance Responsivity Calibrations with Uniform Sources (SIRCUS), lasers are introduced into integrating spheres to generate a uniform irradiance at a reference plane. The laser-based irradiance responsivity results are compared to a traditional lamp-monochromator-based irradiance responsivity calibration obtained at the NIST Spectral Comparator Facility (SCF). A narrowband filter radiometer with a 24 nm bandwidth and an effective band-center wavelength of 801 nm was used as the artifact. The results of the comparison between the different facilities, reported for the first time in the near-infrared wavelength range, demonstrate agreement at the uncertainty level of less than 0.1%. This result has significant implications in radiation thermometry and in photometry as well as in radiometry.

OCIS codes: 120.3940, 120.5630.

1. Introduction

Many national metrology institutes (NMIs) have adopted the practice of realizing an absolute detector-based spectral irradiance scale [1–5] using cryogenic radiometers as the primary standard because it offers a relatively short traceability chain and low uncertainties compared with the traditional source-based method. Several different calibration techniques for the absolute spectral irradiance responsivity of filter radiometers are commonly in use [6–10]. The uncertainties achievable in spectral responsivity measurements based on traditional approaches using a lamp and a monochromator as a radiation source are limited by the low radiant flux available and the relatively broad spectral width of the source [6,7]. Laser-based methods overcome these limitations as they offer orders of magnitude more power and, for cw lasers, inherently narrow linewidth [8–10]. However, because of the high spatial and temporal coherence of the laser sources, care has to be taken to avoid errors attributable to the interference arising from the reflections between parallel surfaces inside the filter radiometer [10].

In this study, two independent laser-based spectral irradiance responsivity calibration methods have been compared in the near-infrared wavelength region using a narrowband filter radiometer, FR800AR, as an artifact. The measurement facilities are at the NIST in the United States and at the Metrology Research Institute of the Helsinki University of Technology (TKK) in Finland, thus having completely independent traceability chains from the two inde-

0003-6935/07/204228-09$15.00/0

pendent primary standard cryogenic radiometers at the two facilities. Wavelength-tunable Ti:sapphire lasers are used at both facilities as the light sources and calibrated trap detectors as the reference standards for spectral power responsivity. However, the method for generating the uniform monochromatic irradiance is completely different. The SIRCUS facility at the NIST uses an integrating sphere to generate a uniform irradiance field [9] while the Laser Scanning Facility (LSF) at TKK [10] is based on the raster scanning technique using a single collimated laser beam; the effective irradiance is determined by calculation. Earlier comparisons of different calibration methods of spectral irradiance responsivity have revealed deviations, which have exceeded the stated uncertainties [11,12]. One reason for these discrepancies has been reported to have been higher than expected uncertainties in the wavelength scales at the comparison laboratories [12]. From this point of view, the laser-based calibration methods are likely to be more exact because of the ability for accurate real-time wavelength monitoring. In addition, different methods for minimization of the effect of the interference fringes, the observation of which is related to the use of monochromatic narrowband laser sources, are used in these facilities. The methods are compared and discussed along with the results obtained at the NIST Spectral Comparator Facility (SCF) [6] using a conventional monochromator-based light source.

In Section 2, the operational principles of the calibration facilities are explained. In Section 3, the construction of the measurement artifact is described, and the experimental procedure on each facility is presented. In Section 4, the uncertainty budgets for the measurement facilities are given. Section 5 presents the calibration results obtained with different methods. In Section 6, the implications of this study for applications in radiation thermometry and in photometry are discussed.

2. Description of the Facilities

In this section we briefly discuss the operational principles of each facility. The detailed descriptions of the SIRCUS, the LSF, and the SCF are found in [9], [10], and [6], respectively.

A. NIST SIRCUS Facility

In the SIRCUS facility, shown schematically in Fig. 1, high-power, tunable lasers are introduced into an integrating sphere producing a uniform, quasi-Lambertian, high radiant flux source. The laser beam is first directed through an intensity stabilizer that controls the relative optical power to within 0.01% of the set point. A portion of the laser beam is sent into a wavemeter that measures the wavelength of the radiation to within 0.001 nm. A beam splitter sends another portion of the laser beam into a Fabry–Perot interferometer to measure the bandwidth and mode stability of the laser. Finally, the laser radiation is introduced into an integrating sphere, often using an optical fiber [9]. Occasionally, a collimator coupled to

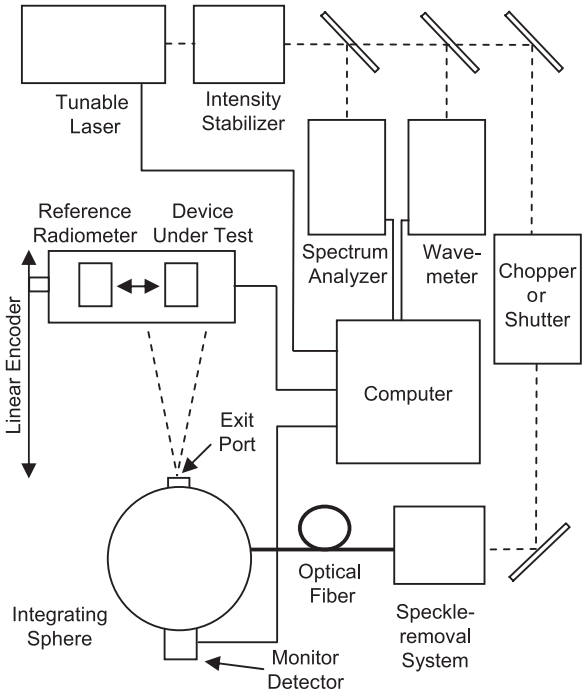

Fig. 1. Schematic of the SIRCUS facility at NIST.

the sphere is used as a calibration source. Speckle in the image from the source, originating from the coherent nature of the laser radiation, is effectively removed by either rastering the beam inside the sphere with a galvanometer-driven mirror or by placing a short length of optical fiber in an ultrasonic bath, thereby mixing the spatial modes in the fiber and the spatial distribution of the light from the fiber that hits the sphere wall.

Reference standard irradiance detectors, calibrated directly against national primary standards for spectral power responsivity [13] and equipped with a precision aperture measured on the NIST Aperture Area facility [14], are used to determine the irradiance at a reference plane. The source irradiance can be readily determined from the measurement geometry as well, which is necessary when the reference plane of the instrument being calibrated and that of the reference standard detector cannot be matched. A monitor photodiode is located on the sphere to correct for any radiant flux changes in the sphere output between measurements with the reference instrument and the device under test (DUT). The sources are located inside a lighttight box. Two baffles are typically installed between the source and the detectors to minimize effects of stray radiation on the measurement.

There are two separate SIRCUS facilities; the UV/Vis/NIR SIRCUS and the IR SIRCUS. The UV/Vis/NIR SIRCUS covers the range from 200 nm to 1.6 μm while the IR SIRCUS facility covers the spectral region from 780 nm to 5 μm. There is some overlap between the two facilities for scale intercomparisons. The two facilities are very similar; the main distinction is in the laser source used to illuminate the integrating spheres and the reference transfer

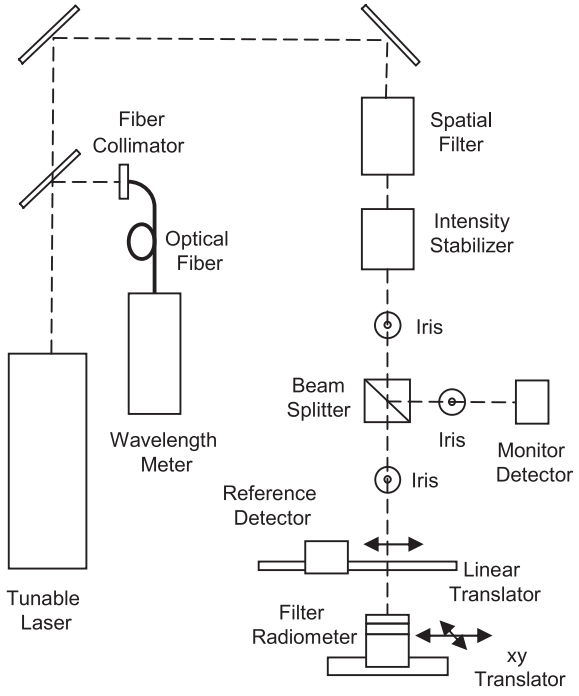

Fig. 2. Schematic of the Laser Scanning Facility at TKK.

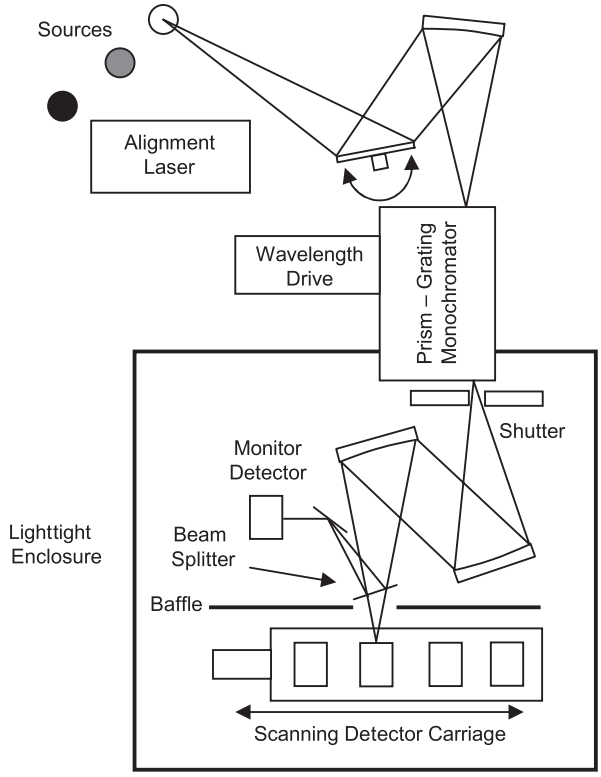

Fig. 3. Schematic of the Visible to Near-Infrared Spectral Comparator Facility at the NIST.

standards used to determine the irradiance at a reference plane. The UV/Vis/NIR SIRCUS was exclusively used in the comparison presented in this paper.

B. TKK Laser Scanning Facility

Figure 2 shows the schematic diagram of the LSF at TKK. The output from a wavelength-tunable cw Ti:sapphire laser is attenuated with a neutral density filter after which it is spatially filtered, collimated, and intensity stabilized. Part of the beam is directed to an optical wavelength meter for real-time wavelength monitoring. The uncertainty of the wavelength scale is estimated to be 0.003 nm. The spectral irradiance responsivity of the filter radiometer, $S(\lambda)$, is obtained by moving the filter radiometer with a high-accuracy translation stage step by step relative to the monochromatic laser beam and measuring the resulting photocurrent $I_{j,k}$ at each point [15]. The irradiance responsivity is then calculated by summing the signals measured, multiplying by the step sizes, and dividing by the incident power as

$$S(\lambda) = \frac{\sum_{j=1}^{n_x} \sum_{k=1}^{n_y} I_{j,k} \Delta x \Delta y}{P_L}. \quad (1)$$

In Eq. (1), n_x and n_y are the numbers of measurement points in the horizontal and vertical directions, Δx and Δy are the horizontal and vertical distances between the measurement points, and P_L is the power of the laser beam. The beam power is measured by moving a reference trap detector in front of the filter radiometer before and after each measurement of $S(\lambda)$. Part of the beam is directed to a monitor detector. During the scanning measurements, the photocurrents of the filter radiometer and the monitor detector are measured simultaneously to reduce the effects of remaining beam power fluctuations. Iris diaphragms are used to reduce stray light and back reflections. The dark currents of the detectors are also measured for the determination of $I_{j,k}$.

C. NIST Spectral Comparator Facility

The Visible to Near-Infrared Spectral Comparator Facility (Vis/NIR SCF) [6] is a monochromator-based system that measures the spectral radiant power responsivity of photodetectors in the 350–1800 nm spectral region as shown in Fig. 3. The main component of the Vis/NIR SCF is a prism-grating monochromator. The monochromator entrance slit is illuminated by a 100 W quartz halogen lamp. The typical exit aperture is a 1.1 mm diameter circular aperture, which is imaged ($\approx f/9$) onto the detectors. The bandwidth of the monochromator is 4 nm. A shutter is located just after the exit slit. A pair of orthogonal linear positioning stages translates the test detectors and the working standards. The detectors and the exit optics are enclosed in a lighttight box. The spatial uniformity of the detector responsivity can also be measured at any wavelength from 350 to 1800 nm.

3. Experimental Procedure

The calibration measurements were performed between November 2005 and March 2006. The mea-

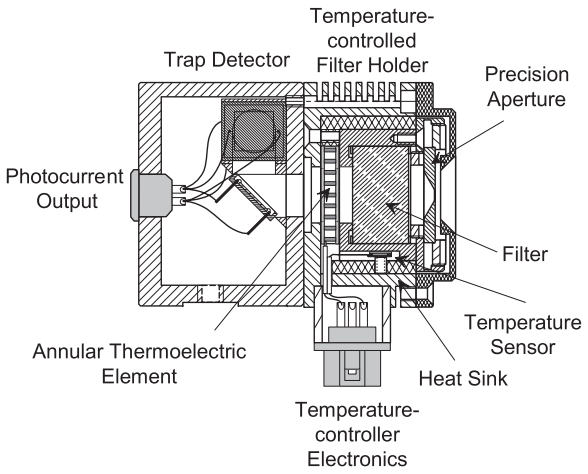

Fig. 4. Schematics of the filter radiometer FR800AR (picture reproduced from [12]).

surement artifact was first calibrated on SIRCUS and on the SCF at the NIST after which it was shipped to TKK for calibration on the LSF.

A. Description of the Measurement Artifact

The filter radiometer, FR800AR, was constructed at TKK and is similar in structure to the filter radiometers presented in [12]. A schematic view of the filter radiometer is shown in Fig. 4. It consists of a precision aperture with a nominal diameter of 3 mm, a bandpass interference filter with an effective central wavelength of 801 nm and a bandwidth of 24 nm (FWHM), and a three-element silicon trap detector. The temperature of the aperture and the filter was stabilized to (25 ± 0.5) °C by a thermoelectric cooling–heating system. The interference effect arising from inter-reflections of the coherent laser light between the layered structures of the filter was minimized by using a filter with slightly wedged surfaces and by applying an antireflection coating on the front surface of the filter. To compare the calibration methods, the spectral irradiance responsivity of FR800AR was measured with each method over a range of 33 nm around the bandcenter wavelength.

B. Measurements on SIRCUS

The spectral irradiance responsivity of the filter radiometer was calibrated on the SIRCUS utilizing the procedure described below. The measurements were made with average spectral intervals of 0.02 nm over the calibration range.

The entire data collection sequence on SIRCUS is automated. Initially, an electronic shutter that blocks the laser radiation before it enters the optical fiber is closed, and a background signal is acquired for both the reference standard trap detector and the sphere monitor. Then the shutter opens and the signals from the trap and the monitor on the sphere are recorded. The signals are initially amplified using a current-to-voltage amplifier and then fed into a digital voltmeter set to average over some number of power line cycles (the signal is averaged for a few seconds at most). Typically three shutter-closed signals and nine shutter-open signals are averaged. The mean reference-to-monitor ratio and the standard deviation of the ratio are recorded. After this, the stage moves to the DUT position, and the data acquisition sequence is repeated. This gives the DUT mean signal-to-monitor ratio and the standard deviation of the ratio. The standard deviations of the ratios are monitored; trap-detector-measurement standard deviations larger than 0.01% are an indication of laser power instabilities.

Under routine calibration conditions, the intensity-stabilized laser wavelength is read by the wavemeter and transferred to the computer during each measurement. Along with mean ratios, the mean and standard deviations of the wavelength are recorded. This enables ready identification of laser wavelength instabilities during a scan. Occasionally, for faster data acquisition, the wavelength is recorded only at the beginning of the acquisition sequence. Following the data acquisition sequence, the wavelength is changed and the sequence is repeated.

C. Measurements on the Laser Scanning Facility and Study of Interference Effects

The spectral irradiance responsivity of the filter radiometer was calibrated at the LSF by making measurements with spectral intervals of exactly 1 nm over the measurement range. The power of the laser beam was set to approximately 100 μW, and the $1/e^2$ diameter of the beam was approximately 3 mm. Step sizes of $\Delta x = 0.5$ mm and $\Delta y = 0.5$ mm and 15 measurement points for both the x and y directions were used as scanning parameters. Before the measurements, the FR800AR was carefully aligned perpendicular to the laser beam. Spurious reflections were eliminated by slightly tilting the optical components in front of the filter radiometer and monitoring the reflections using a CCD camera.

The effect of interference inside the filter radiometer gave rise to responsivity oscillation, as a function of laser wavelength, whose period was approximately 0.15 nm and the amplitude approximately 0.3% of the absolute responsivity when measured near the maximum of the responsivity curve. To compensate for this interference effect, oscillation patterns around every measurement point were determined by making relative responsivity measurements with spectral intervals of 0.02 nm over a full period of oscillation. The measured patterns were then fitted to the responsivity curve obtained from the absolute scanning measurements, and the absolute irradiance responsivity values at the measurement points were corrected to correspond to the average of the surrounding oscillation pattern. The method of least squares was used when fitting the data.

Because of the 10–15 min duration of the raster scanning measurements, relative measurements using a single laser beam rather than absolute scanning measurements were used in the determination of the

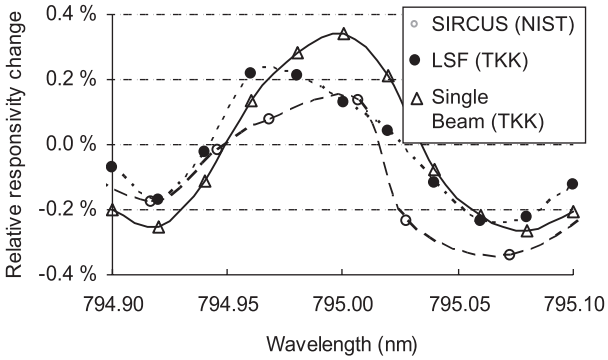

Fig. 5. Interference pattern measured close to 795 nm on SIRCUS, LSF, and with the single beam technique (see text).

oscillation pattern. The applicability of the single-beam method was confirmed by measuring a period of an oscillation pattern with single beam and raster scanning techniques. Figure 5 shows the result of such a measurement at approximately 795 nm together with the result from SIRCUS. In Fig. 5 the average value of the data obtained with the single-beam measurements is fixed to be the same as the average of absolute LSF raster scanning measurements. The results from the SIRCUS measurements share the same absolute scale with the raster scanning data, thus the true difference between these measurements can be evaluated. From Fig. 5 it is seen that, with the exception of a few measurement points, single-beam measurements match well with the raster scanning measurements, thus justifying the technique for oscillation pattern determination. Also, the results of the SIRCUS measurements are well in compliance with raster scanning measurements.

D. Measurements on the Spectral Comparator Facility

The spectral radiant power responsivity of the filter radiometer was determined over the measurement range in 1 nm wavelength increments by direct substitution comparisons to the silicon photodiode working standards. The effective aperture area of the filter radiometer was determined by scanning the monochromator output beam over the radiometer's entrance aperture in 0.125 mm increments to simulate a uniform irradiance. This method has been used by the NIST since 1991 [16]. The effective aperture area is proportional to the ratio of the total integrated signal of the scanned area and the signal from the center position. The spectral irradiance responsivity is the product of the spectral power responsivity and the effective aperture area [17].

4. Facility Uncertainty

This section summarizes the uncertainty budgets of each facility and the origins of the main uncertainty components. It should be noted that wavelength uncertainties are not included in the uncertainty budgets of SIRCUS and LSF because the effects of wavelength deviations are compared via the effective wavelength measurements.

Table 1. Uncertainty Budget of SIRCUS (NIST)

Source of Uncertainty	Relative Standard Uncertainty $\times 10^{-4}$
Reference detector responsivity	
Radiant power responsivity (400–920 nm)	2.5
Aperture area	0.4
Response uniformity	0.5
Cosine dependence	1.0
Temperature	0.3
Source characteristics	
Radiant flux	0.5
Irradiance uniformity	0.5
Determination of the reference plane	1.0
I-V Gain	1.0
Voltmeter reading	0.5
Transfer to device under test (estimated)	3.0
Temperature instability of device under test	2.8
Combined standard uncertainty	5.2

A. SIRCUS

The SIRCUS uncertainty budget is given in Table 1. Reference standard tunnel trap detectors hold the spectral irradiance responsivity scale on SIRCUS. The relative combined standard uncertainty in the detector responsivity is 2.5×10^{-4} at approximately 800 nm. To propagate the low uncertainties in power responsivity to irradiance responsivity, the detector's spatial response uniformity must be measured as well as the area of the defining aperture. The relative standard uncertainty of the area determination for a 5 mm diameter aperture is 4×10^{-5}. The response of a reference trap detector was found to be uniform to within 5×10^{-5} over the entire area of the entrance window (with the aperture removed). The uncertainty attributable to the responsivity deviation from the cosine function is 1×10^{-4} within a 6° field of view (FOV).

The radiant power uncertainty attributable to source instability is 5×10^{-5}. The irradiance is uniform to within 1×10^{-3} over the central ± 2 cm in both the horizontal and vertical directions, resulting in an uncertainty component of 5×10^{-5} attributable to irradiance uniformity in filter radiometer calibration. Given a 50 μm uncertainty in the trap reference plane, the uncertainty in the irradiance at a given reference plane for distances of 1 m or greater is 1×10^{-4}. The uncertainty of the current-to-voltage (I–V) conversion was 1×10^{-4} for gain selections between 10^4 V/A and 10^7 V/A. The estimated uncertainty in the transfer to the filter radiometer is listed in Table 1 as 3×10^{-4}. We have also included a term from the estimated uncertainty arising from temperature fluctuations. Taking the root-sum square of the individual uncertainty components, the combined

Table 2. Uncertainty Budget of LSF (TKK)

Source of Uncertainty	Relative Standard Uncertainty $\times 10^{-4}$
Irradiance	
Power of the laser beam	6.5
Step size of the *xy* translator	1.0
Interference effect	5.0
Temperature	2.8
Photocurrent of the filter radiometer	1.7
Combined standard uncertainty	8.9

relative standard uncertainty for the SIRCUS measurements is 5.2×10^{-4}.

B. Laser Scanning Facility

The summary of the relative combined standard uncertainty for the LSF facility is given in Table 2 according to the estimation presented in [10]. The main uncertainty components arise from the calibration of the power responsivity of the reference trap detector against the cryogenic radiometer (6.5×10^{-4}), from the interference effect inside the filter (5×10^{-4}), and from the temperature instability of the filter radiometer (2.8×10^{-4}). The fact that the filter radiometer was not tilted with respect to the laser beam, but other means were used for the elimination of spurious reflections, led to the exclusion of the uncertainty components related to the tilt of the radiometer reported earlier [10]. The combined relative standard uncertainty for the LSF is approximately 8.9×10^{-4}.

C. Spectral Comparator Facility

The uncertainty budget of the SCF at 800 and 818 nm is shown in Table 3. The former wavelength (800 nm) corresponds to the peak of the filter transmittance and the latter wavelength (818 nm) is located at the higher end of the measured wavelength range. The largest uncertainty components are attributable to the irradiance scanning calibration method, wavelength determination, and repeatability. Smaller uncertainty components are caused by amplifier gains, digital voltmeter, and stray light.

Table 3. Uncertainty Budget of SCF (NIST)

Source of Uncertainty	Relative Standard Uncertainty $\times 10^{-4}$ 800 nm	818 nm
Repeatability and random noise	2	46
Irradiance method (scanning)	58	58
Working standard calibration	9	9
Working standard amplifier gain	4	4
Test detector amplifier gain	4	4
Voltmeter reading	1	1
Wavelength ($\pm$0.1 nm)	3	415
Spectral stray light	0	2
Combined standard uncertainty	59	422

The combined standard uncertainty is 59×10^{-4} at 800 nm and 422×10^{-4}, at 818 nm. The relatively high value of uncertainty at 818 nm is attributable mainly to the uncertainty in the wavelength determination, which causes high uncertainty when measuring at the regions where the transmittance of the filter changes rapidly as a function of the wavelength.

5. Results

The absolute spectral irradiance responsivity curves of the FR800AR obtained with the three methods are plotted over the entire measurement range on a logarithmic scale in Fig. 6(a) and close to the responsivity maximum on a linear scale in Fig. 6(b). The irradiance responsivity curves obtained with the two laser-based methods are in good agreement with each other. It should be noted that the LSF points plotted in Fig. 6 represent the interference-corrected values, i.e., values that are spectrally averaged over the surrounding interference cycle, while the SIRCUS points represent absolutely measured values at each wavelength. The shape of the responsivity curve obtained from the measurements on SCF is highly affected by the large bandwidth of the source, which makes the individual measurement points represent values that are spectrally averaged over several nanometers. Therefore the SCF data deviates significantly from the other two data sets and cannot be directly compared with them at precise wavelengths.

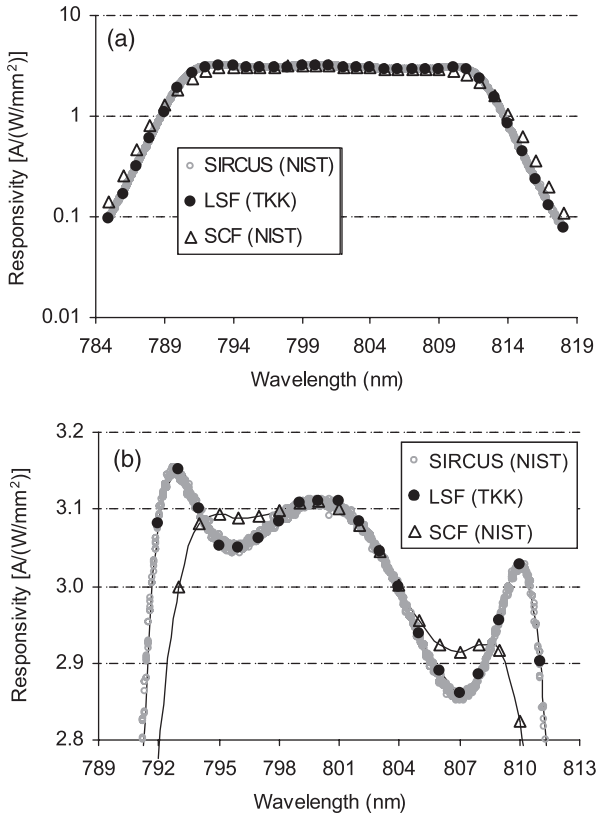

Fig. 6. Spectral irradiance responsivity of the filter radiometer measured on SIRCUS, LSF, and SCF (a) over the entire measurement range, (b) close to the responsivity maximum.

Table 4. Integrated Irradiance Responsivity of FR800AR[a]

	Integrated Response [A/(W/mm^2) nm]	Relative Standard Uncertainty $\times 10^{-4}$	Relative Difference to Weighted Average $\times 10^{-4}$
SIRCUS (NIST)	72.830	5.2	−1.0
LSF (TKK)	72.859	8.9	3.0
SCF (NIST)	72.833	59	−0.6

[a]The data were calculated over the wavelength range 785–818 nm from the results of spectral irradiance calibrations on SIRCUS, LSF, and SCF. The corresponding relative standard uncertainties are shown and the results are compared to the weighted average of all the methods.

The agreement between the calibration methods was evaluated by calculating the integrated response [12]

$$S = \int_{785\ \mathrm{nm}}^{818\ \mathrm{nm}} S(\lambda)\mathrm{d}\lambda \tag{2}$$

for spectral responsivity results over the calibration range. The integrated responses corresponding to each calibration are given in Table 4 and are compared with the weighted average of the results calculated as

$$\bar{S} = \frac{\sum_{i=1}^{3} S_i u_i^{-2}}{\sum_{i=1}^{3} u_i^{-2}}, \tag{3}$$

where S_i are the integrated responses obtained from the three different calibrations, and parameters u_i are the corresponding standard uncertainties. The integrated responsivity values for all compared methods are well within the stated standard uncertainties.

The effective wavelength values

$$\lambda_{eff} = \frac{\int_{785\ \mathrm{nm}}^{818\ \mathrm{nm}} \lambda S(\lambda)\mathrm{d}\lambda}{\int_{785\ \mathrm{nm}}^{818\ \mathrm{nm}} S(\lambda)\mathrm{d}\lambda}, \tag{4}$$

for each calibration were calculated to reveal possible discrepancies in the determinations of the wavelength scales between different methods. The results are presented in Table 5 and are compared with the weighted average of the results calculated as

$$\bar{\lambda}_{eff} = \frac{\sum_{i=1}^{3} \lambda_{eff_i} w_i^{-2}}{\sum_{i=1}^{3} w_i^{-2}}, \tag{5}$$

where λ_{eff_i} are the effective wavelengths obtained from the three different calibrations, and parameters w_i are the corresponding standard uncertainties. The effective wavelengths given by the laser-based calibrations match well with each other. The results are within the stated expanded ($k = 2$) uncertainties of 0.002 nm for SIRCUS and 0.006 nm for the LSF. The effective wavelength extracted directly from the SCF calibration is also in agreement with the other two, deviating 0.016 nm from the weighted average, but its expanded uncertainty of 0.2 nm is approximately 2 orders of magnitude higher compared to the uncertainties of the laser-based methods. The effect of convolution, attributable to the broad spectral width of the source, causes a slight wavelength shift in the SCF data. This can be compensated by deconvolving the data using the monochromator's slit function. It is estimated that the deconvolution would cause approximately a 0.01 nm shift to the SCF effective wavelength.

Table 5. Effective Wavelength of FR800AR[a]

	Effective Wavelength [nm]	Standard Uncertainty [nm]	Difference to Weighted Average [nm]
SIRCUS (NIST)	801.194	0.001	0.001
LSF (TKK)	801.187	0.003	−0.006
SCF (NIST)	801.209	0.1	0.016

[a]The data calculated over the wavelength range 785–818 nm from the results of spectral irradiance calibrations on SIRCUS, LSF, and SCF. The corresponding standard uncertainties are shown, and the results are compared to the weighted average of all the methods.

6. Discussion

Both laser-based methods in this study are based on a wavelength-tunable Ti:sapphire laser. The main difference between the methods lies in the mechanism by which a uniform irradiance is generated from the laser source. On SIRCUS, integrating spheres with a precision aperture are employed, while on LSF the uniform irradiance is generated using the raster scanning technique. The advantage of the raster scanning technique is that it removes the need for the determination of the distance between the source and the detector, which is needed on SIRCUS when the reference plane of the instrument being calibrated and that of the reference detector cannot be matched. On the other hand, the time needed for a scan measurement is relatively long, which restricts the number of measurement points. This has an impact on how the effect of interference is treated. On SIRCUS it is possible to measure the whole band with a spectral resolution good enough to follow the interference pattern continuously. On the LSF, in contrast, the

interference effect is taken into account by determining the interference pattern around every measurement point and calculating a correction factor for every measurement point. In any case, care has to be taken when designing the filter radiometer to minimize interference effects, for example, by the use of wedged optical elements and antireflection coatings.

The results of this comparison have implications for a number of radiometric applications where high-accuracy spectral radiance and irradiance measurements are crucial. In one example, the uncertainty in an absolute detector-based radiometric temperature scale, studied extensively at different NMIs [11,18–20] depends mostly on the accuracy of the NMIs spectral radiance and irradiance responsivity scales. The freezing temperatures of gold, silver, and aluminum fixed points, defined by the International Temperature Scale of 1990 (ITS-90) [21], have been measured by using radiometric detectors traceable to absolute cryogenic radiometers, with uncertainties similar to the thermodynamic measurements of temperature reported in the ITS-90 [18,19]. However, before the detector-based radiometric temperature scales can be considered as suitable alternatives to the relative fixed-point-based method of ITS-90, more studies on the reliability of these different detector-based methods have to be conducted. While in most of the radiometric temperature measurements radiometers that measure the radiance of blackbody sources are used, the spectral irradiance measurements are usually an essential part of their spectral radiance responsivity calibration [9]. Significant improvements in the spectral irradiance scales have been made, especially in the shortwave IR region [3,4].

For temperatures above the freezing temperature of silver, the ITS-90 is defined in terms of spectral radiance ratios of the silver-, gold- or copper-freezing temperature blackbodies using the Planck radiance law. In the ITS-90, the assigned temperatures for the Ag, Au, and Cu freezing points result from thermometry using ratio pyrometry from the mean of two different and conflicting constant-volume gas thermometry measurements at lower temperatures. There are thermodynamic temperature uncertainties of the freezing points of the primary metal blackbodies that arise primarily from the uncertainties in the lower-temperature gas thermometry. Because of the use of spectral radiance ratios, the temperature uncertainties of the ITS-90 assigned blackbodies, $u(T_{BB})$, increase as the square of the temperature ratios according to

$$u(T_{BB}) = \frac{u(T_{FP})}{{T_{FP}}^2}\,{T_{BB}}^2, \tag{6}$$

where T_{FP} and $u(T_{FP})$ are the temperature and the uncertainty of the fixed-point blackbody, and T_{BB} is the temperature of the higher-temperature blackbody. The increases in the temperature uncertainties can be reduced by using absolute radiometry with pyrometers traceable to cryogenic radiometers, and the resulting temperature uncertainties can be smaller than those measured using the ITS-90 techniques [22].

The results of this comparison may also have implications in photometry. The redefinition of the candela in 1979 coupled photometric and radiometric units [23] and made it possible to realize and maintain photometric units using detectors as well as sources. Following the redefinition, many NMIs, including TKK and the NIST, derive and maintain the candela (and the derived photometric units) by using calibrated standard detectors traceable to cryogenic radiometers [24,25] rather than standard lamps traceable to primary standard blackbodies and international temperature scales. By using tunable lasers to measure the spectral responsivity of photometers, the present uncertainties, at the 0.5% level [26] may be reduced to approximately 0.1%, primarily because of the improved accuracy of the wavelength scale. In this case, the uncertainty budget may be dominated by the radiometric stability of the instrument (filter and detector) not the calibration itself.

7. Conclusions

In this paper, we have presented the results of a study of two laser-based calibration methods for absolute spectral irradiance responsivity in the near-infrared wavelength region. A narrow bandwidth filter radiometer was calibrated as an artifact on two National Metrology Institutes' laser-based calibration facilities, on SIRCUS at the NIST and on the LSF at TKK. A calibration was also performed on the NIST SCF to compare laser-based methods with a conventional monochromator-based method. The agreement between the methods was evaluated with respect to the integrated irradiance responsivities and effective wavelengths calculated from the calibration data.

The results of all three methods were found to agree with each other in terms of the integrated responsivities within the limits of stated uncertainties, the laser-based methods offering significantly lower uncertainties than the monochromator-based method. The study of the effective wavelength values showed that the wavelength scales used on SIRCUS and LSF match quite well with each other. The spectral averaging attributable to the broad spectral width of the monochromator source causes a slight wavelength shift in the SCF data. However, the difference between the effective wavelengths extracted from the SCF data and from the average of the laser-based methods is well within the expanded ($k = 2$) uncertainty of the SCF wavelength scale.

This study has validated the stated low uncertainties, somewhat below 0.1% ($k = 1$), of the studied laser-based spectral irradiance calibration methods in the near-infrared region. The study also showed that the wavelength scale for the calibration can be realized with high accuracy using laser-based methods. As explained in Section 6, the results are significant for applications in radiation thermometry as well as in photometry.

References

1. V. E. Anderson and N. P. Fox, "A new detector-based spectral emission scale," Metrologia **28,** 135–139 (1991).
2. P. Sperfeld, K.-H. Raatz, B. Nawo, W. Möller, and J. Metzdorf, "Spectral-irradiance scale based on radiometric blackbody temperature measurements," Metrologia **32,** 435–439 (1996).
3. T. Kübarsepp, P. Kärhä, F. Manoocheri, S. Nevas, L. Yliantila, and E. Ikonen, "Spectral irradiance measurements of tungsten lamps with filter radiometers in the spectral range 290 nm to 900 nm," Metrologia **37,** 305–312 (2000).
4. H. W. Yoon, C. E. Gibson, and P. Y. Barnes, "Realization of National Institute of Standards and Technology detector-based spectral irradiance scale," Appl. Opt. **41,** 5879–5890 (2002).
5. M. Durak and F. Samadov, "Realization of a filter radiometer-based irradiance scale with high accuracy in the region from 286 nm to 901 nm," Metrologia **41,** 401–406 (2004).
6. T. C. Larason, S. S. Bruce, and A. C. Parr, *Spectroradiometric Detector Measurements: Part I–Ultraviolet Detectors and Part II–Visible to Near-Infrared Detectors,* Natl. Inst. Stand. Technol. Spec. Publ. 250-41 (U.S. Government Printing Office, 1998).
7. P. Kärhä, A. Haapalinna, P. Toivanen, F. Manoocheri, and E. Ikonen, "Filter radiometry based on direct utilization of trap detectors," Metrologia **35,** 255–259 (1998).
8. V. E. Anderson, N. P. Fox, and D. H. Nettleton, "Highly stable, monochromatic and tunable optical radiation source and its application to high accuracy spectrophotometry," Appl. Opt. **31,** 536–545 (1992).
9. S. W. Brown, G. P. Eppeldauer, and K. R. Lykke, "Facility for spectral irradiance and radiance responsivity calibrations using uniform sources," Appl. Opt. **45,** 8218–8237 (2006).
10. M. Noorma, P. Toivanen, F. Manoocheri, and E. Ikonen, "Characterization of filter radiometers with a wavelength-tunable laser source," Metrologia **40,** S220–S223 (2003).
11. H. W. Yoon, P. Sperfeld, S. Galal Yousef, and J. Metzdorf, "NIST-PTB measurements of the radiometric temperatures of a high-temperature blackbody using filter radiometers," Metrologia **37,** 377–380 (2000).
12. P. Kärhä, N. J. Harrison, S. Nevas, W. S. Hartree, and I. Abu-Kassem, "Intercomparison of characterization techniques of filter radiometers in the ultraviolet region," Metrologia **40,** S50–S54 (2003).
13. J. M. Houston and J. P. Rice, "NIST reference cryogenic radiometer designed for versatile performance," Metrologia **43,** S31–S35 (2006).
14. J. Fowler and M. Litorja, "Geometric area measurements of circular apertures for radiometry at NIST," Metrologia **40,** S9–S12 (2003).
15. P. Toivanen, F. Manoocheri, P. Kärhä, E. Ikonen, and A. Lassila, "Method for characterization of filter radiometers," Appl. Opt. **38,** 1709–1713 (1999).
16. J. M. Bridges and C. L. Cromer, *Final Report on Calibration and Characterization of I-Line Exposure Meters,* Report 91 090 678A-ENG (International SEMATECH, Austin, Tex., USA, 1991).
17. G. P. Eppeldauer, M. Racz, and T. C. Larason, "Optical characterization of diffuser-input standard irradiance meters," Proc. SPIE **3573,** 220–224 (1998).
18. N. P. Fox, J. E. Martin, and D. H. Nettleton, "Absolute spectral radiometric determination of the thermodynamic temperatures of the melting/freezing points of gold, silver and aluminium," Metrologia **28,** 357–374 (1991).
19. H. W. Yoon, C. E. Gibson, D. W. Allen, R. D. Saunders, M. Litorja, S. W. Brown, G. P. Eppeldauer, and K. R. Lykke, "The realization and dissemination of the detector-based kelvin," in *Proceedings of Tempmeko 04* (Dubrovnik, 2004), pp. 59–70.
20. M. Noorma, P. Kärhä, T. Jankowski, F. Manoocheri, T. Weckström, L. Uusipaikka, and E. Ikonen, "Absolute detector-based radiometric temperature scale," in *Proceedings of Tempmeko 04* (Dubrovnik, 2004), pp. 101–106.
21. H. Preston-Thomas, "The international temperature scale of 1990 (ITS-90)," Metrologia **27,** 3–10 (1990).
22. H. W. Yoon, D. W. Allen, C. E. Gibson, M. Litorja, R. D. Saunders, S. W. Brown, G. P. Eppeldauer, and K. R. Lykke, "Temperature determination of the Ag and Au freezing points using a detector-based radiation thermometer," in *Proceedings of Tempmeko 04* (Dubrovnik, 2004), pp. 113–118.
23. "Principles governing photometry," Metrologia **19,** 97–101 (1983).
24. P. Toivanen, P. Kärhä, F. Manoocheri, and E. Ikonen, "Realization of the unit of luminous intensity at the HUT," Metrologia **37,** 131–140 (2000).
25. Y. Ohno, "Improved photometric standards and calibration procedures at NIST," J. Res. Natl. Inst. Stand. Technol. **102,** 323–331 (1997).
26. R. Köhler, M. Stock, and C. Garreau, "Final report on the international comparison of luminous responsivity CCPR-K3.b," Metrologia **41,** Tech. Suppl. 02001 (2004).

II

Publication II

V. Ahtee, M. Merimaa, and K. Nyholm, "Fiber-based acetylene-stabilized laser," IEEE Trans. Instrum. Meas. **58**, 1211–1217 (2009).

Fiber-Based Acetylene-Stabilized Laser

Ville Ahtee, Mikko Merimaa, and K. Nyholm

***Abstract*—We describe a fiber-based acetylene-stabilized laser system in which light is coupled to free space only to pass through the acetylene cell. The system is constructed using standard components used in telecommunication networks, making the approach straightforward to implement. The Doppler-free spectrum of acetylene can be detected, even without a lock-in amplifier using simple collinear pump–probe geometry, when the length of the optical path in the spectroscopy arrangement is dithered to cancel interference that is inevitably present in a fiber-based setup. The laser was stabilized to five different transitions of $^{13}C_2H_2$ at the $(\nu_1 + \nu_3)$ band using the third-harmonic technique, and the absolute frequencies were measured with an optical frequency comb generator. All the results are in good agreement with the values recommended by the International Committee for Weights and Measures (CIPM). The method for canceling the interference presented here can conceivably be generalized to other types of stabilized lasers as well.**

***Index Terms*—Acetylene-stabilized laser, Doppler-free spectroscopy, optical frequency measurement, telecommunication wavelength reference.**

I. Introduction

HIGH-PRECISION frequency standards at the 1.5-μm wavelength range offer important tools for the development of modern optical telecommunication networks. Such standards are needed, for instance, in the development of dense wavelength-division multiplexing systems with ever-tighter channel spacing. This need has motivated the study of lasers stabilized on the Doppler-free spectrum of acetylene, which was initiated by the early experiments of de Labachelerie *et al.* in the mid-1990s [1]–[3]. Current highly accurate knowledge on the acetylene spectrum at this wavelength region stems from the work performed by numerous research groups [4]–[16]. As a result of these efforts, a laser stabilized on the Doppler-free spectrum of the acetylene $(^{13}C_2H_2)$ is adopted as a primary wavelength standard at this wavelength region, and the International Committee for Weights and Measures (CIPM) has published a list of frequency intervals for transitions in, e.g., the $(\nu_1 + \nu_3)$ band, which are given relative to the recommended frequency value of the P(16) transition $(194\,369\,569\,384 \pm 5$ kHz) [17].

In this paper, we report a fiber-based acetylene-stabilized laser, using standard fiber-optic components, that is readily available at the telecommunication wavelengths [18]. The use of optical fibers, instead of free-space optics, almost completely eliminates the need to align or adjust the optical setup and allows a relatively straightforward design of the optics. A simple pump–probe spectroscopic arrangement without a resonance cavity and the standard third-harmonic detection technique are used to lock the laser to the Doppler-free spectrum of acetylene.

We have characterized the laser and performed absolute frequency measurements using a Ti:S optical frequency comb generator (OFCG) on the laser locked to five different lines of $^{13}C_2H_2$ at the $(\nu_1 + \nu_3)$ band. Here, we also show that a technique previously used in spectroscopy with multipass absorption cells [19] can be used in laser stabilization to suppress the interference originating from the optical surfaces at the interfaces of the setup.

Manuscript received June 12, 2008; revised October 6, 2008. First published December 9, 2008; current version published March 10, 2009. This work was supported by the Academy of Finland. The Associate Editor coordinating the review process for this paper was Mr. Thomas Lipe.

The authors are with the Centre for Metrology and Accreditation (MIKES), 02151 Espoo, Finland (e-mail: ville.ahtee@mikes.fi).

Color versions of one or more of the figures in this paper are available online at http://ieeexplore.ieee.org.

Digital Object Identifier 10.1109/TIM.2008.2008476

II. Acetylene-Stabilized Laser

Fig. 1 shows a schematic of the setup. A fiber-coupled commercial external-cavity diode laser (ECDL, Photonetics Tunics-PRI) provides approximately 5 mW of power over a tuning range of 1520–1600 nm. To increase the stability of the ECDL, the laser head was removed from its chassis and placed on a vibration-isolated optical table. To further improve vibration isolation, the head was mounted on vibration-isolated pads and surrounded by a 2-cm-thick plastic box. To minimize optical feedback to the laser cavity, an external fiber-optic isolator is used, in addition to the optical isolator integrated to the ECDL head. After these modifications, the measured 2-ms linewidth of the laser is less than 800 kHz. The ECDL signal is amplified to approximately 130 mW in a 10-m-long erbium-doped fiber (Liekki, Er16-8/125) pumped with a distributed-feedback laser diode emitting at 1480 nm with a maximum output power of 250 mW. The signal and pump beam are coupled to the erbium fiber through a fiber-optic wavelength-division multiplexer (WDM). An isolator after the erbium fiber ensures that the possible spurious back reflections from the spectroscopy setup are not amplified in the active fiber.

In the spectroscopy setup, the amplified signal is directed to an acetylene cell using a three-port fiber-optic circulator, which provides an isolation of more than 50 dB (manufacturer specification) for the back-reflected light. The pressure in the 50-cm-long acetylene $(^{13}C_2H_2)$ cell was determined from the Doppler-broadened P(16) transition in the $(\nu_1 + \nu_3)$ band. Using the line area, the Gaussian line shape function, cell length, and published value for the line strength [20], the gas pressure was determined to be (2.8 ± 0.1) Pa.

The spectroscopic arrangement is realized in collinear geometry using a reflected pump beam to probe the absorption. An aspheric lens $(f = 11$ mm$)$ at the output of the circulator collimates the pump beam and couples the reflected beam

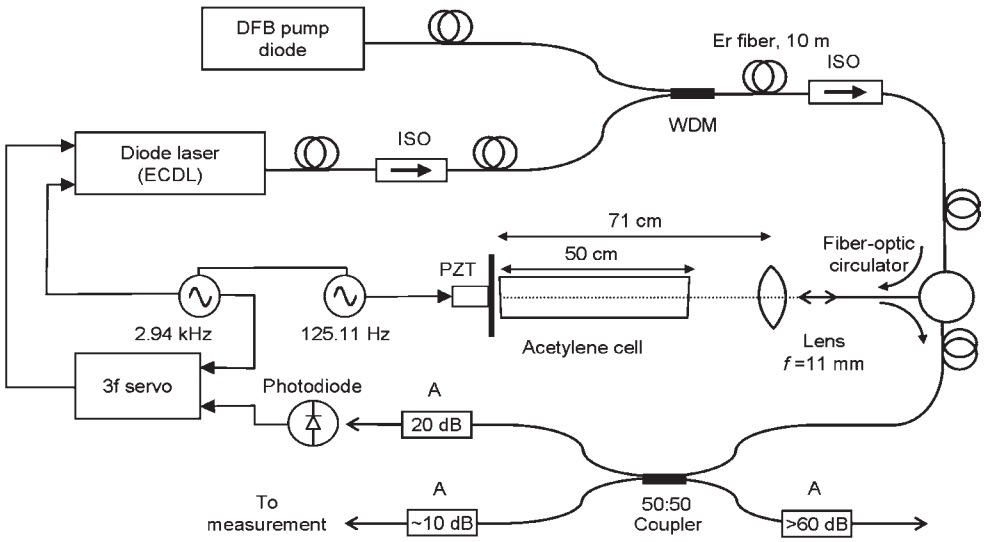

Fig. 1. Acetylene-stabilized laser setup (A: fiber-optic attenuator; ISO: fiber-optic isolator; PZT: piezoelectric transducer; WDM: wavelength-division multiplexer).

back into the fiber. The collimation of the beam was carefully adjusted to locate the beam waist at the end mirror right behind the acetylene cell. A lens with a relatively long focal length is employed to maximize the Rayleigh range of the Gaussian beam and thus minimize the curvature of field along the free-space beam traveling inside the acetylene cell. This is important for the minimization of the frequency shifts of the saturated absorption signal due to the angular mismatch of the wave fronts traveling in opposite directions [21]. Optimization of the waist position was done by maximizing the amount of light coupled back to the fiber. When positioned at a distance of 71 cm from the collimation lens, the $1/e^2$ diameter of the waist is approximately 0.7 mm. This leads to a one-way power density of 26 W/cm^2 at the waist with 100 mW of optical power.

After going through the circulator, the probe signal is divided with a 2×2 fiber coupler having a $50:50$ splitting ratio. One output arm directs the signal to the frequency measurement arrangement, and the other arm directs to an InGaAs photodiode for frequency locking. Attenuation is added to the output arms to reduce the intensity of the signal to a level suitable for detection and to suppress the reflections from the open fiber ends. The unused input arm of the coupler has been terminated with more than 60 dB of one-way attenuation to avoid any effects caused by reflection from its open end.

Great care was taken to avoid reflections from the optical interfaces in the setup. To achieve this, the fiber–fiber connections were done using a fusion splicer, except at the output of the ECDL, where angled physical contact fiber optic connectors (FC/APC) were used as the fiber pigtail was too short for welding. Coupling to free space is also done using FC/APC connectors.

The residual reflection from the open end of the fiber at the acetylene cell is on the order of 10^{-4}, which is enough to cause approximately 1% interference term in the detected signal.

To cancel the interference through averaging at a time scale that is suitable for frequency stabilization, the mirror used to reflect the pump beam is dithered with a piezoelectric transducer (PZT). The mirror is moved 3 μm peak to peak,

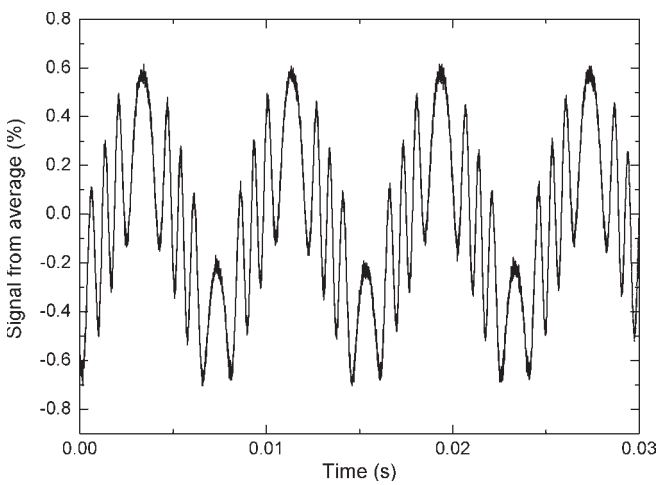

Fig. 2. High-pass-filtered signal from the photodiode amplifier when the end mirror at the spectroscopy arrangement is dithered with a PZT.

which corresponds to several interference maxima and minima, leading to an effective multiplication of the dithering frequency. The dithering frequency of the mirror (125.11 Hz), the modulation frequency of the laser (2.94 kHz), and the time constant of the lock-in amplifier (3 ms) have been selected in such a way that the signal arising from dithered interference is sufficiently averaged, whereas the time constant is still short enough for frequency stabilization. In fact, the dithering frequency is synchronized to the modulation frequency, and their ratio has been chosen to be exactly a half-integer to avoid shifting the harmonics of the dither frequency to the detection band of the lock-in amplifier. Fig. 2 shows the high-pass-filtered signal from the photodiode amplifier, when the amplitude of the mirror movement is tuned to provide a local maximum for the interference suppression. Several interference fringes are seen in the course of a dither cycle. The movement of the mirror causes a small amplitude modulation to the signal, but as it is not frequency dependent, it does not show up at the phase-sensitive detection. Using this method, interference is suppressed by more than two orders of magnitude.

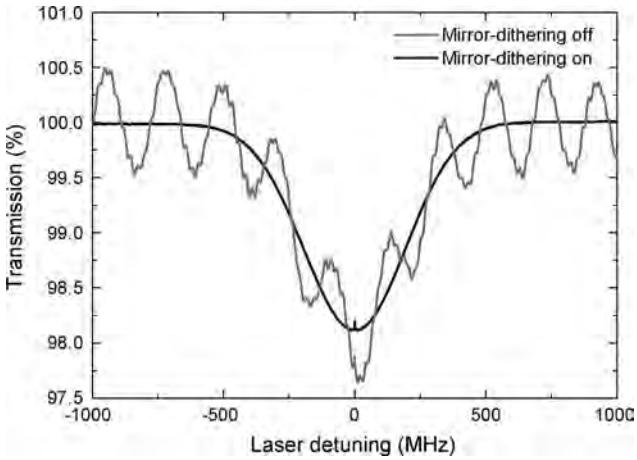

Fig. 3. Unmodulated laser tuned over the Doppler-broadened transition of the P(16) line in the $(\nu_1 + \nu_3)$ band of $^{13}C_2H_2$ (gray) when the end mirror is not dithered and (black) when dithering of the end mirror is applied. The laser power used was 100 mW. (Note: Due to the low-pass filtering, the strength of the Lamb dip shown here is slightly lower than its true value.)

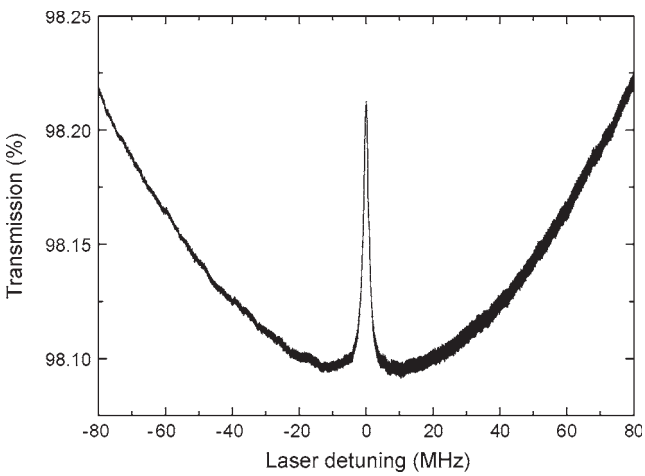

Fig. 4. Unmodulated laser tuned over the Doppler-free transition of the P(16) line in the $(\nu_1 + \nu_3)$ band of $^{13}C_2H_2$. The laser power used was 100 mW.

We have recorded the Doppler-broadened transition of the P(16) of $^{13}C_2H_2$ at the $(\nu_1 + \nu_3)$ band from the low-pass filtered output of the photodiode amplifier by tuning the frequency of the unmodulated laser over the resonance. In the measurements, 100 mW of laser power was used. In Fig. 3, the graph in gray shows the result of the measurement when the end mirror is not dithered. The interference arising from the spurious reflections clearly dominates the signal. The graph in black shows the result of a similar measurement when mirror dithering is applied. The result shows approximately 2% absorption of the line. The strength of the Lamb dip seen at the middle is slightly reduced from its true value due to low-pass filtering.

The true shape of the Lamb dip is shown in Fig. 4, which shows the result of a measurement in which the unmodulated laser was slowly tuned over the Doppler-free transition of the P(16) line.

The strength of the Lamb dip is about $1.2 \cdot 10^{-3}$ of the total intensity incident on the detector and $6.3 \cdot 10^{-2}$ of the peak of the Doppler-broadened absorption. The full-width at half-maximum linewidth of the Lamb dip is 1.9 MHz. The

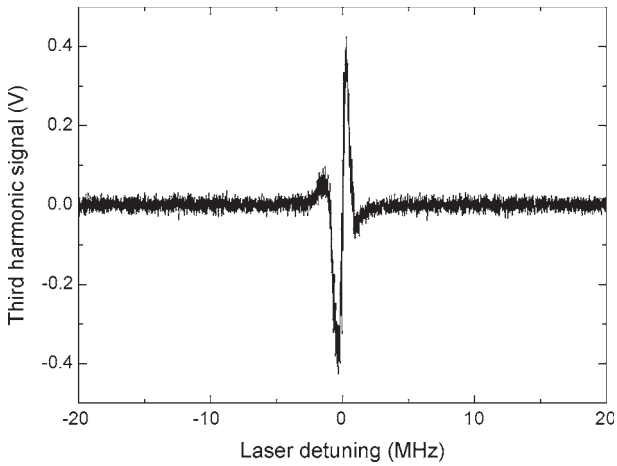

Fig. 5. Third-harmonic signal when the laser frequency was tuned over the P(16) line. The laser was modulated at 2.94 kHz, with a modulation amplitude of (1.0 ± 0.2) MHz peak to peak.

width of the resonance is dominated by the laser linewidth and transit time broadening of approximately 600 kHz arising from the 0.7-mm waist of the pump beam. Other contributions to the width of the resonance arise from the power and pressure broadening.

Fig. 5 shows the third harmonic of the signal recorded from the output of the lock-in amplifier (SRS SR830), when the modulated laser frequency is swept 0.7 MHz/s over the P(16) line. The laser is modulated at 2.94 kHz with a modulation amplitude of (1.0 ± 0.2) MHz peak to peak. (The uncertainty of the modulation amplitude is limited by the measurement and not the instability of the modulation depth.) The laser power was 100 mW, and the time constant of the lock-in amplifier was set to 3 ms. No additional filtering for data acquisition was used. Using the same operating parameters, it is possible to stabilize the laser to the lines between P(1) and P(28) at the $(\nu_1 + \nu_3)$ band using a simple proportional–integral servo.

III. Absolute Optical Frequency Measurement

The absolute frequency measurements of the stabilized laser were performed using MIKES's Ti:S laser OFCG [22] referenced to an active H-maser (Kvarz CH1-75A). The nominal repetition rate of the MIKES OFCG is 1 GHz, and the output spectrum covers the wavelength range from approximately 500 to 1150 nm.

The experimental arrangement for the absolute frequency measurement is shown in Fig. 6. The output of the acetylene-stabilized laser was amplified with a polarization-maintaining fiber amplifier (Pritel, PMFA-27) to 250 mW and frequency doubled using a fiber-pigtailed periodically poled lithium niobate (PPLN) waveguide device (HC-Photonics). The poling of the waveguide has a chirped structure along the length of the 30-mm-long chip, allowing a wide phase-matched bandwidth without any adjustment of the chip. The device provides approximately 1 mW of power at the second harmonic when 250 mW of the power within the wavelength range of 1530–1570 nm is taken to its input.

To achieve a comb spectrum that would simultaneously provide a reasonably good signal-to-noise ratio (SNR) for the

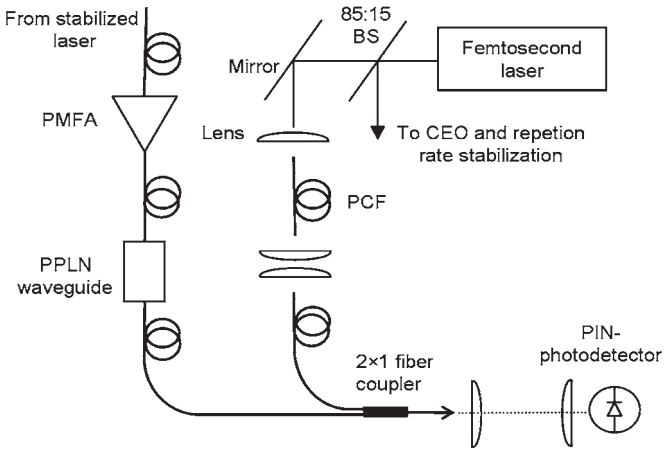

Fig. 6. Experimental arrangement for the absolute frequency measurements of the acetylene-stabilized laser (BS: beam splitter; PCF: photonic crystal fiber; PMFA: polarization-maintaining fiber amplifier; PPLN: periodically poled lithium niobate).

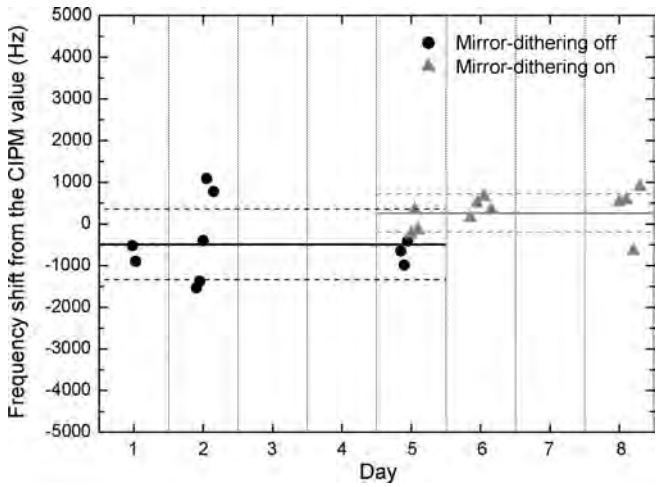

Fig. 7. Absolute frequency measurements of the laser stabilized to the P(16) line of $^{13}C_2H_2$ at the $(\nu_1 + \nu_3)$ band. (Black dot) Measurements without dithering the end mirror at the acetylene cell. (Gray triangle) Measurements with mirror dithering. (Solid line) Average value and (dashed line) standard deviation (one sigma) of the corresponding set of measurements.

comb's carrier-envelope-offset (CEO) determination and for the beat-note signal in the absolute frequency measurements of the acetylene-stabilized laser, the OFCG was slightly modified from its earlier configuration. A mirror that was used to direct the output of the femtosecond laser to the CEO frequency and repetition rate stabilization was replaced with a beam splitter. In the new configuration, 85% of the power is directed to the comb stabilization, and 15% is transmitted through the beam splitter and directed to a 0.15-m-long piece of photonic crystal fiber (PCF) (Crystal Fibre, NL-2.3-790-02) specifically selected for this measurement. This fiber has zero dispersion at 790 nm and broadens the laser spectrum so that sufficient power is available at 770 nm.

The beat frequency arrangement is realized using a 2×1 single-mode fiber coupler and a p-i-n photodiode. A beat note with an SNR of more than 30 dB at a bandwidth of 300 kHz was routinely achieved. This is sufficient for reliable counting when filtered with a relatively narrow bandpass filter.

IV. Result

We performed several sets of absolute frequency measurement with the OFCG to characterize the acetylene-stabilized laser system. The systematic shifts as a function of modulation amplitude and laser power were investigated. The pressure dependence was estimated based on a previously published value for the pressure shift of acetylene. The frequency repeatability and stability of the system were evaluated by performing frequency measurements of the laser locked to the P(16) line over a period of one week. Altogether, we determined the absolute frequency of the laser locked to five different lines of $^{13}C_2H_2$ at the $(\nu_1 + \nu_3)$ band.

A. Laser Frequency Parameter Dependence

The sensitivity of this system to the change in modulation amplitude was determined by performing several 100-s-long absolute frequency measurements of the P(16) line with eight different modulation amplitudes ranging from 0.6 to 3.2 MHz. A least-square fit to these measurements showed a (-3.1 ± 0.1)-kHz/MHz dependence.

The frequency dependence on the laser power was investigated within the range of 70–110 mW. The measured dependence is (1 ± 3) Hz/mW and is found to be negligible, compared with the standard deviation of the measurements under fixed conditions.

With our sealed acetylene cell, we could not investigate the pressure dependence. The pressure shift of (-1.7 ± 0.2) kHz/Pa of the P(16) line is estimated from [7].

B. Frequency Repeatability

To study frequency repeatability, we performed a series of absolute frequency measurements for five days over a period of a week on the laser stabilized to the P(16) line of $^{13}C_2H_2$ at the $(\nu_1 + \nu_3)$ band. The duration of the measurements in the series was between 350 and 5000 s long. The modulation amplitude in these measurements was (1.0 ± 0.2) MHz, and the laser power varied between 70 and 100 mW. The temperature of the laboratory was within (20.15 ± 0.1) °C 90% of the measurement time.

Fig. 7 shows the averaged results of the measurements with respect to the CIPM-recommended value. The results have been corrected for the pressure shift to correspond to the CIPM value reported for 3-Pa cell pressure. The laser was relocked before each set of measurements. The measurements taken on the first three days and marked with black dots were obtained without the dithering of the end mirror in the spectroscopy setup, whereas the latter measurements marked with gray triangles were obtained with mirror dithering applied. The standard error of each measurement is less than 100 Hz and, thus, is not shown in the figure. The solid lines represent the averages of the two data sets, and the dashed lines represent the corresponding standard deviations of the averaged frequency measurements (one sigma). The average value for the first set of measurements is 490 Hz below the CIPM value, and that for the latter set is 260 Hz above the CIPM value. The standard deviation of the

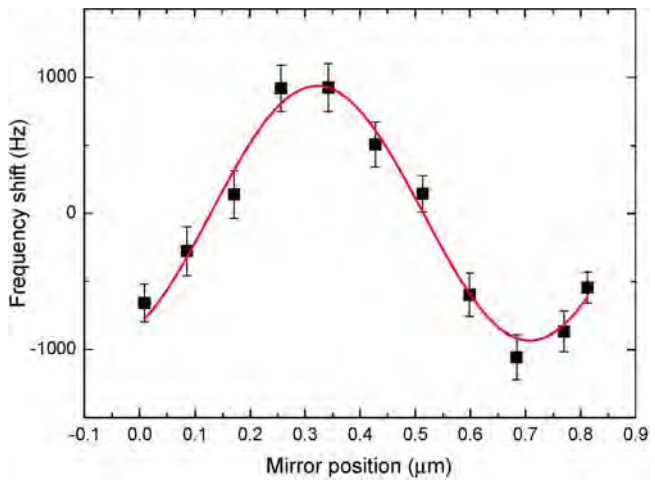

Fig. 8. Measured frequency shift of the laser lock point as a function of the end mirror position.

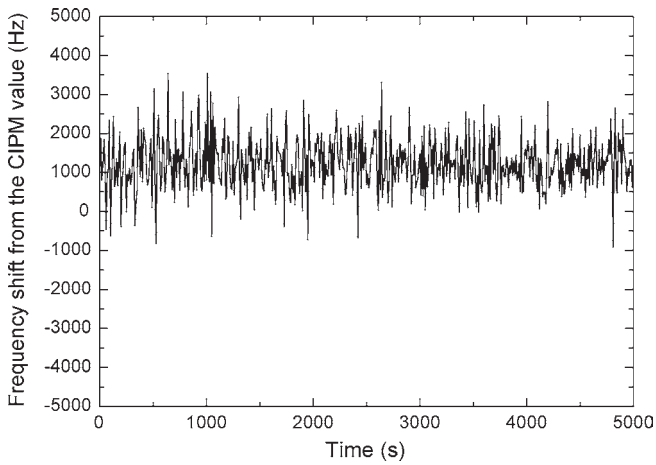

Fig. 9. Typical absolute frequency measurement of the laser stabilized to the P(16) line of $^{13}C_2H_2$ at the $(\nu_1 + \nu_3)$ band. A gate time of 10 s was used.

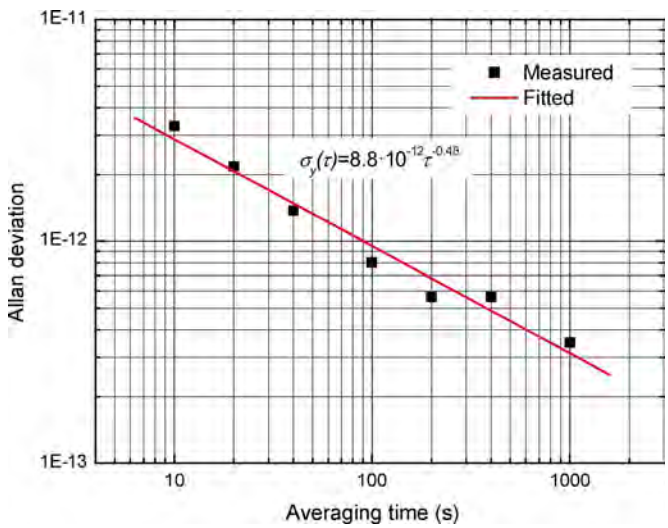

Fig. 10. Typical Allan deviation of the frequency measurements of the P(16) line.

measurements without mirror dithering is 840 Hz, which is almost twice the 450-Hz standard deviation of the measurements when mirror dithering is applied. We address the difference on the magnitude of deviations due to interference, which is effectively canceled out when the end mirror is dithered.

The discrepancy between the averages of the two sets of measurements is also likely caused by interference. Although the effect is basically random, the stable laboratory conditions induce correlation between the successive measurements biasing the data when the mirror is not dithered. Another factor possibly affecting the discrepancy could be the slight change in alignment of the setup due to the introduction of mirror dithering.

The effect of interference was studied in more detail by measuring the frequency of the locked laser as a function of the mirror position over one interference fringe. In Fig. 8, a sine function is fitted to the measurement results. A clear dependence of the laser's lock point to the phase of the reflected light can be observed. The figure shows that the frequency shift due to the interference is $\pm$900 kHz. All the results presented in the succeeding sections have been obtained while utilizing the mirror-dithering technique.

C. Frequency Stability

Fig. 9 shows the result of a typical 5000-s-long absolute frequency measurement of the laser locked to the P(16) line. No bad data points have been removed. The measurement points were taken with a 10-s gate time.

Fig. 10 shows a typical Allan deviation of the frequency measurements of the P(16) line. The Allan deviation indicates that the laser has white frequency noise at least up to an integration time of 1000 s. At 1000 s integration time, a relative frequency stability of $3.2 \cdot 10^{-13}$ is reached.

D. Absolute Frequencies of the Measured $^{13}C_2H_2$ Transitions

The absolute frequency of the P(16) line converted to correspond to the 3-Pa cell pressure was determined to be $(194\,369\,569\,384.3 \pm 1.8)$ kHz based on the measurements shown in Fig. 7 (gray). The standard uncertainty of 1.8 kHz (one sigma) is a conservative estimate based on the repeatability of the measurements, uncertainty of the modulation amplitude, and uncertainty of the cell pressure. Frequency shifts due to changes in alignment have also been taken into account in the uncertainty estimate.

In addition to the absolute frequency of the P(16) line, we measured the absolute frequencies of lines P(10), P(11), P(14), and P(15) to allow a comparison with previously published values [9], [10], [13], [14]. The operating parameters used were the same as those described in Section IV-B. The results of these measurements are summarized in Table I. The absolute frequencies reported are averages of the two sets of measurements that are 350–850-s long at 2.8-Pa cell pressure. All the results are in good agreement with the values recommended by the CIPM.

V. Conclusion

In this paper, we have described an acetylene-stabilized laser, based on standard components used in fiber-optic telecommunication networks. A simple pump–probe geometry in spectroscopic arrangement was found to be sufficient for locking the laser to various transitions in the $(\nu_1+\nu_3)$ band of $^{13}C_2H_2$.

TABLE I
ABSOLUTE FREQUENCIES OF LASER LOCKED TO FOUR TRANSITIONS OF $^{13}C_2H_2$

$^{13}C_2H_2$ transition	Frequency (kHz)	u_c (kHz)	Difference from the CIPM value (kHz)
P(15)	194446632391.8	1.8	0.8
P(14)	194523020608.7	1.8	-1.3
P(11)	194748141655.4	1.8	-0.6
P(10)	194821826415.7	1.8	-0.3

The determined absolute frequencies for five transitions were in agreement with the values recommended by the CIPM and have been measured with an uncertainty of less than 3.6 kHz $(k=2)$. To improve the repeatability of the measurements through interference cancelation, the mirror used to back reflect the pump beam as the probe was position dithered. Although it is vital in the fiber-based laser, the same idea can conceivably also be used to improve the long-term stability of other types of stabilized lasers through the reduction of slowly varying frequency-dependent intensity changes caused by interference.

The results demonstrate that a frequency-stabilized laser with a relatively straightforward fiber-based design can be used as an accurate frequency standard at the telecommunication wavelengths. In addition, the approach taken here provides a potential for developing compact and portable optical frequency standards for applications in the telecommunications industry.

ACKNOWLEDGMENT

The authors would like to thank T. Hieta for experimental help with the fiber optics.

REFERENCES

[1] M. de Labachelerie, K. Nakagawa, and M. Ohtsu, "Ultranarrow $^{13}C_2H_2$ saturated-absorption lines at 1.5 μm," *Opt. Lett.*, vol. 19, no. 11, pp. 840–842, Jun. 1994.

[2] M. de Labachelerie, K. Nakagawa, Y. Awaji, and M. Ohtsu, "High-frequency-stability laser at 1.5 μm using Doppler-free molecular lines," *Opt. Lett.*, vol. 20, no. 6, pp. 572–574, Mar. 1995.

[3] K. Nakagawa, M. de Labachelerie, Y. Awaji, and M. Kourogi, "Accurate optical frequency atlas of the 1.5-μm bands of acetylene," *J. Opt. Soc. Amer. B, Opt. Phys.*, vol. 13, no. 12, pp. 2708–2714, Dec. 1996.

[4] A. Onae, K. Okumura, Y. Miki, T. Kurosawa, E. Sakuma, J. Yoda, and K. Nakagawa, "Saturation spectroscopy of an acetylene molecule in the 1550 nm region using an erbium doped fiber amplifier," *Opt. Commun.*, vol. 142, no. 1–3, pp. 41–44, Oct. 1997.

[5] A. Onae, K. Okumura, J. Yoda, K. Nakagawa, A. Yamaguchi, M. Kourogi, K. Imai, and B. Widiyatomoko, "Toward an accurate frequency standard at 1.5 μm based on the acetylene overtone band transition," *IEEE Trans. Instrum. Meas.*, vol. 48, no. 2, pp. 563–566, Apr. 1999.

[6] F.-L. Hong, A. Onae, J. Jiang, R. Guo, H. Inaba, K. Minoshima, T. R. Schibli, H. Matsumoto, and K. Nakagawa, "Absolute frequency measurement of an acetylene-stabilized laser at 1542 nm," *Opt. Lett.*, vol. 28, no. 23, pp. 2324–2326, Dec. 2003.

[7] A. Czajkowski, A. A. Madej, and P. Dubé, "Development and study of a 1.5 μm optical frequency standard referenced to the P(16) saturated absorption line in the $(\nu_1+\nu_3)$ overtone band of $^{13}C_2H_2$," *Opt. Commun.*, vol. 234, no. 1–6, pp. 259–268, Apr. 2004.

[8] J. Jiang, A. Onae, H. Matsumoto, and F.-L. Hong, "Frequency measurement of acetylene-stabilized lasers using a femtosecond optical comb without carrier-envelope offset frequency control," *Opt. Express*, vol. 13, no. 6, pp. 1958–1965, Mar. 2005.

[9] A. Czajkowski, J. E. Bernard, A. A. Madej, and R. S. Windeler, "Absolute frequency measurement of acetylene transitions in the region of 1540 nm," *Appl. Phys. B, Lasers Opt.*, vol. 79, no. 1, pp. 45–50, Jul. 2004.

[10] C. S. Edwards, H. S. Margolis, G. P. Barwood, S. N. Lea, P. Gill, and W. R. C. Rowley, "High-accuracy frequency atlas of $^{13}C_2H_2$ in the 1.5 μm region," *Appl. Phys. B, Lasers Opt.*, vol. 80, no. 8, pp. 977–983, Jun. 2005.

[11] K. Nakagawa, Y. Sato, M. Musha, and K. Ueda, "Modulation-free acetylene-stabilized lasers at 1542 nm using modulation transfer spectroscopy," *Appl. Phys. B, Lasers Opt.*, vol. 80, no. 4/5, pp. 479–482, Apr. 2005.

[12] C. S. Edwards, G. P. Barwood, H. S. Margolis, P. Gill, and W. R. C. Rowley, "High-precision frequency measurements of the $\nu_1+\nu_3$ combination band of $^{12}C_2H_2$ in the 1.5 μm region," *J. Mol. Spectrosc.*, vol. 234, no. 1, pp. 143–148, 2005.

[13] P. Balling, M. Fischer, P. Kubina, and R. Holzwarth, "Absolute frequency measurement of wavelength standard at 1542 nm: Acetylene stabilized DFB laser," *Opt. Express*, vol. 13, no. 23, pp. 9196–9201, Nov. 2005.

[14] A. A. Madej, J. E. Bernard, A. J. Alcock, A. Czajkowski, and S. Chepurov, "Accurate absolute frequencies of the $(\nu_1+\nu_3)$ band of $^{13}C_2H_2$ determined using an infrared mode-locked Cr:YAG laser frequency comb," *J. Opt. Soc. Amer. B, Opt. Phys.*, vol. 23, no. 4, pp. 741–749, Apr. 2006.

[15] H. S. Moon, W.-K. Lee, and H.-S. Suh, "Absolute-frequency measurement of an acetylene-stabilized laser locked to the P(16) transition of $^{13}C_2H_2$ using an optical-frequency comb," *IEEE Trans. Instrum. Meas.*, vol. 56, no. 2, pp. 509–512, Apr. 2007.

[16] H. Y. Ryu, S. H. Lee, H. S. Moon, and H. S. Suh, "Absolute frequency measurement of an acetylene stabilized laser using a selected single mode from a femtosecond laser fiber comb," *Opt. Express*, vol. 16, no. 5, pp. 2867–2873, Mar. 2008.

[17] R. Felder, "Practical realization of the definition of the metre, including recommended radiations of other optical frequency standards (2003)," *Metrologia*, vol. 42, no. 4, pp. 323–325, Aug. 2005. With revision by the Working Group on the Mise en Pratique (MEP2005).

[18] V. Ahtee, M. Merimaa, and K. Nyholm, "Fiber-based acetylene-stabilized laser," in *CPEM Tech. Dig.*, Jun. 2008, pp. 180–181.

[19] J. A. Silver and A. C. Stanton, "Optical interference fringe reduction in laser absorption experiments," *Appl. Opt.*, vol. 27, no. 10, pp. 1914–1916, May 1988.

[20] M. Kusaba and J. Henningsen, "The $\nu_1+\nu_3$ and the $\nu_1+\nu_2+\nu_4^1+\nu_5^{-1}$ combination bands of $^{13}C_2H_2$. Linestrengths, broadening parameters, and pressure shifts," *J. Mol. Spectrosc.*, vol. 209, no. 2, pp. 216–227, Oct. 2001.

[21] S. E. Park, H. S. Lee, T. Y. Kwon, and H. Cho, "Dispersion-like signals in velocity-selective saturated-absorption spectroscopy," *Opt. Commun.*, vol. 192, no. 1/2, pp. 49–55, May 2001.

[22] M. Merimaa, K. Nyholm, M. Vainio, and A. Lassila, "Traceability of laser frequency calibrations at MIKES," *IEEE Trans. Instrum. Meas.*, vol. 56, no. 2, pp. 500–504, Apr. 2007.

Ville Ahtee was born in Helsinki, Finland, on August 11, 1977. He received the M.Sc. (Tech.) degree from the Helsinki University of Technology (TKK), Espoo, Finland, in 2003.

From 2003 to 2006, he was with the Metrology Research Institute, TKK, as a Researcher, working on optical radiometry and quantum optics. Since 2006, he has been with the Centre for Metrology and Accreditation (MIKES), Espoo. His current research interests include optical frequency metrology and stabilized lasers.

Mikko Merimaa was born in Helsinki, Finland, on November 25, 1972. He received the M.Sc. and Ph.D. degrees from the Helsinki University of Technology, Espoo, Finland, in 1997 and 2001, respectively, both in technology (electrical engineering). His dissertation was on frequency standards based on diode lasers.

After a two-year postdoctoral period at the Helsinki University of Technology, he joined the Centre for Metrology and Accreditation (MIKES), Espoo, where he is currently a Senior Research Scientist. His current research interests include optical frequency metrology and stabilized lasers.

K. Nyholm, photograph and biography not available at the time of publication.

III

Publication III

V. Ahtee, M. Merimaa, and K. Nyholm, "Single-frequency synthesis at telecommunication wavelengths," Opt. Express **17**, 4890–4896 (2009).

Single-frequency synthesis at telecommunication wavelengths

V. Ahtee,[*] M. Merimaa, and K. Nyholm

Centre for Metrology and Accreditation, P.O. Box 9, FI-02151 Espoo, Finland
[*]Corresponding author: ville.ahtee@mikes.fi

Abstract: We report an optical single-frequency synthesizer at the 1.55 μm telecommunications band. Output from a continuous-wave external cavity diode laser is frequency doubled and phase locked to a predetermined component of a Ti:S laser frequency comb. The synthesizer is capable of generating a single user-specified frequency from an atomic time base within the 192–196 THz gain bandwidth of an erbium-doped fiber amplifier. By tuning the repetition rate of the femtosecond laser the synthesized optical frequency can be swept with sub-kilohertz step size. Frequency sweeps of several GHz are realized by automatically re-locking the diode laser to adjacent comb components during frequency sweep. We demonstrate the operation of the device by presenting results of Doppler-free spectroscopy on acetylene using synthesized frequencies.

OCIS codes: (120.3930) Metrological instrumentation; (120.6200) Spectrometers and spectroscopic instrumentation; (140.3600) Lasers, tunable; (300.6320) Spectroscopy, high-resolution

References and links

1. D. J. Jones, S. A. Diddams, J. K. Ranka, A. Stentz, R. S. Windeler, J. L. Hall, and S. T. Cundiff, "Carrier-envelope phase control of femtosecond mode-locked lasers and direct optical frequency synthesis," Science **288**, 635-639 (2000).
2. R. Holzwarth, Th. Udem, T. W. Hänsch, J. C. Knight, W. J. Wadsworth, and P. St. J. Russell, "Optical frequency synthesizer for precision spectroscopy," Phys. Rev. Lett. **85**, 2264-2267 (2000).
3. J. D. Jost, J. L. Hall, and J. Ye, "Continuously tunable, precise, single frequency optical signal generator," Opt. Express **10**, 515-520 (2002).
4. T. R. Schibli, K. Minoshima, F.-L. Hong, H. Inaba, Y. Bitou, A. Onae, and H. Matsumoto, "Phase-locked widely tunable optical single-frequency generator based on a femtosecond comb," Opt. Lett. **30**, 2323-2325 (2005).
5. H. Inaba, T. Ikegami, F.-L. Hong, Y. Bitou, A. Onae, T. R. Schibli, K. Minoshima, and H. Matsumoto, "Doppler-free spectroscopy using a continuous-wave optical frequency synthesizer," Appl. Opt. **45**, 4910-4915 (2006).
6. H. S. Moon, E. B. Kim, S. E. Park, and C. Y. Park, "Selection and amplification of modes of an optical frequency comb using a femtosecond laser injection-locking technique," Appl. Phys. Lett. **89**, 181110 (2006).
7. S. E. Park, E. B. Kim, Y.-H. Park, D. S. Yee, T. Y. Kwon, C. Y. Park, H. S. Moon, and T. H. Yoon, "Sweep optical frequency synthesizer with a distributed-Bragg-reflector laser injection locked by a single component of an optical frequency comb," Opt. Lett. **31**, 3594-3596 (2006).
8. T. M. Fortier, Y. Le Coq, J. E. Stalnaker, D. Ortega, S. A. Diddams, C. W. Oates, and L. Hollberg, "Kilohertz-resolution spectroscopy of cold atoms with an optical frequency comb," Phys. Rev. Lett. **97**, 163905 (2006).
9. Y.-J. Kim, J. Jin, Y. Kim, S. Hyun, and S.-W. Kim, "A wide-range optical frequency generator based on the frequency comb of a femtosecond laser," Opt. Express **16**, 258-264 (2008).
10. H. Y. Ryu, S. H. Lee, W. K. Lee, H. S. Moon, and H. S. Suh, "Absolute frequency measurement of an acetylene stabilized laser using a selected single mode from a femtosecond fiber laser comb," Opt. Express **16**, 2867-2873 (2008).
11. M. Merimaa, K. Nyholm, M. Vainio, and A. Lassila, "Traceability of laser frequency calibrations at MIKES," IEEE Trans. Instrum. Meas. **56**, 500-504 (2007).
12. B. R. Washburn, R. W. Fox, N. R. Newbury, J. W. Nicholson, K. Feder, P. S. Westbrook, and C. G. Jørgensen, "Fiber-laser-based frequency comb with a tunable repetition rate," Opt. Express **12**, 4999-5004 (2004).

#105904 - $15.00 USD Received 5 Jan 2009; revised 26 Feb 2009; accepted 6 Mar 2009; published 13 Mar 2009

13. R. Felder, "Practical realization of the definition of the metre, including recommended radiations of other optical frequency standards (2003)," Metrologia **42**, 323-325 (2005). With revision by the Working Group on the Mise en Pratique (MEP2005).
14. V. Ahtee, M. Merimaa, and K. Nyholm, "Fiber-based acetylene-stabilized laser," IEEE Trans. Instrum. Meas. (In press, doi: 10.1109/TIM.2008.2008476)
15. C. J. Bordé, J. L. Hall, C. V. Kunasz, and D. G. Hummer, "Saturated absorption line shape: Calculation of the transit-time broadening by a perturbation approach," Phys. Rev. A **14**, 236-263 (1976).

1. Introduction

The introduction of a full-octave optical frequency comb generator at the turn of millennium enabled practical absolute optical frequency measurements by providing a direct link between microwave and optical frequencies [1,2]. Since then ever sophisticated optical frequency metrology tools have been developed, one example being continuous-wave (cw) optical frequency synthesizers [3-10]. Such devices are indispensable, as unlike conventional frequency comb generators that produce a multitude of rather weak frequency components, a cw synthesizer provides a single selectable frequency. Such a light source is directly suitable for, e.g., spectroscopy, high precision characterization of optical components, or as a frequency reference in calibration of stabilized lasers.

Here we report on a cw synthesizer capable of generating a single user-specified frequency from an atomic time base on wavelengths around 1.55 μm within the 192–196 THz gain bandwidth of an erbium-doped fiber amplifier (EDFA). This frequency range is important for telecommunication networks as most of the long-haul data transmission takes place on this so called optical C-band due to the convenience provided by EDFAs. The synthesizer also directly provides an output at the second harmonic of these frequencies, i.e., at wavelengths around 775 nm.

The construction and characteristics of the synthesizer are presented below. We demonstrate the operation of the device in an experiment where we have used the synthesizer to conduct Doppler-free spectroscopy on P(16) line of acetylene ($^{13}C_2H_2$) at the $\nu_1+\nu_3$ overtone band.

2. Synthesizer construction

The general structure of the experimental setup resembles that of some radio frequency (rf) synthesizers; an optical frequency comb is used to phase coherently down-convert an optical frequency to the rf-regime, where conventional rf-techniques are employed to phase lock the frequency to a reference using a digital phase-locked loop-circuit (PLL). Figure 1 shows a schematic block diagram of the synthesizer.

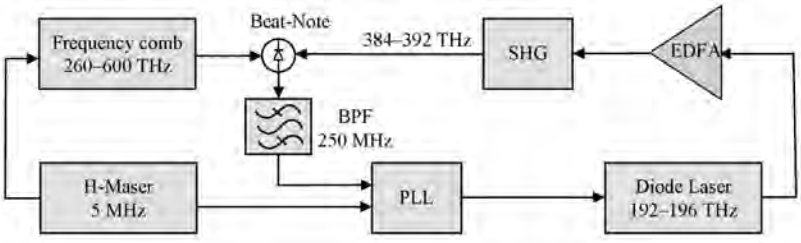

Fig. 1. Schematic block diagram of the optical frequency synthesizer.

A tunable external cavity diode laser (ECDL) (Photonetics Tunics-PRI) provides >5 mW of output power over the 192–196 THz gain bandwidth of an EDFA. The signal is amplified with a polarization maintaining EDFA (Pritel PMFA-27) to 250 mW for efficient second harmonic generation (SHG). The frequency-doubled signal is heterodyned with a predetermined component of an optical frequency comb generator, whose repetition rate and carrier-envelope-offset (CEO) are referenced to a hydrogen-maser (Kvarz CH1-75A). The resulting beat-note frequency is band-pass filtered and fed to a H-maser referenced digital

#105904 - $15.00 USD Received 5 Jan 2009; revised 26 Feb 2009; accepted 6 Mar 2009; published 13 Mar 2009

PLL-circuit, which phase locks the ECDL frequency to the comb output, and hence, to the H-maser.

The optical frequency comb generator is based on a Kerr-lens mode-locked Ti:S laser with 1 GHz repetition rate and its offset frequency is stabilized using self-referencing [11]. The output spectrum of the frequency comb generator extending from 500 nm to 1150 nm is relatively strongly structured and exhibits several minima 15 – 35 dB below the highest power spectral density. Unfortunately, the original configuration had a power minimum at 770 nm around which the spectral power was found to be too low to obtain sufficient beat-note signal for reliable phase locking. Because of this, 15 % of the output power of the Ti:S-laser is taken to a microstructure fiber (Crystal Fibre, NL-2.3-790-02) specifically selected to provide high-intensity output around 775 nm.

The second-harmonic generation of the ECDL is carried out using a fiber-pigtailed periodically poled lithium niobate waveguide (PPLN WG, HC-Photonics). The poling of the device has a chirped structure along the length of the 30 mm long chip, allowing wide phase-matched bandwidth without any adjustment of the chip. The device provides approximately 1 mW of power at the second harmonic when 250 mW of power from the output of the polarization maintaining EDFA is taken to its input.

The beat-frequency signal between the second harmonic signal and the comb is obtained by overlapping the laser modes in a single-mode fiber using a 2×1 fiber coupler. A Si PIN-photodetector is used for detection. A beat-frequency signal with more than 30 dB signal-to-noise ratio (SNR) using a 300-kHz resolution bandwidth is routinely achieved. This is sufficient for reliable phase locking when filtered with a relatively narrow (25 MHz) band-pass filter.

The frequency stability of the synthesizer follows that of the microwave frequency reference [11] for integration times longer than the time constant of the servo-loops. The H-maser used in the experiment has a relative frequency stability of 2×10^{-12} at an integration time of 1 s. Frequency stabilities below 10^{-14} are reached after an integration time of a few hundred seconds. An upper limit for short-term (2 ms) linewidth of the synthesizer was measured to be 800 kHz.

3. Frequency control

Prior to phase locking to the frequency comb, the optical frequency of the ECDL is set approximately to the targeted value. A coarse frequency tuning of the ECDL steps the output frequency with 100-MHz resolution over the entire tuning range. Continuous fine-tuning of the frequency is allowed over about ± 3 GHz range around the coarsely set operating frequency. A calibrated wavelength meter (HP86120B) is used to provide frequency information with an accuracy of 100 MHz.

After the ECDL is set close to the targeted frequency, the comb spectrum is tuned by the repetition rate until the beat-frequency signal appears inside the 25 MHz band of the band-pass filter. Then the PLL is switched on and the frequency of the ECDL attains a value defined by the frequency comb as $(nf_{rep}\pm f_{CEO}\pm f_{beat})/2$ where n is the number of the comb component to which the ECDL is locked. The frequency information from the wavelength meter is sufficient for direct determination of n.

The PLL-block consists of a digital charge pump phase-locked loop circuit (Analog devices, LMX1501A) and an operational amplifier integrator circuit as a loop filter. Digital dividers integrated in the PLL circuit allow phase comparison at kHz level. This ensures sufficient averaging of signal jitter to avoid cycle slips. The feedback to the ECDL is realized by controlling the laser cavity with a piezoelectric actuator.

The locking range at the output of the integrator is limited to ± 5 MHz. Due to the rather narrow locking range, a DC-bias voltage is added to the integrator output using a data acquisition card (NI PCI-6035E) and a summing operational amplifier circuit. The output voltage of the integrator is read to the computer and its deviation from the range center is measured. A corresponding voltage is summed to the control signal for the integrator output voltage to return to the center level. This is needed to compensate slow drifts of the ECDL

#105904 - $15.00 USD Received 5 Jan 2009; revised 26 Feb 2009; accepted 6 Mar 2009; published 13 Mar 2009

locking point during long measurements or when the synthesized frequency is tuned over the range allowed by the integrator output. The frequency sweeps are realized using the approach proposed in Ref. 12. The comb repetition rate is stepped in small increments (δf_f), which steps the frequency of the n^{th} comb component by $n\delta f_r$, and hence, also the second harmonic frequency of the ECDL locked to this component by the same amount. The repetition rate is synthesized from the H-maser with a rf-signal generator (Agilent E4424B), which allows stepping the frequency with millihertz-resolution. When mapped to target optical frequencies (i.e. multiplied by $n/2 \approx 195\,000$), this corresponds to a few hundred hertz resolution.

With our Ti:S-laser based comb the practical tuning range of a single frequency component by the repetition rate is limited to around 1 GHz. To achieve larger frequency sweeps, the second harmonic of the ECDL frequency locked to a certain comb component can be handed-over on the fly to the adjacent component during a sweep. The principle is depicted in Fig. 2. The repetition rate is stepped until the comb component n to which the ECDL is locked reaches the initial position of the adjacent component ($n+1$). Then the repetition rate is set back to the starting value and the PLL locks the laser to this $(n+1)^{th}$ component, after which the sequence can be repeated. Although the lock is momentarily lost during the hand-over process, the DC-bias voltage applied to the output of the PLL loop filter keeps the ECDL-frequency within the locking range in respect to the $(n+1)^{th}$ component. The speed of the sweep is mainly limited by a few hundred millisecond settling time of the PLL after each frequency step. With this approach the synthesized frequency can be swept over 6 GHz, which is the range allowed by the ECDL fine-tuning. However, frequency sweeps over several THz would be possible in principle.

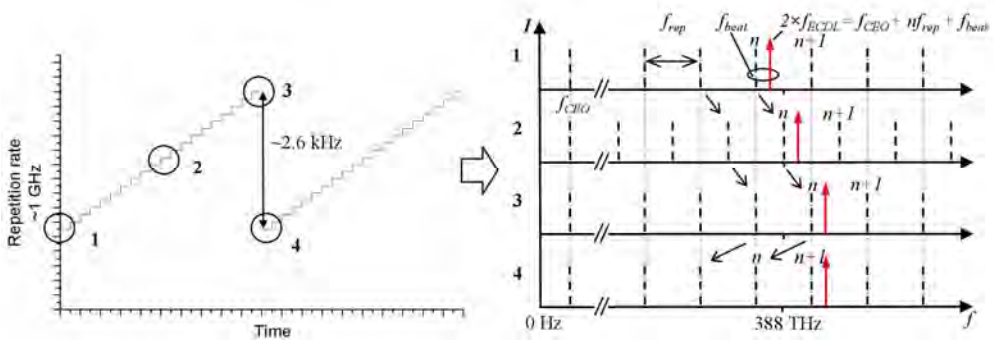

Fig. 2. Tuning of the synthesized frequency. The left part of the figure illustrates the stepping of the repetition rate and the right part that of the optical frequencies. 1) The second harmonic of the synthesized frequency is locked to the n^{th} frequency component of the comb. 2-3) By stepping the repetition rate, the n^{th} component is shifted to the initial position of the $(n+1)^{th}$ component. 4) The repetition rate is set back to the start value and the synthesizer locks to the $(n+1)^{th}$ component.

4. Doppler-free spectroscopy on acetylene

We demonstrate the operation of the synthesizer by using it for Doppler-free spectroscopy of acetylene. We studied the P(16) line of $^{13}C_2H_2$ at the $\nu_1+\nu_3$ overtone band, which serves as a wavelength reference at 1.54 μm [13]. The experimental arrangement is realized using a slightly modified version of a fiber-based setup that we have previously applied with our acetylene-stabilized laser scheme [14].

4.1. Setup

Figure 3 shows a general structure of the complete measurement arrangement. The spectroscopy setup is connected to the synthesizer between the ECDL output and the EDFA input. In the figure, the blocks that are part of the synthesizer are shaded in gray whereas the blocks belonging specifically for the acetylene measurement are unshaded. As the details of the spectroscopy setup are given in Ref. 14, we give here only a brief description.

#105904 - $15.00 USD Received 5 Jan 2009; revised 26 Feb 2009; accepted 6 Mar 2009; published 13 Mar 2009

The output signal from the ECDL is amplified to approximately 125 mW in a 10 meter long erbium-doped fiber, pumped with a distributed feedback (DFB) laser diode at 1480 nm. Fiber-optic isolators are placed at the outputs of the ECDL and the erbium fiber to suppress possible feedbacks. Small amount of power is branched off after the erbium fiber with a 90:10 fiber coupler and taken to a photodiode, which provides a feedback signal to the DFB laser for intensity stabilization. Attenuation is added to the open arms of the fiber coupler to reduce the intensity of the signal to a level suitable for detection and to suppress the reflections from the open fiber ends. The rest of the amplified signal is directed to an acetylene cell using a three-port fiber-optic circulator.

The spectroscopic arrangement is realized in a collinear geometry using reflected pump beam to probe the absorption. An aspheric lens at the output of the circulator collimates the pump beam and couples the reflected beam back into the fiber. The collimation of the beam is carefully adjusted in order to locate the beam waist at the end mirror right behind the acetylene cell. The $1/e^2$-diameter of the waist is approximately 0.7 mm. This leads to one-way power density of 19 W/cm^2 at the waist where 75 mW of optical power is left after insertion losses due to the fiber optic components. Pressure in the 50-cm long acetylene cell is 2.8 Pa.

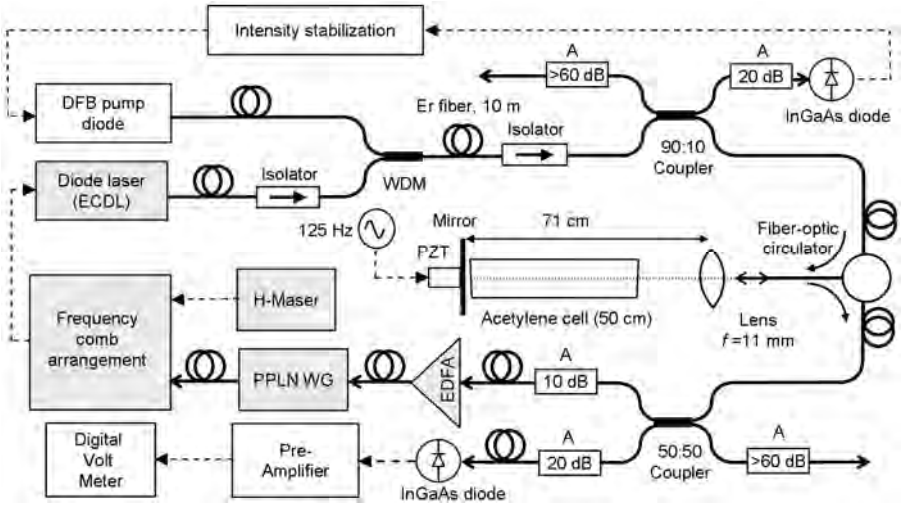

Fig. 3. Experimental arrangement for Doppler-free spectroscopy on acetylene. The blocks that are part of the synthesizer are shaded in gray. A=Attenuation, PZT = piezoelectric transducer, WDM = wavelength division multiplexer.

After going through the circulator the probe signal is divided with a 50:50 fiber coupler. One output arm directs the signal to the synthesizer arrangement and the other arm to a temperature stabilized InGaAs photodiode for detection. As with the first fiber coupler, also here attenuation is added to the output arms of the coupler. The signal from the photodiode is amplified with a low-noise current preamplifier (SR570) and measured with a digital volt meter (Agilent 34410A).

The reflections from the interfaces of the setup are minimized by fusion splicing the fiber connections. However, the inevitable reflection from the open end of the fiber at the acetylene cell, although minimized using an angled fiber connector, is of the order of 10^{-4} and causes approximately one percent interference term in the detected signal. To cancel the interference through averaging, the mirror used to reflect the pump beam is dithered with a piezoelectric transducer. When the signal is appropriately low pass filtered at detection the interference term is effectively averaged out.

4.2. Results

We studied the intensity stability of the measurement system while scanning the frequency. Figure 4(a) shows a result of 23 consecutive measurements where the synthesized frequency

#105904 - $15.00 USD Received 5 Jan 2009; revised 26 Feb 2009; accepted 6 Mar 2009; published 13 Mar 2009

was swept over an 8 MHz frequency range with 100 steps at a region well outside the acetylene absorption. The signal was low pass filtered with 10 Hz band. The delay between successive measurement points within a frequency sweep was 480 ms and at each measurement point the signal was averaged 200 ms. The dead-time between sweeps was typically 30 s, which was needed for sweep initialization. The overall measurement time was 1800 s. The relative standard deviation of the 2300 intensity measurement points is 9×10^{-6}.

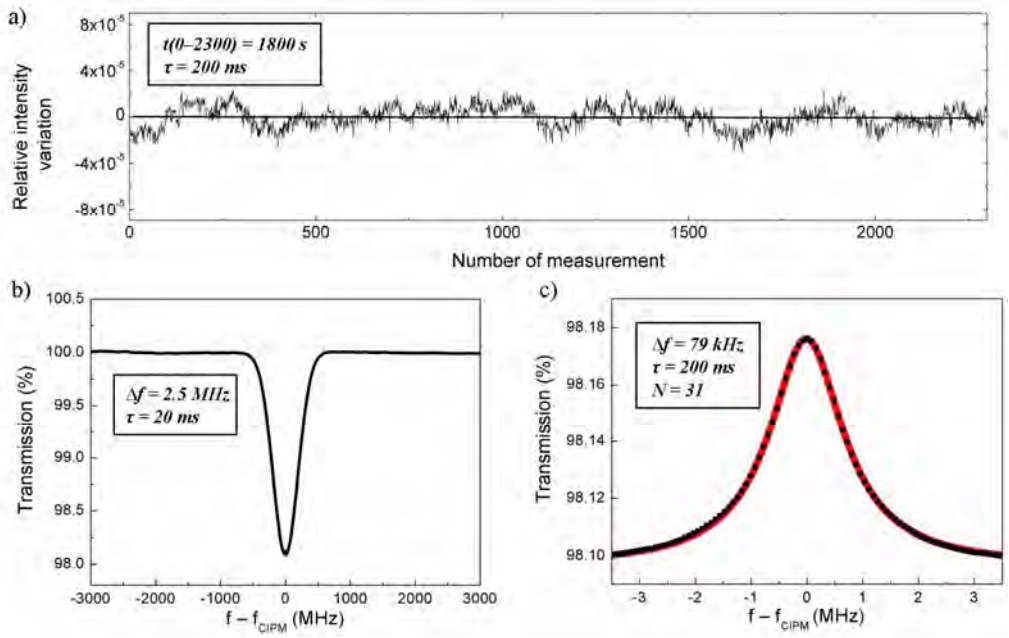

Fig. 4. (a). Intensity stability of the synthesizer: Detected signal from 23 consecutive 8 MHz frequency sweeps each consisting of 100 frequency steps. (b) Doppler-broadened P(16)-transition. (c) Doppler-free line shape of the P(16)-transition. Lorentzian fit (in red) gives a center frequency 9 kHz below the CIPM value. τ = integration time per measurement point, Δf = frequency step size, N = number of averaged frequency sweeps.

Figure 4(b) shows a result of a measurement where the frequency was swept 6 GHz over the Doppler-broadened transition of P(16)-line. The frequency step size was 2.5 MHz. At each measurement point the signal was averaged 20 ms. Due to the frequency resolution, the Doppler-free line shape is not properly shown. Figure 4(c) shows measurement of the Doppler-free line shape at higher resolution. The graph is an average of 31 similar frequency sweeps over the line center. The frequency step is 79 kHz and integration time used at each point is 200 ms. The graphs in Figs. 4(b) and 4(c) are plotted on absolute frequency scale with the scale center at 194 369 569.384 MHz, which is the value adopted by International Committee for Weights and Measures (CIPM) for this transition when measured with the third-harmonic technique using 1-MHz modulation amplitude [13]. A Lorentzian fitted to the Doppler-free line shape gives a center frequency of 9 kHz below the CIPM value. We performed four equivalent sets of measurements over the Doppler-free line shape on two separate days. The standard deviation of the line center frequencies given by Lorentzian fits was 0.8 kHz. The deviation from the CIPM value is assumed to be primarily due to line shape asymmetries arising from imperfections of the beam alignment in the spectroscopic arrangement [15]. This effect can also be observed with stabilized lasers employing the third-harmonic technique. However, in that case the effect is less pronounced as usually only the peak of the line is examined.

#105904 - $15.00 USD Received 5 Jan 2009; revised 26 Feb 2009; accepted 6 Mar 2009; published 13 Mar 2009

5. Conclusion

We have presented an optical single-frequency synthesizer operating within the gain bandwidth of an EDFA. The construction is based on a wavelength tunable ECDL whose output is phase-locked to a predetermined component of a H-maser referenced Ti:S laser frequency comb. The synthesized frequency can be swept over several GHz limited only by the continuous tuning range of the ECDL. In principle, the frequency tuning by adjustment of the Ti:S laser repetition rate combined with the comb component handover process demonstrated here would allow frequency sweeps over the entire gain bandwidth of an EDFA.

We have demonstrated the performance of the synthesizer in high precision spectroscopy on acetylene. The capability of repeating the measurements on absolute frequency scale with the relative intensity stability at 10^{-5} level enabled recording the line shapes with great accuracy. Even a Doppler-free absorption feature, as small as 8×10^{-4} of total detected power, could be observed at high signal-to-noise ratio without modulation techniques. A Lorentzian fit to the result gives a line center frequency of 9 kHz below that of the CIPM recommendation. These values can not, however, be directly compared without further investigation of line shape asymmetries, which might cause a shift to the line center given by the fit. The line shape asymmetries are also a potential source of error when determining the line center frequencies using the conventional third-harmonic technique.

Here we demonstrated sweeping the frequency by frequency comb's repetition rate. An alternative approach could be to vary the comb's offset frequency by altering the pump power. This would leave the Ti:S laser cavity untouched and hence lead to more stable operation during frequency scans. However, the obtainable tuning range would in practice be restricted to less than 100 MHz.

In addition to the applications in spectroscopy, the stabile frequency and intensity properties of the developed system makes the synthesizer directly suitable, e.g., for high precision characterization of components used in optical telecommunications networks or as a frequency reference when calibrating acetylene-stabilized lasers. The output at wavelengths around 775 nm could be useful also in atomic physics experiments.

Acknowledgments

V. Ahtee is grateful for the financial support of the Academy of Finland. The authors would like to thank T. Hieta for experimental help with the fiber optics.

#105904 - $15.00 USD Received 5 Jan 2009; revised 26 Feb 2009; accepted 6 Mar 2009; published 13 Mar 2009

IV

Publication IV

V. Ahtee, M. Merimaa, and K. Nyholm, "Precision spectroscopy of acetylene transitions using an optical frequency synthesizer," Opt. Lett. **34**, 2619–2621 (2009).

Precision spectroscopy of acetylene transitions using an optical frequency synthesizer

V. Ahtee, M. Merimaa, and K. Nyholm*

Centre for Metrology and Accreditation (MIKES), P.O. Box 9, FI-02151 Espoo, Finland
**Corresponding author: kaj.nyholm@mikes.fi*

Received April 17, 2009; revised June 12, 2009; accepted June 29, 2009;
posted July 30, 2009 (Doc. ID 110261); published August 21, 2009

An optical frequency synthesizer is used for saturation spectroscopy of acetylene near 1540 nm. In the synthesizer, a user-specified frequency is generated from an atomic time base by phase locking the second harmonic of a cw near-IR external-cavity diode laser (ECDL) to a Ti:sapphire frequency comb. By stepping the repetition rate of the frequency comb, the ECDL frequency is swept over an acetylene transition in a saturated absorption spectroscopy setup. Hence, a spectral lineshape is measured with an absolute frequency scale. Line-center frequencies determined by fitting theoretical line profiles to the measured data are in good agreement with values measured with the ECDL stabilized to acetylene by third-harmonic locking and with the values recommended by the International Committee for Weights and Measures (CIPM). © 2009 Optical Society of America

OCIS codes: 300.6390, 300.6320, 120.6200.

Optical frequency combs have become invaluable tools in optical frequency metrology, as they produce a multitude of precisely known frequencies over a wide spectrum and thus enable absolute frequency measurements of lasers stabilized to atoms or molecules. Moreover, frequency combs can be used directly for spectroscopy [1]. However, in some applications the low optical power in each comb component and the dense comb structure may hinder direct comb spectroscopy. One way to circumvent this problem is to perform spectroscopy using an optical single-frequency synthesizer. In such a device, a tunable cw laser is electronically phase locked [2,3] or injection locked [4] to a frequency comb. Scans are usually carried out by stepping the comb repetition rate [4], and hence the frequency of the cw laser, or by sweeping the frequency of the cw laser by an electro-optic modulator [3].

In this Letter, we report on saturated absorption spectroscopy of acetylene ($^{13}C_2H_2$) using an optical frequency synthesizer [5]. The good signal-to-noise ratios (SNR) of the recorded spectra allow determination of line centers by fitting theoretical line profiles to the measured data. Thus, information on line-center frequencies that are not shifted by modulation is accessible.

Our synthesizer is based on the idea presented in [2]: to scan a cw laser precisely in frequency by phase locking it to a frequency comb with a tunable repetition rate, except that instead of a fiber-laser comb we use a self-referenced Ti:sapphire (Ti:S) frequency comb (500–1100 nm) to which the second harmonic of a tunable (1520–1600 nm) near-IR external-cavity diode laser (ECDL) is phase locked. In Fig. 1 the experimental setup for saturation spectroscopy of acetylene using our optical frequency synthesizer is shown. Here we describe only the parts that are essential for spectroscopy. More detailed descriptions of the synthesizer and the self-referenced frequency comb can be found in [5,6], respectively.

The repetition rate and the carrier-envelope-offset frequency of the comb are phase locked to a hydrogen maser. In order to phase lock the fiber-coupled ECDL to the frequency comb, its output is amplified in a fiber amplifier (FA) and frequency doubled in a periodically poled lithium niobate waveguide (PPLN WG) with a chirped structure that allows second-harmonic generation over the entire operational range of the fiber amplifier. Direct synthesis of an optical frequency from a time base is achieved when the heterodyne beat note between the second harmonic of the ECDL and the nearest comb component is phase locked to the H-maser. The SNR of this beat note (over 30 dB in 300 kHz resolution bandwidth) when filtered with a 25 MHz bandpass filter allowed reliable phase locking over long time periods.

To perform spectroscopy with an absolute frequency scale, the synthesized frequency is scanned by stepping the comb's repetition rate. As the tuning range of the repetition rate is limited, longer scans were realized by phase locking the ECDL frequency automatically to the next comb line every time the scan of the comb had extended roughly the comb line spacing (~1 GHz) [5]. To minimize intensity

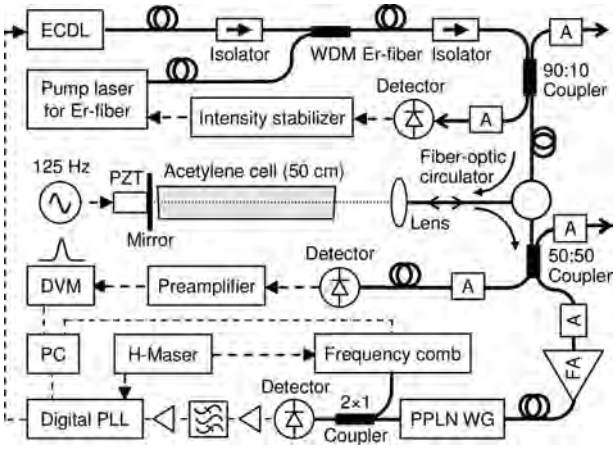

Fig. 1. Experimental setup: A, attenuator; DVM, digital volt meter; PC, computer; PZT, piezoelectric transducer; WDM, wavelength division multiplexer. PLL, phase-locked loop. Other abbreviations defined in text.

changes, part of the light was coupled to an intensity stabilizer that controls the output power of the pump laser for the Er-fiber amplifier.

In the spectroscopy setup, an aspheric lens at the output of a 3-port fiber-optic circulator collimated the pump beam in such a way that the beam waist was located at the end mirror placed right after the acetylene cell (2.8 Pa) and coupled the reflected beam back into the fiber. The one-way power density was 19 W/cm^2 at the waist. The collimation was carefully optimized by maximizing the amount of light coupled back into the fiber, in order to minimize frequency shifts due to the angular mismatch of two wavefronts [7,8]. The probe beam was produced by retroreflecting the pump beam and detected with a temperature-stabilized InGaAs photodiode. Interference arising mainly from the retroreflecting mirror and the output end of the circulator was suppressed more than 2 orders of magnitude by dithering the optical path length with a piezoelectric transducer attached to the mirror [9]. Other reflections were minimized by fusion splicing all fiber connections.

Figure 2 shows a scan in 2.5 MHz frequency steps over the Doppler profile of the $P(16)$ line in the $(\nu_1 + \nu_3)$ band of $^{13}C_2H_2$. The inset in Fig. 2, which is a scan over the Lamb dip measured with better resolution (step size 146 kHz), demonstrates the good SNR achievable with our setup. The relative intensity stability of 10^{-5} sets the limit for the minimum detectable signal. In Fig. 3 is shown a measured saturated absorption spectrum of the $P(16)$ line together with fitted line profiles. The 7-MHz-wide spectrum is an average of 34 frequency scans in which the step size was ~79 kHz and the signal was integrated for 200 ms at each point. A Gaussian fit to the measured Doppler profile of Fig. 2 is removed from the spectrum before fitting. The Doppler-free linewidth (FWHM) of the $P(16)$ line determined from four such measurement series was (1599±6) kHz resulting from a Lorentzian laser line, 0.5 MHz transit-time broadening, and ~0.3 MHz pressure broadening. The 2 ms linewidth of the free-running ECDL is 0.8 MHz. However, in the measurements the laser line was slightly broader due to low frequency acoustic disturbances.

Although the Lorentzian fit appears indistinguishable from the measured data, a closer investigation of

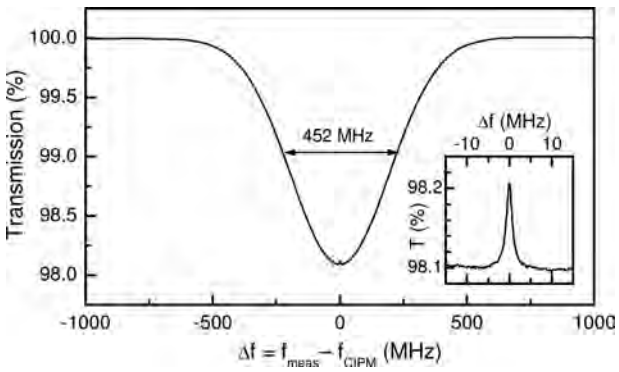

Fig. 2. Scan over the $P(16)$ line. The inset is a scan with better resolution over the Lamb dip.

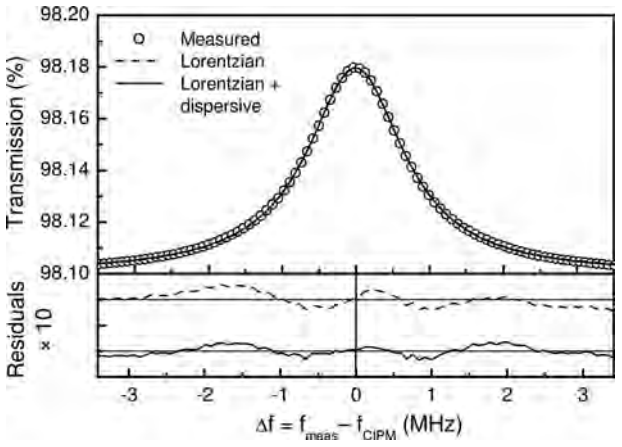

Fig. 3. (a) Measured $P(16)$ line (circles), a Lorentzian fit (dashed curve), Lorentzian+dispersive fit (solid curve). (b) Residuals of the fits respectively, on the same scale but with the residual values multiplied by 10 and shifted vertically for clarity. The average of the residuals is one order of magnitude lower for the Lorentzian+dispersive fit.

the residuals reveals a systematic difference between the data and the fit function, indicating an asymmetry in the measured line profile. The asymmetry was present in all studied lines and leads to a shift in the line centers. The average frequency difference between the line centers (determined from altogether nine measurement series on five lines) and the values recommended by the CIPM [10] was (−10.2±1.1) kHz. The asymmetry did not depend on the scan direction and was not due to intensity changes during the scan or improper interference cancellation. This was verified by recording spectral lines in both scan directions and taking scans of the same frequency extent but outside the line.

Thus, the asymmetry origins from other contributions to the line profile, the most important one being the angular mismatch of the pump and probe beam wavefronts [7,8]. Although, the collimation was carefully adjusted, a small angular mismatch may have remained. This can be taken into account by fitting a Lorentzian as well as a dispersive line profile to the data [8]. Figure 3 shows that this fit agrees better with the data, and the shape of the residual curve is now symmetrical. However, the residuals indicate that the signal is still slightly too peaked at the line center for the fit. This might be a result of the increased relative contribution of slow molecules to the signal. When the linewidth is transit-time limited as in our measurements, the saturation becomes inhomogeneous for low pump laser powers and low gas pressures, and the line shape tends towards sharper peaking [7,11]. This deviation from the Lorentzian line shape in saturated absorption signals of acetylene lines has been reported in [12,13]. Hence, by taking into account the effect from slow molecules an even better agreement of the fit may be reached.

The experimental setup in absolute frequency measurements with our acetylene-stabilized laser [9] was essentially the same as in measurements with the optical frequency synthesizer except the following two differences. The detector measuring the saturated absorption signal was used for third-harmonic

Table 1. Measured Frequencies of Five $^{13}C_2H_2$ Lines[a]

Line	Synthesizer f_{synth} (kHz)	$^{13}C_2H_2$-Stab. Laser f_{stab} (kHz)	CIPM Value (kHz)	$f_{synth}-f_{stab}$ (kHz)
$P(10)$	194 821 826 415.9	194 821 826 415.7	194 821 826 416	0.2
$P(11)$	194 748 141 655.5	194 748 141 655.4	194 748 141 656	0.1
$P(14)$	194 523 020 606.4	194 523 020 608.7	194 523 020 610	−2.3
$P(15)$	194 446 632 391.4	194 446 632 391.8	194 446 632 391	−0.4
$P(16)$	194 369 569 382.1	194 369 569 384.2	194 369 569 384	−2.1

[a]Calculated modulation shifts are added to synthesizer frequencies.

detection in stabilization of the ECDL, and instead of locking the second harmonic of the ECDL to the comb, its frequency difference to the nearest comb component was measured. Moreover, we did not realign the spectroscopy part of the setup between these two measurement series. To check that the alignment had not changed we remeasured the absolute frequency of the $P(16)$ line with the acetylene-stabilized laser right after its line shape was measured with the synthesizer. The obtained frequency value 194 369 569 384.2 kHz agrees well with the value reported in [9] and is used in Table 1. Hence, the results of the two methods are comparable, when the shift arising from the 1 MHz modulation amplitude of the stabilized laser is taken into account.

This can be done either by extrapolating to zero modulation amplitude using a known modulation shift or by calculating the shift to the third-harmonic signal using the 1 MHz modulation amplitude and the asymmetric line shape from the fit with Lorentzian and dispersive profiles. As the modulation shift was known only for the $P(16)$ line [9], we used the latter method. We also determined the shifts using MATLAB/Simulink for simulating third-harmonic locking to the asymmetric lines with the same lock-in amplifier parameters that were used in the actual acetylene-stabilized laser measurements. The two methods gave essentially the same frequency shifts (within 0.2 kHz). The obtained shift (-3.6 ± 0.9) kHz for the $P(16)$ line (an average from four measurement series performed in two days) agrees with the measured shift of (-3.1 ± 0.1) kHz/MHz for modulation amplitudes between 0.6 MHz and 3.2 MHz.

In Table 1 are listed line-center frequencies determined from averaged spectral lines (typically averages of ~30 scans) measured with the optical frequency synthesizer, frequencies measured with our acetylene-stabilized laser [9], and the values recommended by the CIPM [10]. The calculated modulation shifts due to the line asymmetry are added to the frequencies obtained by the synthesizer in order to compare them with the other values that are reported for third-harmonic detection with 1 MHz modulation amplitude. The line-center frequency for the $P(16)$ line determined by the optical frequency synthesizer is an average of four measurements series with a standard deviation of 1.4 kHz. This value is a reasonable uncertainty estimate for all measured lines, as the SNR in detection dominates the uncertainty budget. All the frequencies are within the standard uncertainty of 5 kHz given for the CIPM values.

In summary, we have performed precision absorption spectroscopy of saturated acetylene line shapes using an optical frequency synthesizer. The high SNR of the recorded spectra allowed determination of line-center frequencies that are not shifted by modulation apparent in methods based on lasers locked to the line center. The line-center frequencies were in excellent agreement with the frequencies obtained with our acetylene-stabilized laser and with the CIPM values. The calculated modulation shift of the $P(16)$ line agreed with the shift determined from acetylene-stabilized laser measurements. The spectroscopic applications of our synthesizer are not limited to the near IR. By using suitable tunable lasers spectroscopy can, in principle, be performed anywhere in the wavelength range of the comb.

The work was financially supported by the Academy of Finland (grant 214128).

References

1. M. C. Stowe, M. J. Thorpe, A. Péer, J. Ye, J. E. Stalnaker, V. Gerginov, and S. A. Diddams, Adv. At. Mol. Opt. Phys. **55**, 1 (2008), and references therein.
2. B. Washburn, R. Fox, N. Newbury, J. Nicholson, K. Feder, P. Westbrook, and C. Jørgensen, Opt. Express **12**, 4999 (2004).
3. H. Inaba, T. Ikegami, F.-L. Hong, Y. Bitou, A. Onae, T. R. Schibli, K. Minoshima, and H. Matsumoto, Appl. Opt. **45**, 4910 (2006).
4. S. E. Park, E. B. Kim, Y.-H. Park, D. S. Yee, T. Y. Kwon, C. Y. Park, H. S. Moon, and T. H. Yoon, Opt. Lett. **31**, 3594 (2006).
5. V. Ahtee, M. Merimaa, and K. Nyholm, Opt. Express **17**, 4890 (2009).
6. M. Merimaa, K. Nyholm, M. Vainio, and A. Lassila, IEEE Trans. Instrum. Meas. **56**, 500 (2007).
7. C. J. Bordé, J. L. Hall, C. V. Kunasz, and D. G. Hummer, Phys. Rev. A **14**, 236 (1976).
8. S. E. Park, H. S. Lee, T. Y. Kwon, and H. Cho, Opt. Commun. **192**, 49 (2001).
9. V. Ahtee, M. Merimaa, and K. Nyholm, IEEE Trans. Instrum. Meas. **58**, 1211 (2009).
10. MEP 2005, CIPM recommended values for absorbing molecule $^{13}C_2H_2$, http://www.bipm.org/utils/common/pdf/mep/M-e-P_C2H2_1.54.pdf.
11. Ch. Chardonnet, F. Guernet, G. Charton, and Ch. J. Bordé, Appl. Phys. B **59**, 333 (1994).
12. L.-S. Ma, J. Ye, P. Dube, and J. L. Hall, J. Opt. Soc. Am. B **16**, 2255 (1999).
13. J. Hald, J. C. Petersen, and J. Henningsen, Phys. Rev. Lett. **98**, 213902 (2007).

V

Publication V

R. Lettow, V. Ahtee, R. Pfab, A. Renn, E. Ikonen, S.Götzinger, and V. Sandoghdar, "Realization of two Fourier-limited solid-state single-photon sources," Opt. Express **15**, 15842–15847 (2007).

Realization of two Fourier-limited solid-state single-photon sources

R. Lettow[1], V. Ahtee[1,2], R. Pfab[1], A. Renn[1], E. Ikonen[2], S. Götzinger[1], and V. Sandoghdar[1]

[1]*Laboratory of Physical Chemistry and optETH, ETH Zürich, CH-8093 Zürich, Switzerland*

[2]*Metrology Research Institute, Helsinki University of Technology (TKK) and Centre for Metrology and Accreditation (MIKES), P.O. Box 3000, FI-02015 TKK, Finland*

Stephan.goetzinger@phys.chem.ethz.ch

http://www.nano-optics.ethz.ch

Abstract: We demonstrate two solid-state sources of indistinguishable single photons. High resolution laser spectroscopy and optical microscopy were combined at $T = 1.4\ K$ to identify individual molecules in two independent microscopes. The Stark effect was exploited to shift the transition frequency of a given molecule and thus obtain single photon sources with perfect spectral overlap. Our experimental arrangement sets the ground for the realization of various quantum interference and information processing experiments.

OCIS codes: 270.5585, 270.5290, 300.6280, 180.1790

References and links

1. Ch. Brunel, B. Lounis, Ph. Tamarat, and M. Orrit, "Triggered Source of Single Photons based on Controlled Single Molecule Fluorescence," Phys. Rev. Lett. **83**, 2722-2726 (1999).
2. B. Lounis and W. E. Moerner, "Single photons on demand from a single molecule at room temperature," Nature **407**, 491–493 (2000).
3. P. Michler, A. Kiraz, C. Becher, W. V. Schoenfeld, P. M. Petroff, L. Zhang, E. Hu, and A. Imamoglu, "A Quantum Dot Single-Photon Turnstile Device," Science **290**, 2282–2285 (2000).
4. C. Kurtsiefer, S. Mayer, P. Zarda, and H. Weinfurter, "Stable Solid-State Source of Single Photons," Phys. Rev. Lett. **85**, 290–293 (2000).
5. A. Kuhn, M. Hennrich, and G. Rempe, "Deterministic Single-Photon Source for Distributed Quantum Networking," Phys. Rev. Lett. **89**, 067901 (2002).
6. M. Keller, B. Lange, K. Hayasaka, W. Lange, and H. Walther, "Continuous generation of single photons with controlled waveform in an ion-trap cavity system," Nature **431**, 1075–1078 (2004).
7. E. Waks, K. Inoue, C. Santori, D. Fattal, J. Vuckovic, G. S. Solomon, and Y. Yamamoto, "Secure communication: Quantum cryptography with a photon turnstile," Nature **420**, 762–762 (2002).
8. R. Alleaume, F. Treussart, G. Messin, Y. Dumeige, J.-F. Roch, A. Beveratos, R. Brouri-Tualle, J.-P. Poizat, and P. Grangier, "Experimental open-air quantum key distribution with a single-photon source," New J. Phys. **6**, 92 (2004).
9. E. Knill, R. Laflamme, and G. J. Milburn, "A scheme for efficient quantum computation with linear optics," Nature **409**, 46–52 (2001).
10. P. Kok, W. J. Munro, K. Nemoto, T. C. Ralph, J. P. Dowling, and G. J. Milburn, "Linear optical quantum computing with photonic qubits," Rev. Mod. Phys. **79**, 135–175 (2007).
11. C. Santori, D. Fattal, J. Vuckovic, G. S. Solomon, and Y. Yamamoto, "Indistinguishable photons from a single-photon device," Nature **419**, 594–597 (2002).
12. T. Legero, T. Wilk, M. Hennrich, G. Rempe, and A. Kuhn, "Quantum Beat of Two Single Photons," Phys. Rev. Lett **93**, 070503 (2004).

#88797 - $15.00 USD Received 18 Oct 2007; revised 9 Nov 2007; accepted 14 Nov 2007; published 15 Nov 2007

13. A. Kiraz, M. Ehrl, T. Hellerer, O. E. Müstecaplioğlu, C. Bräuchle, and A. Zumbusch, "Indistinguishable photons from a single molecule," Phys. Rev. Lett. **94**, 223602 (2005).
14. J. Beugnon, M. P. A. Jones, J. Dingjan, B. Darqui, G. Messin, A. Browaeys, and P. Grangier, "Quantum interference between two single photons emitted by independently trapped atoms," Nature **440**, 779–782 (2006).
15. P. Maunz, D. L. Moehring, S. Olmschenk, K. C. Younge, D. N. Matsukevich, and C. Monroe, "Quantum interference of photon pairs from two remote trapped atomic ions," Nat. Phys **3**, 538–541 (2007).
16. L. Mandel, "Photon interference and correlation effects produced by independent quantum sources," Phys. Rev. A **28**, 929–943 (1983).
17. L. Kador, T. Latychevskaia, A. Renn and U. P. Wild, "Radio-frequency Stark effect modulation of single-molecule lines," J. Lumin. **86**, 189–194 (2000).
18. S. M. Mansfield and G. S. Kino, "Solid immersion microscope," Appl. Phys. Lett. **57**, 2615–2616 (1990).
19. G. Wrigge, I. Gerhardt, J. Hwang, G. Zumofen, and V. Sandoghdar, "Efficient coupling of photons to a single molecule and the observation of its resonance fluorescence," submitted, ArXiv, http://arxiv.org/abs/0707.3398 .
20. K. Koyama, M. Yoshita, M. Baba, T. Suemoto, and H. Akiyama, "High collection efficiency in fluorescence microscopy with a solid immersion lens," Appl. Phys. Lett. **75**, 1667–1669 (1999).
21. M. Orrit and J. Bernard, "Single Pentacene Molecules Detected by Fluorescence Excitation in a p-Terphenyl Crystal," Phys. Rev. Lett. **65**, 2716–2719 (1990).
22. A.-M. Boiron, B. Lounis, and M. Orrit, "Single molecules of dibenzanthanthrene in n-hexadecane," J. Chem. Phys. **105**, 3969–3974 (1996).
23. T. Nonn and T. Plakhotnik, "Fluorescence excitation spectroscopy of vibronic transitions in single molecules," Chem. Phys. Lett. **336**, 97–104 (2001).
24. A. Kiraz, M. Ehrl, C. Bräuchle, and A. Zumbusch, "Low temperature single molecule spectroscopy using vibronic excitation and dispersed fluorescence detection," J. Chem. Phys. **118**, 10821–10824 (2003).
25. F. Jelezko, B. Lounis, and M. Orrit, "Pump-probe spectroscopy and photophysical properties of single dibenzanthanthrene molecules in a naphthalene crystal," J. Chem. Phys. **107**, 1662–1702 (1997).
26. C. Santori, S. Götzinger, Y. Yamamoto, S. Kako, K. Hoshino, and Y. Arakawa, "Photon correlation studies of single GaN quantum dots," Appl. Phys. Lett. **87**, 051916 (2005).

Single-photon sources have been demonstrated in the solid state with molecules [1, 2], quantum dots [3] and nitrogen-vacancy color centers in diamond [4] as well as with atoms [5] and ions [6] in the gas phase. Single photons have been successfully used for applications in quantum cryptography [7, 8], but complex schemes of quantum information processing require a large number of indistinguishable photons [9, 10]. The first efforts in this direction have used consecutively emitted photons by single quantum dots, atoms in cavities or molecules [11, 12, 13]. More recently experiments with two independently trapped atoms or ions have been also reported [14, 15]. Here, we show that two molecules embedded in solid samples can also be used to generate lifetime-limited photons for use in the investigation of photon interference and correlation effects [16]. The solid-state aspect of our system offers many advantages including well defined polarization and a nearly indefinite measurement time using the same single emitter.

The experimental arrangement is sketched in Fig. 1 (a). Two independent low temperature microscopes are separated by an opaque wall in a liquid helium bath cryostat at $T = 1.4\,\mathrm{K}$. Light from a tunable dye laser (Coherent 899-29, $\lambda = 590$ nm, linewidth 1 MHz) is coupled into the microscopes via galvo-optic mirror scanners and telecentric lens systems. Each sample is prepared by sandwiching a solution of dibenzanthanthrene (DBATT) in *n*-tetradecane (concentration of $10^{-7}/mol$) between a glass substrate that contains interdigitating gold electrodes (spacing 18 μm) [17] and a hemispherical cubic zirconia solid immersion lens (SIL) [18]. The electrodes can be used to apply electric fields of up to 5×10^6 V/m resulting in a Stark shift of more than 5 GHz for the molecular resonance. The SILs combined with aspheric lenses of high numerical aperture (NA=0.55) provide an effective NA of 1.12 [19], allowing a high spatial resolution and an enhanced fluorescence collection efficiency [20]. Three piezoelectric slider systems in each microscope make it possible to position the sample/SIL unit precisely with respect to the aspheric lens. The collected photons of the microscopes can be sent either to an avalanche photodiode (APD), a spectrometer with a resolution of 0.3 nm, an imaging CCD

#88797 - $15.00 USD Received 18 Oct 2007; revised 9 Nov 2007; accepted 14 Nov 2007; published 15 Nov 2007

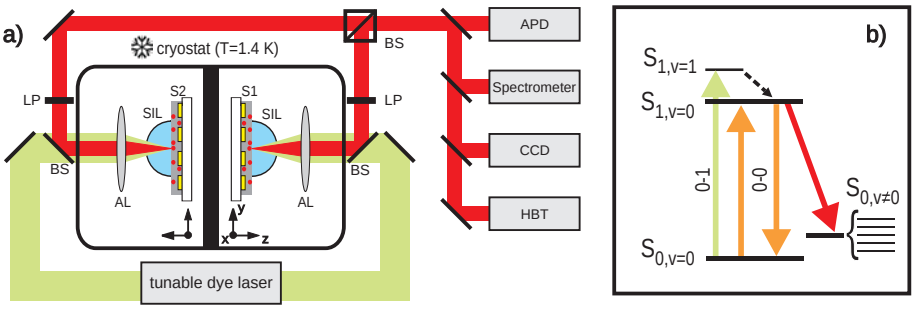

Fig. 1. a) Experimental setup: Two low temperature microscopes with solid immersion lenses are placed in a liquid helium bath cryostat. AL: aspheric lens, SIL: solid-immersion lens, S: sample, LP: long pass filter, BS: beam splitter, HBT: Hanbury Brown and Twiss autocorrelator, consisting of a beam splitter, two APDs and a time correlator card (Pico Harp, Pico Quant). Details are given in the text. b) Jablonsky diagram of a dye molecule with the relevant energy levels.

camera or a Hanbury Brown and Twiss (HBT) type photon correlator. Long-pass cut-off and band-pass filters are used to block undesired photons.

The energy spectrum of a dye molecule embedded in a solid at low temperatures is composed of electronic and vibrational levels. In what follows, we denote the states corresponding to the electronic ground and the first excited states of DBATT by $S_{0,v}$ and $S_{1,v}$, respectively (see fig. 1(b)). It turns out that each vibrational transition is composed of a narrow zero-phonon line (ZPL) and a phonon wing that stems from the vibrational coupling of the molecule with the host matrix. The ratio of the photons emitted into the ZPL to the total number of photons emitted into that particular vibronic transition is given by the Debye-Waller (α_{DW}). The ZPL of the transition between $S_{0,v=0}$ and $S_{1,v=0}$ (from now on referred to as 0-0 ZPL) in DBATT becomes natural linewidth limited at $T \leq 2\ K$, providing an ideal source of Fourier-limited single photons.

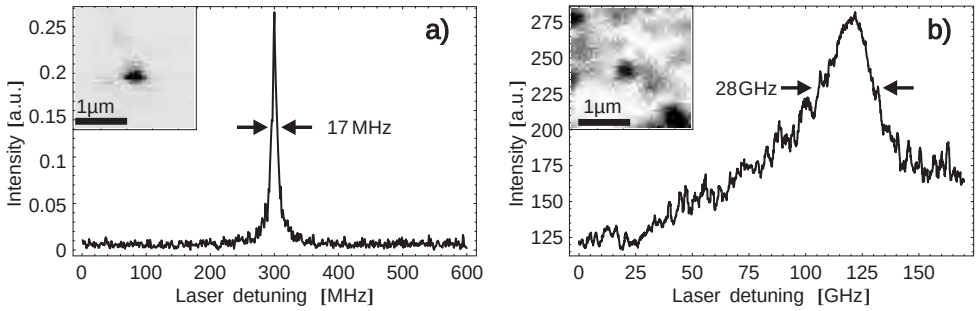

Fig. 2. (a) Fluorescence excitation spectrum of a single molecule excited via the 0-0 zero photon line. (b) Fluorescence excitation spectrum of the same molecule excited via the 0-1 transition. Insets: Laser scanning images of the molecule and its surrounding recorded at T=1.4 K under respective excitation conditions.

In standard fluorescence excitation spectroscopy [21] a narrow-band laser resonantly excites the molecule via the 0-0 ZPL. The molecular excitation decays consequently via the vibrational

#88797 - $15.00 USD Received 18 Oct 2007; revised 9 Nov 2007; accepted 14 Nov 2007; published 15 Nov 2007

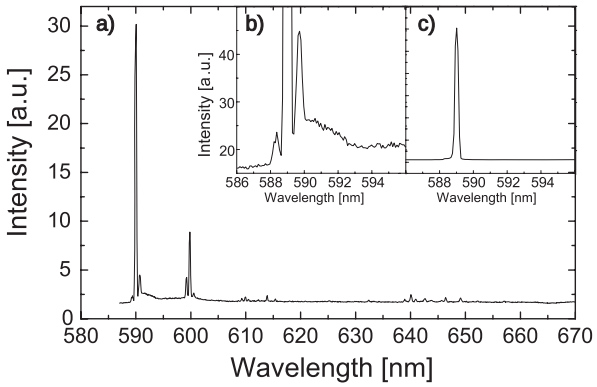

Fig. 3. a) Spectrum of a single DBATT molecule in *n*-tetradecane under 0-1 excitation. The linewidth is limited by the spectrometer resolution. b) Zoom around the 0-0 ZPL. c) The 0-0 ZPL isolated by inserting a 0.5 nm bandpass filter.

levels $S_{0,v}$, emitting Stokes-shifted photons (figure 1 (b)). To achieve a high signal-to-noise ratio and a low background in detecting single molecules, however, the 0-0 ZPL emission is cut off by using filters in detection. Figure 2 (a) displays an excitation spectrum from a single DBATT molecule. The full width at half-maximum (FWHM) of 17 ± 1 MHz corresponds to the excited state lifetime of 9.4 ± 0.5 ns [22].

In order to capture the *emission* on the narrow 0-0 ZPL transition, we apply a second version of fluorescence excitation spectroscopy by exciting the molecule to $S_{1,v=1}$ [23, 24] at 242 cm^{-1} higher frequency than the 0-0 ZPL [25]. This state quickly relaxes into $S_{1,v=0}$ where it decays further to the electronic ground state and emits a visible photon as in the previous case (figure 1 (b)). Figure 2 (b) shows such an excitation spectrum for the same molecule studied in Fig. 2 (a). The observed FWHM of 28 GHz is about three orders of magnitude broader than the ZPL transition and is caused by the short lifetime of about 5 ps for the $S_{1,v=1}$ state.

The large linewidth of the 0-1 transition implies its low absorption cross section. As a result, more than two orders of magnitude higher pump power (100 nW) is needed to obtain a signal comparable to the conventional excitation scheme used in Fig. 2 (a). This high laser intensity increases the background fluorescence because together with broad resonance lines it facilitates the excitation of neighboring molecules, reducing the spectral selectivity that has been the central asset in cryogenic single molecule detection. To get around this problem, we have worked with samples that are 100 times more dilute than commonly studied in single molecule spectroscopy. Furthermore, we have exploited the high resolution provided by SILs to identify single molecules spatially. The insets in Figs. 2 (a) and (b) show confocal scan images recorded when the laser frequency was set to the resonances shown in each figure. The FWHM of 290 nm is very close to the diffraction limited value of 270 nm expected from NA=1.12 and allows us to verify that the same molecule is the source of signals in both cases.

The next step toward the preparation of a Fourier-limited single photon source is to filter the 0-0 phonon wing and the Stokes shifted emission to extract the 0-0 ZPL. Figure 3 (a) shows the emission spectrum of a single DBATT molecule obtained by a 0-1 excitation. The dominant line at 590 nm represents the 0-0 ZPL. Several emission lines and the phonon wings (see also Fig. 3 (b)) are clearly visible. The recorded spectrum is in good agreement with ensemble measurements reported in the literature [25]. By comparing the different areas under the measured spectrum, we can estimate the Franck-Condon and the Debye-Waller factors to be 0.4 and

#88797 - $15.00 USD Received 18 Oct 2007; revised 9 Nov 2007; accepted 14 Nov 2007; published 15 Nov 2007

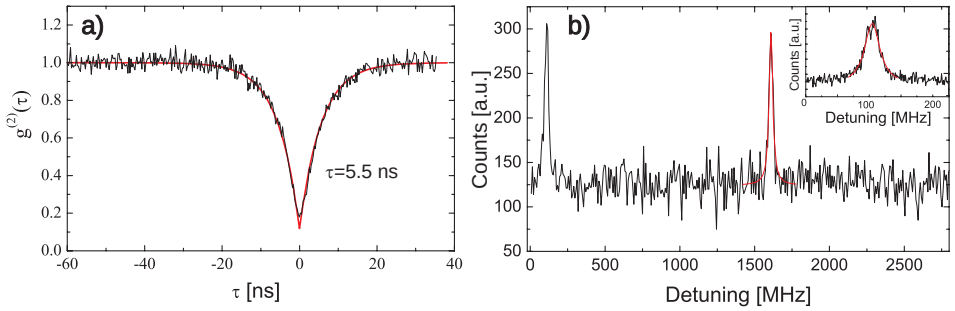

Fig. 4. (a) Second order photon correlation measurement of the zero-phonon line for a molecule excited via the 0-1 transition. Strong antibunching is clearly visible. (b) Fluorescence of the 0-0 ZPL analyzed by a Fabry-Perot cavity. Inset: A high resolution scan.

0.7, respectively. Figure 3 (c) shows the 0-0 ZPL after inserting a 0.5 nm bandpass filter in the detection path. In saturation experiments we were able to measure more than 3.5×10^5 photons per second emitted by this line.

To verify the realization of a single photon source, we have measured the second order autocorrelation function $g^{(2)}(\tau)$ on the 0-0 ZPL isolated according to the above-mentioned procedure. As shown in Fig. 4 (a), a strong antibunching is observed with $g^{(2)}(0) = 0.18$. We attribute the deviation from the ideal value of 0 to a limited time resolution of the single photon counters. The antibunching characteristic time of 5.5 ns is shorter than the decay time of 9.4 ns for the $S_{1,v=0}$ state because of the strong pumping of the population out of the ground state [26]. To ensure that the emitted 0-0 ZPL photons are nevertheless natural linewidth limited, we sent the emitted photons through a Fabry-Perot cavity with a finesse of 200 and a free spectral range of 1.5 GHz. Figure 4 (b) clearly shows a single peak within the free spectral range of the spectrum analyzer. The zoom in the inset highlights the narrow linewidth when accounting for the instrument FWHM of 7.5 MHz.

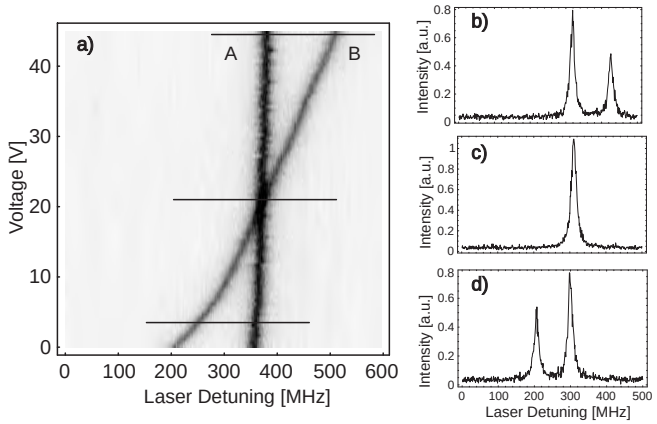

Fig. 5. (a) Fluorescence excitation spectra of two molecules. Molecule (B) is shifted with respect to molecule (A) with increasing voltage. (b)-(d) cross sections as indicated in (a). At $V = 21$ V, the two spectra are fully overlapped.

#88797 - $15.00 USD Received 18 Oct 2007; revised 9 Nov 2007; accepted 14 Nov 2007; published 15 Nov 2007

Having demonstrated the generation of narrow-band single photons from single DBATT molecules, we searched for two molecules, one in each microscope, that had 0-0 ZPLs within a few GHz of each other. By applying a constant electric field to the electrodes embedded in the glass substrates, we could tune the 0-0 ZPLs of the molecules independently via the Stark effect. Figure 5 shows the 0-0 fluorescence excitation spectra from two molecules recorded on one APD as the voltage applied to one sample was varied. The 0-0 ZPL of one molecule shifts with increasing voltage and sweeps through the resonance of the second molecule. At an applied field of about 1.2×10^6 V/m the spectra of the two molecules can be no longer distinguished. Given the well-defined orientation of the transition dipole moment in DBATT, the emission of single molecules can be linearly polarized with an extinction ratio of the order of 300:1 [19], making it a simple task to obtain the same polarization state for both single photon sources. Overlapping Fourier-limited spectral lines and polarization states establish the two molecules as sources of indistinguishable single photons.

In conclusion, we have combined cryogenic optical microscopy and spectroscopy to identify and prepare two single molecules that generate indistinguishable photons. A spectral analysis using a Fabry-Perot cavity and antibunching measurements gave direct proof for the generation of lifetime-limited single photons. The solid-state arrangement in this experiment using SILs makes it possible to miniaturize each single-photon source and to integrate several of them on one chip. Together with the nearly indefinite photostability and the long coherence times of dye molecules, these features make our approach promising for performing complex quantum operations. We are currently working to trigger the emission of single photons by incorporating a pulsed laser for the 0-1 excitation.

Acknowledgments

This work was supported by the ETH Zurich via the INIT program Quantum Systems for Information Technology (QSIT), the Swiss National Science Foundation and the Academy of Finland (grant number 210857). We thank G. Wrigge and I. Gerhardt for experimental help.

#88797 - $15.00 USD Received 18 Oct 2007; revised 9 Nov 2007; accepted 14 Nov 2007; published 15 Nov 2007

VI

Publication VI

V. Ahtee, R. Lettow, R. Pfab, A. Renn, E. Ikonen, S. Götzinger, and V. Sandoghdar, "Molecules as sources for indistinguishable single photons," J. Mod. Opt. **56**, 161–166 (2009).

Journal of Modern Optics
Vol. 56, Nos. 2–3, 20 January–10 February 2009, 161–166

Taylor & Francis
Taylor & Francis Group

Molecules as sources for indistinguishable single photons

Ville Ahtee[a,b], Robert Lettow[a], Robert Pfab[a], Alois Renn[a], Erkki Ikonen[b], Stephan Götzinger[a]* and Vahid Sandoghdar[a]

[a]*Laboratory of Physical Chemistry and optETH, ETH Zürich, Zürich, Switzerland;* [b]*Metrology Research Institute, Helsinki University of Technology (TKK) and Centre for Metrology and Accreditation (MIKES), Finland*

(*Received 31 January 2008; final version received 9 September 2008*)

We report on the triggered generation of identical photons by solid-state single-photon sources in two separate cryogenic laser scanning microscopes. Organic fluorescent molecules were used as emitters and investigated by means of high resolution laser spectroscopy. Continuous-wave photon correlation measurements on individual molecules proved the isolation of single quantum systems. By using frequency selective pulsed excitation of the molecule and efficient spectral filtering of its emission, we produced triggered Fourier-limited single photons. In a further step, local electric fields were applied to match the emission wavelengths of two different molecules via Stark effect. Identical single photons are indispensable for the realization of various quantum information processing schemes proposed. The solid-state approach presented here paves the way to the integration of multiple bright sources of single photons on a single chip.

Keywords: quantum information processing; single molecule spectroscopy; single-photon source; two-photon interference

1. Introduction

Interference effects of light produced by two independent, unrelated sources were already studied in 1955 [1]. Since then experiments have become more sophisticated and detectors more sensitive, showing that interference exists even for a few photons. In fact, it was as late as 1983 that Mandel theoretically investigated interference and correlation effects of single photons emitted by independent sources [2], likely inspired by new experimental techniques for studying resonance fluorescence from single atoms. First experiments in this direction utilized a spontaneous parametric down-conversion (SPDC) process where indistinguishable photon pairs are generated from higher frequency pump photons in a nonlinear crystal [3]. However, such photons cannot be considered fully independent since they were produced by the same pump photons and the same region of a crystal in a coherent process. In a step towards independent sources, photons were created in spatially separated crystals [4], but since the crystals were still pumped by the same laser, the resulting photons are still not completely independent. Only very recently indistinguishable photons from independent SPDC sources were reported where different crystals were pumped by electrically synchronized but otherwise independent femtosecond lasers [5]. An inherent drawback of SPDC sources remains, however, that their photon statistics is governed by a Poissonian distribution. In other words, the probability of emitting more than one photon can only be reduced, but it is never zero. As a result, one is limited to a weak photon flux to ensure the creation of single photon pairs. Furthermore, photons created by SPDC are spectrally broad and additional spectral filtering is often needed, resulting in a further reduction of the photon flux.

Motivated by the limitations of SPDC, active research has been undertaken to develop true single-photon sources that are capable of emitting indistinguishable photons. Photon indistinguishability is indispensable in any realization of quantum computation with single photons [6]. It is important to note that not only consecutively emitted photons from one emitter need to be identical, but also photons from different sources must be indistinguishable. In fact, schemes proposing efficient quantum computation require multiple single-photon sources emitting mutually indistinguishable single photons. Several two-level emitters, such as single quantum dots [7], single atoms in cavities [8], and single molecules [9] have successfully been operated as sources for indistinguishable single photons. In these experiments, consecutively emitted photons of the very same emitter were overlapped on a beam splitter. In another approach, atomic ensembles have been used for the

*Corresponding author. Email: stephan.goetzinger@phys.chem.ethz.ch

ISSN 0950–0340 print/ISSN 1362–3044 online

DOI: 10.1080/09500340802464657
http://www.informaworld.com

generation of indistinguishable photon pairs [10]. Very recently a milestone was reached when indistinguishable photons were produced from independently trapped atomic emitters [11,12]. Atoms and ions are very attractive for demonstrating proofs of principle. However, trapping single atoms requires sophisticated technology and the experimental procedure becomes particularly challenging if a large number of independently trapped atoms is desired.

Emitters in solid matrices offer a promising alternative. The position of the emitter is fixed so that no elaborate trapping techniques are required. The resulting devices can be very small and densely packed due to the monolithic nature of a solid-state system, and electrical pumping is often possible [13]. Semiconductor quantum dots, for example, are attractive for several reasons. First, they are well known to be photostable. Second, fabrication technology from semiconductor industry is readily available for micro- and nano-processing of chips that contain hundreds of quantum dots. On the other hand, their photon indistinguishablity is limited by dephasing [14] and their linewidth is usually not lifetime limited. As a solution, it is proposed to switch off spontaneous emission and use schemes similar to a stimulated Raman adiabatic passage for generating photons [14,15]. The experimental realization can be challenging and the proof of principle has not yet been demonstrated.

Organic molecules in a crystalline host matrix offer another powerful system. At low temperatures some molecular transitions become lifetime limited and offer almost unity quantum yield. Molecules, like any other system that generates photons by spontaneous emission, offer another important advantage compared to SPDC. Even though the same laser excites two molecules, coherence is destroyed by the spontaneous emission process, making the emitted photons truly independent. Recently we realized two independent Fourier-limited solid-state single-photon sources [16]. The solid-state arrangement of this approach enables nearly indefinite measurement times using the same emitter and a straightforward method for scaling and miniaturization. This paper characterizes the system further, reports on our recent developments, and discusses future prospective.

2. Method

Figure 1(*a*) shows a schematic of the experimental setup. Two independent low temperature microscopes in a liquid helium bath cryostat ($T = 1.4\,\mathrm{K}$) are separated by an opaque wall. As excitation sources we used either a continuous wave (cw) or a pulsed

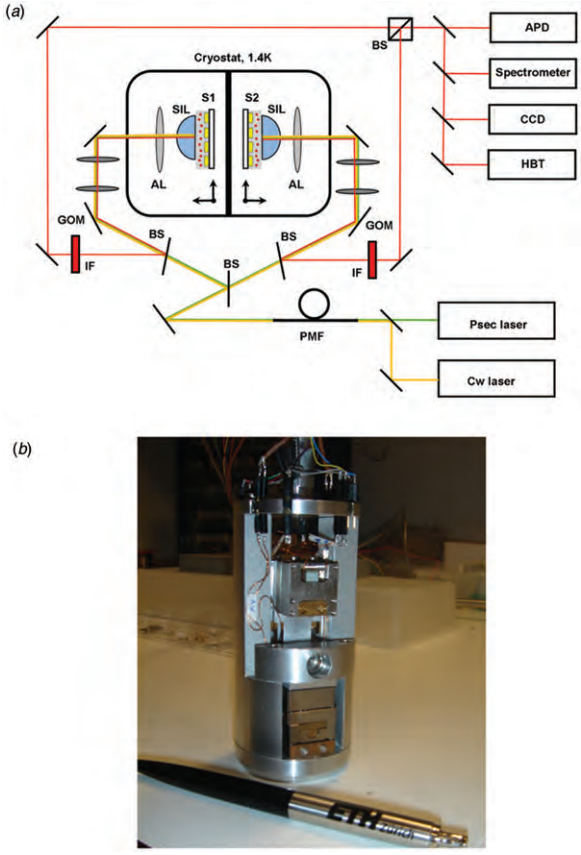

Figure 1. (*a*) Experimental setup: two low temperature microscopes with solid immersion lenses (SIL) are placed in a liquid helium bath cryostat. Light from the excitation lasers is coupled into a polarization maintaining fiber (PMF) and guided to the microscopes equipped with galvo-optic mirror scanners (GOM) and telecentric lens systems. Fluorescence is collected by the same optical arrangement and directed to different detectors. S: sample, AL: aspheric lens, BS: beam splitter, IF: set of interference filter, APD: avalanche photodetector, HBT: Hanbury Brown and Twiss autocorrelator. Further details are given in the text. (*b*) Photograph of the low temperature sample holder with piezoelectric slider positioners and AL-SIL imaging system. (The color version of this figure is included in the online version of the journal.)

dye laser. Both lasers could be coarsely frequency tuned by several tens of nanometers around 590 nm. The cw laser system (Coherent 899-29) is also continuously tunable over several hundred GHz and has a linewidth of about 1 MHz. The pulsed laser produces pulses of 700 ps with a repetition rate of 76 MHz. A cavity dumper can reduce this rate by a factor of 20 to guarantee well separated photons emitted by a single molecule. Light from both lasers is coupled into a polarization maintaining single mode fiber and directed to the microscope objectives via galvo-optic mirror scanners and telecentric lens systems to provide beam scanning confocal microscopes. As emitters we used dibenzanthanthrene (DBATT) molecules

embedded in Shpolskii matrices of *n*-tetradecane with a concentration of about 10^{-7} mol l^{-1}. The samples were sandwiched between hemispherical cubic zirconia solid immersion lenses (SIL) and glass substrates that contained interdigitating gold electrodes for Stark shifting the resonances of the molecules. Voltages up to 90 V, equivalent to electric fields of up to 5×10^6 V m^{-1}, could be applied to the electrodes spaced by 18 μm.

Aspheric lenses with a numerical aperture (NA) of 0.55 were placed inside the cryostat to focus the excitation beams onto the SILs and the samples [16,17]. Such a lens combination leads to an overall NA of 1.12. The sample/SIL package was mounted on a home-made three-axis piezoelectric slider system that enabled adjustments with sub-micrometer precision. The emission from the molecules was collected by the same SIL/aspheric lens combination and was directed to an avalanche photodiode (APD), a spectrometer, an imaging CCD camera, or a Hanbury Brown and Twiss (HBT) type photon correlator. A set of optical interference filters cut out the excitation wavelength and other unwanted spectral components. Figure 1(*b*) shows a photograph of the sample holder. The diameter of the holder is 50 mm limited by the dimensions of the cryostat chamber.

There are two principal ways to excite the narrow band molecules at cryogenic temperatures. The first method excites the ground state molecule into the $S_{1,v=0}$ state (see Figure 2(*a*)). From there the molecule decays into the ground state $S_{0,v=0}$, and into a manifold of states with $v \neq 0$. These red shifted photons are detected, but the photons from the narrow 0–0 zero phonon line (ZPL) cannot be separated from the excitation laser. This technique of photoluminescence excitation spectroscopy can directly measure the linewidth of the 0–0 ZPL by scanning a narrowband laser across its resonance [18]. In a second method, one excites the molecule into a higher vibrational level of the electronically excited state ($S_{1,v=1}$). This state decays nonradiatively within a few ps into $S_{1,v=0}$, from where the molecule decays, giving access to photons of the lifetime limited 0–0 ZPL. Associated with the short lifetime of $S_{1,v=1}$ is a broadening of the energy level to about 30 GHz. Therefore, we need about two orders of magnitude larger pump power (100 nW) compared to conventional excitation of molecules via the 0–0 ZPL. Vibronic excitation also severely decreases the spectral selectivity. Molecules with 0–0 ZPLs separated by more than 10 GHZ can be simultaneously excited owing to the broad $S_{1,v=1}$ level. For this reason we dilute our samples by about two orders of magnitude compared to commonly used samples in low temperature single molecule spectroscopy. Figure 2(*b*) shows a typical emission spectrum

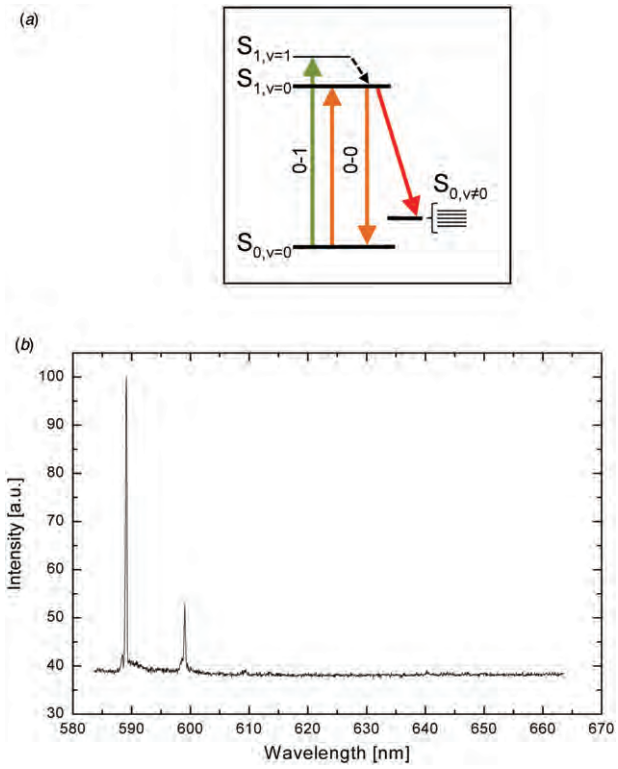

Figure 2. (*a*) Jablonsky diagram of a dye molecule with relevant energy levels. (*b*) Typical emission spectrum of a single DBATT molecule in *n*-tetradecane under vibronic excitation. The spectrum is dominated by the 0–0 ZPL at about 590 nm. (The color version of this figure is included in the online version of the journal.)

of a single DBATT molecule in *n*-tetradecane under vibronic excitation. The spectrum is dominated by the narrow 0–0 ZPL. In fact, we observe about 30% of the emitted photons in the 0–0 ZPL [16]. It is worth mentioning that DBATT in a crystalline host matrix does not suffer from photobleaching at cryogenic temperatures. We typically perform experiments with the very same molecule over hours or days.

3. System characterization

Figure 3(*a*) shows an image recorded by one of the confocal microscopes over an area of 10 μm × 10 μm. Molecules are excited on 0–1 transitions and their red shifted fluorescence is collected. Several single molecules can be distinguished. Relatively high background fluorescence caused by the increase in the laser power reveals the shape of the crystalline host matrix with characteristic cracks. Figure 3(*b*) displays the high spatial resolution of the system. It shows a 2.5 μm × 2.5 μm scan around the molecule marked in Figure 3(*a*). A Gaussian profile is fitted to the cross-section of the graph. The resulting full width at

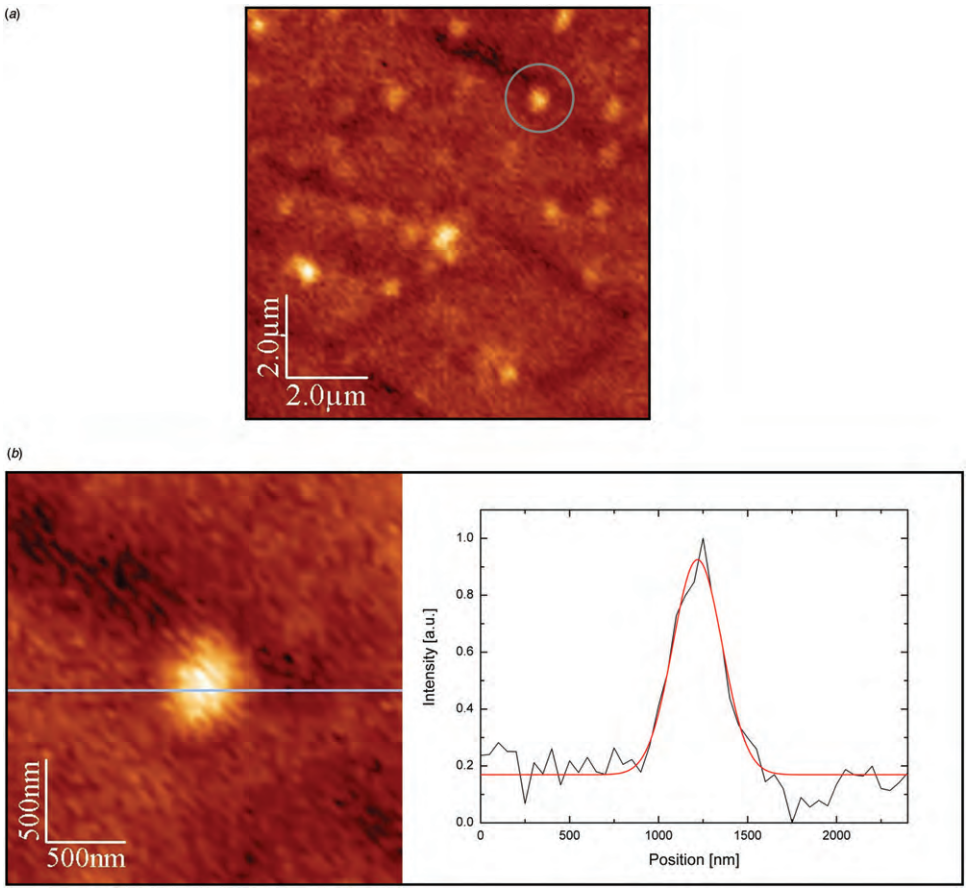

Figure 3. (*a*) Confocal image (10 µm × 10 µm) of a sample using vibronic excitation. Individual molecules can be seen as bright spots. (*b*) 2.5 µm × 2.5 µm scan over the molecule marked in (*a*). A Gaussian profile fitted to the cross-section estimates the focus size to be as small as 330 nm.

half-maximum (FWHM) of 330 nm indicates that the diameter of the laser focus is close to the theoretical diffraction-limited value of 270 nm expected from a NA = 1.12 objective. Such a tight focus is rather important for suppressing the probability of exciting more than one molecule via the broad vibronic excited state.

After having identified a molecule that is spatially well separated from others (see Figure 3(*b*)), we confirmed the lifetime limited linewidth of the 0–0 ZPL by photoluminescence excitation spectroscopy. Typically we measured 18 MHz full width at half-maximum, a value that corresponds well to the excited state lifetime of 9.4 ± 1 ns reported in the literature [19]. Photon correlation measurements using the HBT setup proved the isolation of a single quantum system. Figure 4(*a*) shows the result of such a measurement performed on a single molecule excited by the cw laser. Antibunching is clearly visible with $g^2(0) = 0.34$. The antibunching decay time of 8.1 ns is a bit shorter than the lifetime of the molecule, indicating that the system was not operated in the weak excitation limit.

In order to realize a triggered single-photon source, we excited the same molecule with the pulsed laser (Figure 4(*b*)). As in the case of the cw measurement, we excited the molecule via $S_{1,v=1}$ and detected its fluorescence on the 0–0 ZPL. Again we observe antibunching with $g^2(0) < 0.5$. The two-photon emission probability is reduced to 44% compared to a Poissonian source. The remaining coincidence counts at $t = 0$ can possibly be attributed to a weak excitation of other slightly detuned molecules in the neighborhood. This performance could be improved by diluting the sample further and incorporating a pinhole in the detection path to ensure exclusive collection of photons from the molecule of interest. To our knowledge, these results constitute the first report of single molecule spectroscopy where pulsed excitation is combined with spectral and spatial resolution. The technical difficulty in this detection scheme is to obtain pulses that are shorter than the fluorescence lifetime but long enough to avoid the excitation of several molecules at the same time. We achieved this by using a linear dye laser pumped by

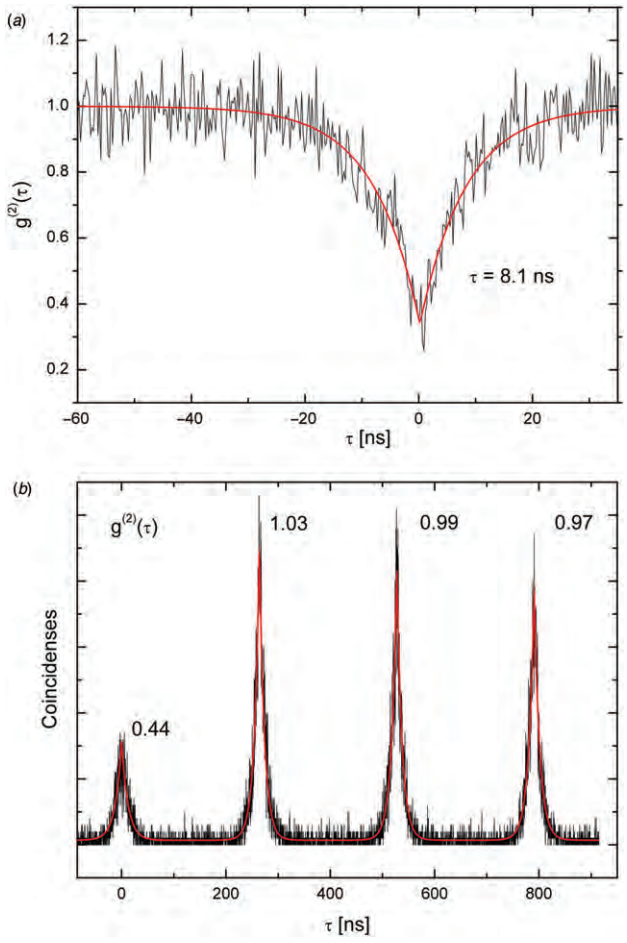

Figure 4. (*a*) Second order photon correlation measurement of the zero-phonon line of a molecule using cw excitation. (*b*) Triggered single photon emission by the same molecule using pulsed excitation. Strong antibunching is clearly visible in both cases. (The color version of this figure is included in the online version of the journal.)

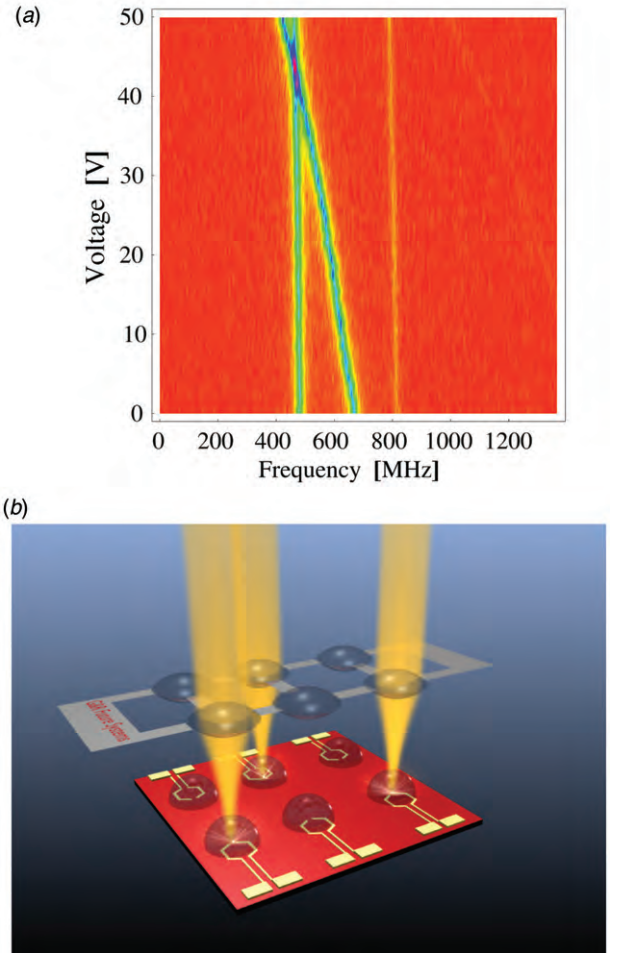

Figure 5. (*a*) Fluorescence excitation spectra of two molecules in different microscopes. An electric field applied to one of the molecules shifts its fluorescence to lower frequencies with increasing voltage. The two molecules become spectrally indistinguishable at a voltage of 42 V. (*b*) Schematics of multiple single-photon sources on a single chip where molecules are individually addressable by laser beams focused by aspheric lens/SIL combinations. Electrodes can be used to shift the emission wavelength of each single-photon source independently. (The color version of this figure is included in the online version of the journal.)

a frequency-doubled Nd:YVO_4 laser with a pulse width of about 13 ps. We then stretched the pulses to about 700 ps by implementing two etalons in the dye laser cavity.

Having shown that the selected molecule has a Fourier-limited linewidth and can be used as a triggered single-photon source, we looked for another molecule in the second microscope. After we found a promising candidate with a 0–0 ZPL within a few GHZ of the first molecule's emission line, we varied the voltage applied to the Stark electrodes in one of the microscopes. Figure 5(*a*) shows an example of Stark tuning where 0–0 ZPL fluorescence excitation spectra were taken simultaneously from both samples as a function of the applied voltage. At zero volts, the 0–0 ZPLs of the molecules are separated by 180 MHz. With increasing voltage the 0–0 ZPL of one of the molecules shifts towards lower frequencies. At a voltage of 42 V, the resonances of the two molecules can no longer be distinguished.

True quantum indistinguishability requires identical photons with respect to wavelength, polarization state, and spatial mode. DBATT molecules embedded in a Shpolskii matrix have well-oriented transition dipole moments whose emission can be linearly polarized [17]. Thus, it should not be a difficult task to obtain the same polarization state for both molecules. Indeed, we could successfully couple the 0–0 ZPL emission from single molecules into a polarization maintaining single mode fiber with an efficiency of 30%, corresponding to more than

10^5 photons per second. Therefore, this system provides ideal properties for the realization of a Hong–Ou–Mandel experiment whereby the exact degree of indistinguishability between photons can be determined. The lifetime limited linewidth of photons emitted from molecules provide a substantial advantage over photons obtained from incoherently pumped quantum dots [7,14].

Our current experiments involve only two molecules in different setups. However, one can easily imagine realizing a dense configuration of electrodes that are individually addressable on one chip as illustrated in Figure 5(*b*). Small solid immersion lenses together with microlens arrays would ensure a high collection efficiency of photons emitted by a large number of single-photon sources. Coupling the photons in a bundle of single mode fibers with polarization control and variable delay lines, would enable a device capable of simultaneously generating many indistinguishable single photons on demand.

4. Conclusion

In this paper we presented the realization of two identical Fourier-limited solid-state single-photon sources. Organic dye molecules were identified by cryogenic high resolution optical microscopy in two independent setups. The utilization of solid immersion lenses together with aspheric lenses was essential to achieve a tight excitation focus and thus a high degree of spatial selectivity. This arrangement also provides large collection efficiency essential for bright single-photon sources. Triggered single-photon emission was realized by introducing a frequency selective pulsed vibronic excitation scheme. The Stark effect was exploited to shift the transition frequency of a given molecule and thus achieve two independent single-photon sources with perfect spectral overlap. The high photostability and the compact solid-state arrangement of the sources allow nearly indefinite measurement times on the same emitter and a straightforward up-scaling to a larger number of identical single-photon sources. These results are promising for miniaturization and integration of several single-photon sources to even smaller volumes on a single chip. Further control and enhancement of the radiation properties of such single-photon sources can be envisioned by using microcavities [20] or nano-antennae [21,22].

Acknowledgements

This work was supported by the ETH Zurich via the INIT program Quantum Systems for Information Technology (QSIT), the Swiss National Science Foundation (SNF) and the Academy of Finland. We thank G. Wrigge and I. Gerhardt for experimental help.

References

[1] Forrester, A.T.; Gudmundsen, R.A.; Johnson, P.O. *Phys. Rev.* **1955,** *99,* 1691–1700.
[2] Mandel, L. *Phys. Rev. A* **1983,** *28,* 929–943.
[3] Hong, C.K.; Ou, Z.Y.; Mandel, L. *Phys. Rev. Lett.* **1987,** *59,* 2044–2046.
[4] de Riedmatten, H.; Marcikic, I.; Tittel, W.; Zbinden, H.; Gisin, N. *Phys. Rev. A* **2003,** *67,* 022301-1–5.
[5] Kaltenbaek, R.; Blauensteiner, B.; Zukowski, M.; Aspelmeyer, M.; Zeilinger, A. *Phys. Rev. Lett.* **2006,** *96,* 240502-1–4.
[6] Knill, E.; Laflamme, R.; Milburn, G.J. *Nature* **2001,** *409,* 46–52.
[7] Santori, C.; Fattal, D.; Vuckovic, J.; Solomon, G.S.; Yamamoto, Y. *Nature.* **2002,** *419,* 594–597.
[8] Legero, T.; Wilk, T.; Hennrich, M.; Rempe, G.; Kuhn, A. *Phys Rev. Lett.* **2004,** *93,* 070503-1–4.
[9] Kiraz, A.; Ehrl, M.; Hellerer, Th.; Müstecaplioglu, Ö.E.; Bräuchle, C.; Zumbusch, A. *Phys. Rev. Lett.* **2005,** *94,* 223602-1–4.
[10] Thompson, J.K.; Simon, J.; Loh, H.; Vuletic, V. *Science* **2006,** *313,* 74–77.
[11] Beugnon, J.; Jones, M.P.A.; Dingjan, J.; Darquié, B.; Messin, G.; Browaeys, A.; Grangier, P. *Nature* **2006,** *440,* 779–782.
[12] Maunz, P.; Moehring, D.L.; Olmschenk, S.; Younge, K.C.; Matsukevich, D.N.; Monroe, C. *Nature Phys.* **2007,** *3,* 538–541.
[13] Yuan, Z.; Kardynal, B.E.; Stevenson, R.M.; Shields, A.J.; Lobo, C.J.; Cooper, K.; Beattie, N.S.; Ritchie, D.A.; Pepper, M. *Science* **2002,** *295,* 102–105.
[14] Kiraz, A.; Atatüre, M.; Imamoğlu, A. *Phys. Rev. A* **2004,** *69,* 032305-1–10.
[15] Yao, W.; Liu, R.-B.; Sham, L.J. *Phys. Rev. Lett.* **2005,** *95,* 030504-1–4.
[16] Lettow, R.; Ahtee, V.; Pfab, R.; Renn, A.; Ikonen, E.; Götzinger, S.; Sandoghdar, V. *Opt. Express* **2007,** *15,* 15842–15847.
[17] Wrigge, G.; Gerhardt, I.; Hwang, J.; Zumhofen, G.; Sandoghdar, V. *Nature Phys.* **2008,** *4,* 60–66.
[18] Orrit, M.; Bernard, J. *Phys. Rev. Lett.* **1990,** *65,* 2716–2719.
[19] Boiron, A.-M.; Lounis, B.; Orrit, M. *J. Chem. Phys.* **1996,** *105,* 3969–3974.
[20] Press, D.; Götzinger, S.; Reitzenstein, S.; Hofmann, C.; Löffler, A.; Kamp, M.; Forchel, A.; Yamamoto, Y. *Phys. Rev. Lett.* **2007,** *98,* 117402-1–4.
[21] Kühn, S.; Håkanson, U.; Rogobete, L.; Sandoghdar, V. *Phys. Rev. Lett.* **2006,** *97,* 017402-1–4.
[22] Rogobete, L.; Kaminski, F.; Agio, M.; Sandoghdar, V. *Opt. Lett.* **2007,** *32,* 1623–1625.